2020

ON THE DETECTION OF GW190814

Matthew E. Gill

Acknowledgements

For my physics colleagues: David, Mello, Nick, Josh, Dillon, Dan, Ryan, thank you for accepting me into your circle, despite my inexperience, and all of your support as you watched me battle through sham after sham. For my oldest friends: The memory of your spirits have looked over my shoulder and helped to guide me as I stumbled through darkness. This is for Fitz & Marcus, who have been there every step of this Richmond journey. This is for Katherine (and Zuna & Elli)- without these sources of light in my life, I would have long ago been too lost to have ever finished. This is for my family.

RIP Mac Miller.

Abstract

ON THE DETECTION OF GW190814

By Matthew E. Gill
A Thesis submitted in partial fulfillment of the requirements for the degree of
Master of Science at Virginia Commonwealth University.

Virginia Commonwealth University, 2020.

Director: Dr. Robert Gowdy,
Associate Professor, Associate Chair, Department of Physics

The field of gravitational wave astronomy is currently at an all time high. The first half of the most recent observing run (April 1, 2019 - September 30, 2019) yielded a total of 39 gravitational wave detections, including 13 from sources which had not been identified by other astronomical observation methods before. This is three times as many detections than were measured in the first two observing runs combined. In this paper, the design sensitivity decisions leading to this unprecedented rate of detection are explored. In particular, we detail the nature of the LIGO and VIRGO gravitational wave interferometers. One recently detected event of particular interest, GW190814, was shown to possess a number of extraordinary properties relative to previous gravitational wave detections. It exhibits the greatest mass asymmetry of any system observed to date, leading to evidence of waveform contributions from higher order multipoles. The mass of the smaller object has generated curiosity in the field over whether the system is a binary black hole or neutron star-black hole merger. The nature of this component and the resulting properties of the system will be explored.

TABLE OF CONTENTS

Chapter Page

LIST OF FIGURES

CHAPTER 1

INTRODUCTION

Its been over a century since general relativity was first theorized by Albert Einstein in a series of papers published over the course of a decade [7]. In this time, the theory has held up to experimental tests on numerous fronts, though it still only gives a classical theory of gravity. Early tests of the theory sought to verify the Newtonian limit of the results which were able to be tested at the time. This helped to explain phenomena such as the precession of Mercury[8] and deflection of light during a total solar eclipse[9].

Even with the many experiments confirming the post-Newtonian consequences of general relativity, gravitational waves, an early prediction, remained undetected[1]. They were initially brought forward by Poincare[10] when he showed gravitational fields would observe similar propagation limits to those recently derived for electromagnetic fields. They were also then predicted by Einstein in 1916 after the initial development of GR. The evasiveness of gravitational waves can not be understated- the path deviations as one reaches the Earth from very far sources are imperceptible to the naked eye, and require complex equipment to validate. The indirect observation of energy transfer by gravitational waves could not occur until the detection of the pulsar PSR-1913+16 in 1974 [11].

However, in 2015, after nearly a century of theorizing, and 2 decades of construction and tuning, the two LIGO gravitational wave observatories achieved the first direct detection of a gravitational wave[12]. This event was the accumulation of a massive number of projects that truly began in 1994 [13]. The project technically was

first proposed in 1984 but due to the typical issues of organization in bureaucracy, it took 10 years to get moving. The two sites in Hanford, Washington and Livingston, Louisiana began construction in 1994 and 1995, respectively, and were completed in 1997. The first run at full initial LIGO design sensitivity occurred from 2005-2007 [2]. In addition to the LIGO detectors, the VIRGO detector began construction in the mid-90's near Pisa, Italy, with the intention of matching LIGO's sensitivity progression. From the beginning, each detector was designed to grow through a series of evolutionary stages in which their techniques and thus the detector sensitivity increases. These detectors are all highly advanced versions of Michelson interferometers, designed to reach dimensionless strain sensitivities of order of magnitude 10^{-21} and beyond.

The advanced LIGO detectors began their first run on September 12, 2015, running until January 19, 2016 [14]. The first gravitational wave was detected just two days later, only 3 detections were made in total, and all were binary black hole (BBH) systems. The second observation run occurred from November 30, 2016 and August 25, 2017, resulting in another 8 detections, of which 1 was a binary neutron star (BNS) system. VIRGO was added to the detection system on August 1, 2017, after finalizing its upgrade to the advanced state. This addition rapidly improved data quality, and in the first half of the third run led to a total of 39 detections [15], one of which is most like a BNS [16]. A handful of these detections exhibit extraordinary properties unlike previously measured detections.

One detection of particular intrigue is that of GW190814, first measured on August 14th, 2019. While only the second binary system ever observed with a significant mass asymmetry between its components, it is the most asymmetric yet, with a mass ratio of about $q = 0.112$ [17]. This property contributes to the production of radiation that is governed by higher order terms in the multipole expansion, analogous to that found in electromagnetism. Furthermore, the secondary mass component of the system is

found to be approximately $M_2 = 2.59 M_\odot$, where $M_\odot$ signifies one solar mass. The system, which given its mass components, is assumed to be either a BBH or a neutron star black hole (NSBH) binary system, making this secondary mass either the lightest black hole or the heaviest neutron star (NS) observed to date.

To reach this point of the conversation however, Chapters 2-5 of this thesis will be used to construct a solid mathematical bases in which to understand gravitational waves. First, we review some of the fundamental aspects of special relativity, and the base mathematical framework for working in four dimensional spacetime. Then, we provide a review of the construction of differential geometry along with motivation for Einstein's equations in curved spacetime. This gives way to the simpler linearized theory of gravity through transformation to the transverse traceless (TT) gauge. The mathematics behind this will be explored.

Chapter 6 is then devoted to bringing these idea to application- focusing first on the simple idea of the interferometer. We then examine how the ideas behind this machine can be used to make accurate measurements of the strain effects of passing gravitational waves. After this, the general setup of the advanced stages of LIGO and VIRGO will be described, along with an explanation of the signal parameters generated by these setups. Then, some of the design choices of the advanced LIGO (aLIGO) and advanced VIRGO (aVIRGO) upgrades leading to the most recent run will be reviewed. This includes a discussion of their design sensitivities both individually, and when the 3 observatories are in conjunction.

Finally, the results and methods of detection GW190814 are covered in Chapter 7. This includes the initial detection and the analytical methods of handling the waveform to deduce the system's physical parameters. These parameters are discussed and compared to previous results. Some of the more exotic features of the system are explored in detail, namely, the nature of the secondary components and the energy

contributions from higher order multipoles. It turns out that the classification of this binary system is inconclusive, due to issues with the explored parameter space in the models of numerical relativity. We explore the capability of the next generation of planned gravitational wave detectors to expand this parameter space, through its ability to obtain better strain sensitivity to systems of this frequency.

CHAPTER 2

REVIEW OF SPECIAL RELATIVITY

In order to build up mathematically to the idea of gravitational waves, we first begin with the theory of special relativity. Throughout this thesis, it is assumed the reader has a thorough understanding of special relativity, though not necessarily tensor algebra; and a solid grasp on linear algebra and mathematical reasoning. This chapter provides a summary of special relativity as covered by [18] [1] [19].

To begin the coverage of modern relativity, the two postulates fundamental to the theory of special relativity should be mentioned:

1. The speed of light is a constant $c = 3 \times 10^8$ m/s relative to any non-accelerating observers.

2. The results of all experiments in one reference frame are independent of its speed relative to other reference frames.

2.1 Spacetime

Setting up the physical structure to accommodate these postulates first requires a well-defined description of space and time. Anyone who has taken a physics class has experience with constructing a coordinate space in conjunction with a time stamp. In classical non-relativistic physics, it is trivial to take a real physical object and define a coordinate system about it such that one can analyze its dynamics. The coordinates chosen, regardless of how complicated, were naturally independent of the actual physics at hand, and yielded the same results. In such a case, gravity was thought of as an instantaneous force across a distance.

However, with the introduction of relativity, it was discovered that nothing could

propagate faster than the speed of light. This changed the nature of physics entirely, requiring a redefined structure of reality to appropriately model gravity. Where before, the absolute time was used to keep track of a system's development, in relativistic physics, the time becomes part of a 4-dimensional spacetime coordinate system. In special relativity, this is best done using the standard Cartesian coordinates and a time coordinate, which yields what is known as Minkowski spacetime. Then any event, $\mathscr{P}$, may be represented by the 4 coordinates $\mathscr{P} = (t, x, y, z)$. Furthermore, by describing a particle at a continuous string of these events, one can form a particle's world-line.

At first glance, this may look counter productive, as it bears a close resemblance to the old pre-relativity coordinate systems. However, the importance in this construction is not in the coordinates themselves, but the way in which they are related to one another.

2.2 Mathematics

A reference frame is defined loosely [collier] as the 4-dimensional coordinate system in which each event can be located by a time and its position. Each reference frame corresponds to a specific set of basis vectors e_0, e_1, e_2, e_3 [gowdy notes], with e_1, e_2, e_3 the basis vectors of a Cartesian coordinate system (x,y,z). It is helpful to think of the time in each frame as being measured by infinitely many, evenly spaced clocks. The time coordinate of an event in any given frame can then be found by checking the nearest clock in that frame.

For a reference frame to be inertial, it must satisfy the following 3 properties, per [18].

1. "The distance between points (x_1, y_1, z_1) and (x_2, y_2, z_2) are independent of time."

2. "The clocks that sit at every point are synchronized, and run at the same rate."

3. "The geometry of space at any time t is Euclidean."

Once established, reference frames and their basis vectors are used to describe the location of events in spacetime. As one has 3-dimensional vectors in pre-relativity physics, one now has 4-dimensional vectors in spacetime. In Minkowski spacetime, these vectors are not really any more abstract than their old counterparts. A vector is most simply defined as an arrow extending between two events in spacetime [19][18]. However for later extensions into curved spacetime, it will be useful to have an alternate representation of this idea.

2.2.1 Vectors

Suppose that, instead of an arrow, there is a line segment connecting the two events in spacetime. Let the position on the line segment be describable by some parameter, λ. Then this line between the two events, $\mathscr{P}_1$ and $\mathscr{P}_2$, can be described by

$$\mathscr{A}(\lambda) = \mathscr{P}_1 + \lambda(\mathscr{P}_2 - \mathscr{P}_1) \tag{2.1}$$

One can see that at $\lambda = 1$, the event $\mathscr{A}(0)$ turns out to be $\mathscr{P}_1$, and on the other hand, $\mathscr{A}(1)$ turns out to be $\mathscr{P}_2$. Taking the derivative with respect to λ, one finds

$$\frac{d\mathscr{A}}{d\lambda} = \frac{d}{d\lambda}(\mathscr{P}_1 + \lambda(\mathscr{P}_2 - \mathscr{P}_1)) = \mathscr{P}_2 - \mathscr{P}_1 \tag{2.2}$$

Note that this derivative is an equivalent representation of the original vector in mind. In flat spacetime, these two representations turn out to be equivalent representations of the same idea. Thus, by creating this line segment, parameterizing it, and producing a tangent vector, the number of points being considered can be

reduced from 2 to 1. This use of the tangent space to simplify the dimensions of our calculation will be essential when the transition to curved space is made. Furthermore, by choosing the parameter λ to be the absolute time τ, the line $\mathscr{A}(\tau)$ becomes representative of the worldline of a particle, and its tangent vector is the 4-velocity, $\mathbf{u}$.

Let this particle be observed from a reference frame, S, with basis vectors e_0, e_1, e_2, e_3 as described above. Then the particle at time τ has coordinate vector

$$x^\mu(\tau)\mathbf{e}_\mu = x^0(\tau)\mathbf{e}_0 + x^1(\tau)\mathbf{e}_1 + x^2(\tau)\mathbf{e}_2 + x^3(\tau)\mathbf{e}_3 \tag{2.3}$$

and four-velocity

$$u^\mu(\tau)\mathbf{e}_\mu = u^0(\tau)\mathbf{e}_0 + u^1(\tau)\mathbf{e}_1 + u^2(\tau)\mathbf{e}_2 + u^3(\tau)\mathbf{e}_3. \tag{2.4}$$

2.2.2 Lorentz Frames

Lorentz frames are the inertial frames of special relativity. In some appropriate coordinate system, a piece of spacetime can be described as Lorentzian if for any two events, A and B, in the same neighborhood, the proper distance and proper time between the two events is related by

$$\begin{aligned} \Delta s^2 &= -\Delta\tau^2 \\ &= -(x^0(A) - x^0(B))^2 + (x^1(A) - x^1(B))^2 \\ &\quad + (x^2(A) - x^2(B))^2 + (x^3(A) - x^3(B))^2 \end{aligned} \tag{2.5}$$

Meeting this condition ensures that the coordinate system has a locally Lorentz geometry. Then, Lorentz transformations preserve the Lorentzian nature of a reference frame, describing transformations from one Lorentz frame into another Lorentz frame. These can be understood simply as a transformation between two frames that are moving at relative velocities to one another, but it also includes rotations in some

spatial plane. Lorentz velocity boosts lead to the well known effects of time dilation and length contractions. For more information on these transformations and their general forms, see [1]. These Lorentz transformations, are typically of the form

$$x^{\mu'} = \Lambda^{\mu'}{}_{\mu} x^{\mu} \tag{2.6}$$

where this uses the standard Einstein index summation notation to express the linear transformations of the components. In this notation, any indices that are identical are summed over by default

$$a_j b^j = \sum_j a_j b_j \tag{2.7}$$

The sum on the right is shown in terms of a "traditional" sum over indices, where the object on the left is what we will use to denote a sum in the Einstein convention. The motivation of the position of the indices in these expressions will be explained later on.

2.2.3 Metric tensor

To measure the length of a four-vector in some reference frame, one must introduce the metric tensor, $\mathbf{g}$. This object acts as a function which takes 2 vectors as inputs and returns their scalar product. If one inserts the same vector twice, the metric tensor yields the scalar squared length of that vector. It is both linear and symmetric, and as such, one can define the metric coefficients in a Lorentz frame by the relation

$$\eta_{\mu\nu} \coloneqq \mathbf{g}(\mathbf{e}_\mu, \mathbf{e}_\nu) \tag{2.8}$$

It should be noted that this holds in any dimension, the value of which is determined by the range of the indices μ of the basis vectors. One can then write the spacetime

interval between any two events as

$$\begin{aligned}(\Delta s)^2 &= \Delta x_\mu \Delta x^\mu = \Delta \mathbf{x} \cdot \Delta \mathbf{x} \\ &= \mathbf{g}(\Delta \mathbf{x}, \Delta \mathbf{x}) = \mathbf{g}(\Delta x^\mu \mathbf{e}_\mu, \Delta x^\nu \mathbf{e}_\nu) = \Delta x^\mu \Delta x^\nu \mathbf{g}(\mathbf{e}_\mu, \mathbf{e}_\nu) \\ &= \Delta x^\mu \Delta x^\nu \eta_{\mu\nu}\end{aligned} \tag{2.9}$$

In any Lorentz frame, these coefficients are

$$\eta_{00} = -1 \qquad\qquad \eta_{kk} = 1. \tag{2.10}$$

One can also choose to insert only one vector into the metric tensor, in which case the object becomes a geometrical object known as a **one-form**. In particular we are concerned with the one-forms that correspond to the tangent vectors described previously. These describe a "pattern of surfaces" [19] in spacetime. If one then introduces a vector $\mathbf{v}$, the scalar output is measured by the number of surfaces which the vector passes through. The pattern of the surfaces is defined by the corresponding four-vector and the metric.

It should be clear from the above that the number of basis one-forms will be equivalent to the dimension of the spacetime in mind. They abide by the relation

$$\boldsymbol{\omega}^\beta(\mathbf{e}_\alpha) = \delta^\beta_\alpha \tag{2.11}$$

For example the one-form corresponding to the position vector can be represented as a linear combination of the basis forms

$$x_\mu(\tau)\boldsymbol{\omega}^\mu = x_0(\tau)\boldsymbol{\omega}^0 + x_1(\tau)\boldsymbol{\omega}^1 + x_2(\tau)\boldsymbol{\omega}^2 + x_3(\tau)\boldsymbol{\omega}^3 \tag{2.12}$$

We will minimize the amount of derivation here and provide a few facts. One forms undergoing a Lorentz transformation like those described for vectors will obey the same transformation law. Furthermore these can be described as existing at singular

points rather than "in spacetime." Using the prior delta function relation, one can write the squared length of a vector as

$$\begin{aligned}\mathbf{g}(\mathbf{x},\mathbf{x}) &= x^{\mu}\mathbf{e}_{\mu}(x_{\nu}\boldsymbol{\omega}^{\nu}) = x^{\mu}x_{\nu}\mathbf{e}_{\mu}(\boldsymbol{\omega}^{\nu}) = x^{\mu}x_{\nu}\delta^{\mu}_{\nu} \\ &= x^{\mu}x_{\mu}\end{aligned} \tag{2.13}$$

An alternative way of expressing this can be achieved by raising (or lowering) the indices of vector components with the components of the metric, such as $x^{\mu} = g^{\mu\nu}x_{\nu}$. Thus, an equivalent way of writing the above expression would be

$$\begin{aligned}\mathbf{g}(\mathbf{x},\mathbf{x}) &= x^{\mu}x_{\mu} \\ &= g_{\mu\nu}x^{\mu}x^{\nu}\end{aligned} \tag{2.14}$$

2.2.4 Tensors

In general, these relations between the bases of a frame are essential for understanding the nature of tensors. A **tensor** is a linear function which takes arguments of vectors and one-forms and returns a scalar function when provided with all arguments. However, depending on the arguments required, and the fraction of these which are provided, the function can produce a scalar, a one-form, a vector, or another tensor.

In general, tensors are constructed from using tensor products. A general tensor, T, which takes m one-forms and n vectors for arguments, will be constructed from m basis vectors, $\mathbf{e}_{\beta_i}$, and n basis one-forms, $\boldsymbol{\omega}^{\alpha_i}$, by taking the tensor product between them.

$$T = T^{\alpha_1\ldots\alpha_m}{}_{\beta_1\ldots\beta_m}\mathbf{e}_{\beta_1}\otimes\ldots\otimes\mathbf{e}_{\beta_n}\otimes\boldsymbol{\omega}^{\alpha_1}\otimes\ldots\otimes\boldsymbol{\omega}^{\alpha_m} \tag{2.15}$$

Tensors can be described according to their rank, such that a rank $\binom{m}{n}$ tensor would require m one-forms and n vectors to output a scalar. Both one-forms and vectors are themselves tensors, of type $\binom{0}{1}$ and $\binom{1}{0}$ respectively. Additionally, the

metric, in the form described thus far, is a type $\binom{0}{2}$. With some bases of a Lorentz frame defined, one can find the components of an $\binom{m}{n}$ tensor in that basis according to

$$T^{\alpha_1 \ldots \alpha_m}{}_{\beta_1 \ldots \beta_m} = \mathbf{T}(\boldsymbol{\omega}^{\alpha_1}, ..., \boldsymbol{\omega}^{\alpha_m}, \mathbf{e}_{\beta_1}, ..., \mathbf{e}_{\beta_n}). \tag{2.16}$$

The tensor components obey the Lorentz transformation law between reference frames just as vectors and one-forms. The indices are raised and lowered just as seen in equation (2.11). This is a limited overview of the nature of an immense class of geometric objects. Some of their properties, such as their symmetries (and anti-symmetries), may be applied without proof through the construction of these mathematics. For further information one should see the resources [1] [19] [18] [20]. It should be noted before proceeding that Lorentz transformations, though with indices that look like a tensor for the purpose of our notation, are not tensorial.

2.3 Energy and Momentum

With all of this in mind, we now take a moment to capture some of the notions of special relativity in the primitive version of component notation that has been constructed thus far. Namely, we wish to describe briefly the core components of the stress-energy tensor. For this section forward, we will use God-given units in which the fundamental constants, such as the speed of light, c, Planck's constant, $\hbar$, Boltzmann's constant, k, and the gravitational constant, G, are all set equal to 1. This creates the following unit scaling

$$[(energy)] = [\text{mass}] = [\text{length}^{-1}] = [\text{time}^{-1}] \tag{2.17}$$

The four-momentum effectively combines the rest mass-energy, $p^0 = E = m$ and

three-momentum p^i into the form

$$p^\mu = mU^\mu. \tag{2.18}$$

The square length of these two vectors, $p^\mu p_\mu = -m^2$, is shown to yield the standard relativistic energy relation $E^2 = \sqrt{p^i p_i + m^2}$. However this is all for one particle, and only gives so much insight into a system. To avoid this in moving to more complex systems, one wishes to also define the stress-energy (or energy-momentum) tensor, $T_{\mu\nu}$. This gives a description of the density of energy and momentum in a large collection of particles, or *dust*, using the total velocity of the system. More accurately, One can think of this as some flux of the four-momentum across some surface, though the idea of a surface does not necessarily hold in curved space, so this should be taken lightly.

This tensor is symmetric, meaning that for the indices μ, ν, $T_{\mu\nu} = T_{\nu\mu}$. The time based components represent the energy and momentum densities where $T_{00} = \rho$ the energy density, and $T_{0i} = T_{i0}$ are the momentum densities in the x_i directions. The spatial components of this tensor, T_{ij}, make up the stress part of the stress-energy tensor name, describing how a volume element in the dust exerts force in the space around it. Thus for some cubic volume element in the fluid, the diagonal components, T_{ii}, describe the pressure, P the faces exert in the direction they face. In contrast, the off diagonal components $T_{ij}, i \neq j$ describe how the faces exert shear force along their edges, effectively warping them.

One is typically interested in the form of the stress-energy tensor for a perfect fluid, as these can be generalized to most astrophysical situations quite well. These are fluids that can be represented entirely by an isotropic rest frame pressure, $T_{ii} = P$, and its rest frame energy density, $T_{00} = \rho$, thus making it diagonal. The general form

for the stress energy tensor of a perfect fluid is expressed as

$$T^{\mu\nu} = (\rho + P)U^{\mu}U^{\nu} + P\eta^{\mu\nu}, \tag{2.19}$$

where it should be noted that the four-velocity is typically normalized according to the condition $\eta_{\mu\nu}U^{\mu}U^{\nu} = -1$. The evolution of matter can then be determined by considering an equation of state defined by the relation $P = P(\rho)$

One final property of the stress energy tensor is that it is conserved, meaning its divergence is required to vanish

$$\partial_{\mu}T^{\mu\nu} = 0 \tag{2.20}$$

The $\nu = 0$ equation describes the conservation of energy, while the spatial equations $\nu = k$ describe the conservation of the kth component of momentum.

CHAPTER 3

DIFFERENTIAL GEOMETRY

This chapter reviews the basic tools of differential geometry which will be used to develop the theory of general relativity from special relativity. This begins with a review of differentiable manifolds, and how vectors, one-forms, and tensors are described in these spaces. Afterwards, the consequences of the metric are explored in the form of the covariant derivative, the connection coefficients, and the curvature tensor. The content of this chapter is primarily a summary of [1].

3.1 Manifolds and Maps

Before proceeding into the physics of curved spacetime, the final touches must be made on the mathematical framework thus far. From a topological point of view, a **manifold** can be defined as a set of points, M, in which each point has an open neighborhood which can be mapped onto an open set of $\mathbb{R}^n$, with the map being continuous and one to one. [20]. In order for this to be possible, the points in M must be continuous and differentiable. This ensures a space that is locally Lorentz.

In introductory classical physics, system dynamics are often modeled using Euclidean coordinate systems. Trivially, these spaces can all be considered manifolds. However, when doing analysis in curved spacetime, the manifolds are more complex, and the resemblance to Euclidean space may vary across it. In these instances, it is necessary to smoothly "patch" these Lorentz-like spaces into a comprehensive manifold.

To make this a little more precise, one can consider some number of sets A_i with maps $\psi_{ij}: A_i \mapsto A_j$ between them. Given three sets for $i = 1, 2, 3$, with maps

ψ_{12}andψ_{23} as defined above, the map ψ_{13} can also be expressed using the **composition** $\psi_{13} = \psi_{23} \circ \psi_{12}$. These maps can also be considered as functions of elements, so that an alternative way of writing this for a map from an element $x \in A_i$ to $y \in A_j$ would be $y = \psi_{ij}(x)$.

To describe the makeup of the different mappings, note that ψ_{ij} is defined as **one-to-one** if there is no more than one map into each element of A_j from the set A_i. ψ_{ij} is defined as **onto** if there is a minimum of one map into each element of A_j. If ψ_{ij} is both one-to-one and onto, each element of A_i maps into each element of A_j exactly once. In such a case, the map ψ_{ij} is invertible, and the inverse map ${\psi_{ij}}^{-1}$ is defined by the function relation $x = {\psi_{12}}^{-1}(y)$.

To consider continuity and differentiability over manifolds, examine the map $\phi : \mathbb{R}^n \mapsto \mathbb{R}^m$, which maps vectors $\mathbf{v} \in \mathbb{R}^n$ with components $(v^1, v^2, ..., v^n)$ to a vector $\mathbf{u} \in \mathbb{R}^m$ with components $(u^1, u^2, ..., u^m)$. It is assumed here that the reader has a sufficient understanding of continuity and differentiability of a single variable function. Then, consider the m functions ϕ_j that define this map, which describe the resulting m components of the vector $\mathbf{u}$ as $u^j = \phi_j(v^1, v^2, ..., v^n)$. One of these function is considered C^p if its pth derivative exists and is continuous, while the overall map ϕ is called C^p if all of its component functions are at least C^p. If a map has a collection of functions that are all infinitely differentiable and continuous, then the map is denoted C^∞ and referred to as **smooth**. Finally, two sets A and B are **diffeomorphic** if there exists a C^∞ map $\phi: A \mapsto B$, along with an inverse map that is also C^∞.

A **chart** (alternatively, a coordinate system) is made up of a set $U \subseteq M$ and a one-to-one map $\phi: U \mapsto \mathbb{R}^n$, such that $\phi(U)$ is open in $\mathbb{R}^n$. A $\mathbf{C^\infty}$ **atlas** can then be constructed by taking a collection of these charts and indexing them as (U_α, ϕ_α) and enforcing the conditions:

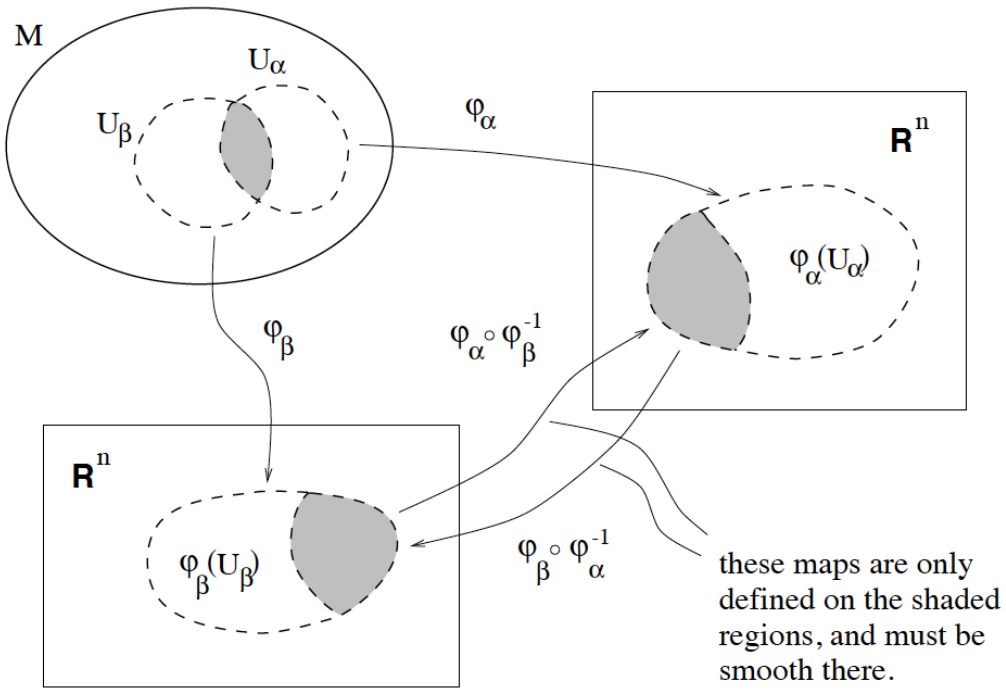

Fig. 1.
A schematic of the mapping between charts that are smoothly sewn together[1]

1. The union of the U_α is equal to M.

2. The charts are smoothly sewn together, so that if two charts, U_α and U_β, intersect, then the map $\phi_\alpha \circ \phi_\beta^{-1}$ takes points in $\phi_\beta(U_\alpha \cap U_\beta)$ onto an open set $\phi_\beta(U_\alpha \cap U_\beta)$ (both of which are in $\mathbb{R}^n$. All of these maps are required to be C^∞.

This second point may be better illuminated by Figure 1. Finally, a **C^∞ n-dimensional manifold** is a set M, along with an atlas containing every compatible chart. The differentiability does not always have to be infinite however, and it can always be assumed that the manifold is as differentiable as need be for the task at hand. The use of an atlas to define the manifold is due to the large variations in the topology of curved spacetimes, and is a formal method for "patching" these locally

Lorentz spaces, as mentioned.

This describes "wrapping" the real physical world with a mathematical coordinate system in order to do calculations. To illustrate this idea, consider a **curve** on a manifold can then be described as a one-to-one map $C: \mathbb{R} \mapsto M$, for some parameter $\lambda \in \mathbb{R}$. To make calculations on this curve, one must refer to the specific chart (ϕ, U) of the constructed atlas, which yields a mathematical representation of the curve in $\phi(U) \in \mathbb{R}^n$, defined by the function $(\phi \circ C)(\lambda) = (x^1(\lambda), x^2(\lambda), ..., x^n(\lambda))$.

3.2 Vectors

Return to the idea of the tangent vector, $\frac{d\mathscr{A}}{d\lambda}$, of the line $\mathscr{A}$ connecting two events in flat spacetime, which was established in the previous chapter. This enforced that vectors can be described as existing at singular points in spacetime, rather than extending between two points. This idea will be necessary in the transition to curved spacetime, as it will be required for all vectors to be described locally in order to appropriately give them meaning.

Topologically speaking, **the tangent vector u to a curve** $\mathscr{A}(\lambda)$ is the directional derivative operator along that curve,

$$\mathbf{u} = \partial_{\mathbf{u}} = \frac{d}{d\lambda} \tag{3.1}$$

where the final derivative is to be evaluated along the curve $\mathscr{A}$ at some particular event, $\mathscr{P}$ [1][19]. This last derivative can also be expanded using the chain rule as

$$\frac{d}{d\lambda} = \frac{dx^\mu}{d\lambda}\frac{\partial}{\partial x^\mu} \tag{3.2}$$

It should be noted that the partial derivative with respect to the curve x^μ can be

written as $\partial_\mu = \frac{\partial}{\partial x^\mu}$. Then, this initial tangent vector $\mathbf{u}$ now has the expansion

$$\mathbf{u} = \frac{dx^\mu}{d\lambda}\partial_\mu \tag{3.3}$$

Thus, it can be seen that the tangent vector $\mathbf{u}$ can be expressed with the directional derivatives ∂_μ chosen as its set of basis vectors. The component notation of vectors described previously for special relativity will not change, as all of the geometrical changes will be contained by the metric. One can also build this idea up by considering all of the curves passing through some point, $\mathscr{P}$. The collection of the tangent vectors at $\mathscr{P}$ from all of these curves makes up the **tangent vector space at** $\mathscr{P}, T_p$.

Choosing the basis vectors for this space to be $\mathbf{e}_{(\alpha)} = \partial_\alpha$ defines a **coordinate basis**. By constructing a tangent vector space in this manner at each point in a manifold, one can define a vector field that gives the value of a vector $\mathbf{v}(\mathscr{P}) \in T_p$ at each point p. Note that since the tangent space at each point in the manifold is constructed from the curves that pass through it, vector fields can also be thought of as a map from C^k functions to C^k functions. More accurately however, it should be said that a **vector field** is a linear, Leibnizian operator on functions. Notationally, vector fields, $\mathbf{v}$ will be referred to without giving it a specific argument of a point, $\mathscr{P}$ on the manifold.

The **commutator** of two vector fields v, w is then defined by its action on some function, f

$$[u, v]f = (uv - vu)f = u(vf) - v(uf). \tag{3.4}$$

This tells us how the resulting function changes as a result of the ordering of the vector field actions. It can easily be shown that this is also a vector field, the components of

which can be expressed as

$$[u, v]^\mu = u^\mu \partial_\lambda v^\lambda - v^\mu \partial_\lambda u^\lambda \tag{3.5}$$

3.3 One-forms & General Tensors

One also wishes to define similar field frameworks for one-forms, and therefore give the ability to form tensor fields. We skimmed past the idea of one-forms last chapter but attempt to give further definition here. One forms are linear functions that take vector arguments and return a real number, but in particular we are interested only in the maps from the tangent vector space. This in particular can be called the dual vector space [1], among other things.

First, it should be noted that the gradient of a function, is a one-form with the function's partial derivatives as its components,

$$\mathbf{d}\phi = \frac{\partial \phi}{\partial x^\mu} \boldsymbol{\omega}^\mu \tag{3.6}$$

The action of the gradient on a vector turns out to be the directional derivative in the direction of the vector. Furthermore, it can be shown that the gradient of the coordinate expressions x^μ are a natural basis to use. In this case, the components of the gradient of the coordinate functions acting on the basis of the function's tangent vectors, note that are written as

$$(dx)^\mu \partial_n u = \partial_n u x^\mu = \frac{x^\mu}{x_\nu} = \delta^\mu_\nu \tag{3.7}$$

Thus, choosing these as our basis vectors and one-forms satisfies the same requirement from flat spacetime. One can then follow similar logic as that which was applied for vector fields to reach form fields. To do this one defines the form field at each point corresponding to the curves passing through that point. This is then extended to all

the points with curves passing through them on the manifold, and the collection of these make up the form field.

Then, once again, we can go through this same process to arrive at tensor fields across the manifold. The first step in this will be to write the tensor in terms of basis tensors constructed from the defined basis vectors and basis forms,

$$T = T^{\alpha_1 \ldots \alpha_m}{}_{\beta_1 \ldots \beta_m} \partial_{\beta_1} \otimes \ldots \otimes \partial_{\beta_n} \otimes (dx)^{\alpha_1} \otimes \ldots \otimes (dx)^{\alpha_m} \tag{3.8}$$

Doing this for every point on the field (or where ever our interests require it), create a tensor field on the manifold on which one can have some semblance of comparison. The actual comparison process will be cleared up moving forward. Throughout this thesis, the choice of notational convention should be obvious. Nonetheless, it should be noted that the math will primarily be covered using component notation, unless otherwise stated.

3.4 The Metric Tensor

The metric tensor in curved spacetime will contain most of the geometric data about the manifold in consideration. As such, we will need a more dynamic metric than the flat spacetime metric, $\eta_{\mu\nu}$. However, this metric will still be a symmetric, type $\binom{0}{2}$ tensor. The covariant components of the metric will now denoted by

$$g_{\mu\nu} = \mathbf{g}(\mathbf{e}_\mu, \mathbf{e}_\nu). \tag{3.9}$$

where the basis vectors $\mathbf{e}_\alpha$ can be orthonormal, such as those described above, but are not necessarily. The contravariant components of the metric tensor are the matrix inverse of its covariant components. These are related by the condition

$$g_{\mu\nu} g^{\nu\sigma} = \delta_\mu{}^\sigma. \tag{3.10}$$

The metric in curved spacetime is responsible for providing calculations of path length and proper time. This relation is similar to that of flat spacetime, where the flat metric, $\eta_{\mu\nu}$, is replaced by the general metric, $g_{\mu\nu}$, to give the spacetime interval

$$ds^2 = g_{\mu\nu}dx^\mu dx^\nu \tag{3.11}$$

Furthermore, it is also responsible for giving a reference for the construction of locally Lorentz frames, as well as defining the motion of test particles by replacing the outdated notion of the gravitational field. To accomplish this first goal, define **a local Lorentz frame at a given event $\mathscr{P}_0$** as "the closest thing there is to a global Lorentz frame at that event." An equivalent representation of this is that at $\mathscr{P}_0$, the metric breaks down into the component form $g_{\mu\nu}(\mathscr{P}_0) = \eta_{\mu\nu}$, where these components vary minimally in the neighborhood of the event, as $\partial_\alpha g_{\mu\nu} = 0$. This is the basic expression of the Principle of Equivalence, the motivating principles behind relativity, and will be further addressed in the next chapter.

3.5 Connection Coefficients & Covariant Derivatives

In one of these locally lorentz frames, calculations can be done between neighboring events as if one was still in flat spacetime. Between any of these events, one can move tensors and vectors trivially- the changes of an object between two events can be described purely by the partial derivatives constituting the basis vectors of the space. However, it is important to remember that the basis components of these tangent spaces do not have to be constant. In fact, they usually change over a manifold. This should be clear, as this chapter has spent many words describing why these tangent vectors should be restricted to single points on a manifold, or to their neighbors in locally flat spaces.

As such, in the transition to curved spacetime, there is no immediate way to

define how a vector changes when the spacetime contains this ambiguity. With this in mind, it would be nice to construct a derivative operator, ∇ that will appropriately account for geometrical variations between points. This operator should be required to be linear and obey the Leibniz rule for all field arguments. So that for some tensor fields $\mathbf{v}, \mathbf{w}$,

1. $\nabla(\mathbf{v} + \mathbf{w}) = \nabla\mathbf{v} + \nabla\mathbf{w}$

2. $\nabla(\mathbf{v} \otimes \mathbf{w}) = \nabla\mathbf{v} \otimes \mathbf{w} + \mathbf{v} \otimes \nabla\mathbf{w}$

Note that just as the partial derivative in flat spacetime, this covariant derivative should act on general tensors in such a way that transforms a type $\binom{k}{l}$ tensor into a type $\binom{k}{l+1}$ tensor. Furthermore, it should be enforced that on scalar functions, the covariant derivative operator reduces to the partial derivative operator. Then, let us consider the action of this derivative on a vector field $\mathbf{u}$ which is written in some arbitrary basis $\mathbf{e}_\alpha$ in the vector space $V_{\mathscr{P}}$ across the manifold. This behaves as

$$\begin{aligned} \nabla_\mu \mathbf{u} &= \nabla_\mu(u^\alpha \mathbf{e}_\alpha) \\ &= (\nabla_\mu u^\alpha)\mathbf{e}_\alpha + u^\alpha(\nabla_\mu \mathbf{e}_\alpha) \end{aligned} \tag{3.12}$$

Since the components u^α are just scalar functions, this first term will reduce to a partial derivative,

$$\nabla_\mu \mathbf{u} = (\partial_\mu u^\alpha)\mathbf{e}_\alpha + u^\alpha(\nabla_\mu \mathbf{e}_\alpha) \tag{3.13}$$

Now comes the tricky part, the covariant derivative of the basis vectors $\mathbf{e}_\alpha$. To treat this, note that the desired geometrical object should express how the vector changes across the manifold. To get a real sense for what is happening, then, it should be clear that any results would be greatly simplified by expressing them in the same space which the original vector was expressed in. As such, we will expand

this derivative as some linear combination of the same basis vectors. Thus, with some brief haphazard notation, the result of this derivative in the second term above can be written in the form

$$\nabla_\mu \mathbf{e}_\alpha = (\nabla_\mu \mathbf{e}_\alpha)^\nu \mathbf{e}_\nu \tag{3.14}$$

The factor on the right hand side is obviously too clunky to seriously consider working with every time a derivative is taken. Instead, this term is replaced by the **connection coefficient**, $\Gamma^\nu_{\mu\alpha}$, such that this can instead be written as

$$\nabla_\mu \mathbf{e}_\alpha = \Gamma^\nu_{\mu\alpha} \mathbf{e}_\nu \tag{3.15}$$

Note that the chosen convention here is to place the differentiating index- μ, in this case -as the inside index. Then, with this definition in hand, the covariant derivative of a vector, $\mathbf{u}$, is thus given by the relation

$$\nabla_\mu \mathbf{u} = (\partial_\mu u^\alpha)\mathbf{e}_\alpha + u^\alpha \Gamma^\nu_{\mu\alpha} \mathbf{e}_\nu. \tag{3.16}$$

By switching the dummy indices in the equation, it should be easy to see that the components of this derivative take the form

$$\nabla_\mu u^\alpha = \partial_\mu u^\alpha + \Gamma^\alpha_{\mu\nu} u^\nu. \tag{3.17}$$

The covariant derivative of a general type $\binom{n}{m}$ tensor can be shown to also be a tensor, though this is a fact that will not be proven here. For further reading, see [[1]/wald/].

Through similar arguments, one can easily arrive at an expression for the components of the covariant derivative of some one-form ω_α. The only difference ends up being the

Similarly for some general type $\binom{m}{n}$ tensor $T_{\alpha_1 \ldots \alpha_n}{}^{\beta_1 \ldots \beta_m}$, the number of additional

correction terms will be equal to m+n. The covariant indices will yield correction terms added on, while the corrections for the contravariant indices will be subtracted, as was the case for the derivative of a single one-form.

Two additional properties that should be demanded of the covariant derivative and its resulting connection are

1. Torsion-free: $\Gamma^{\nu}_{\mu\alpha} = -\Gamma^{\nu}_{\alpha\mu}$
2. Metric-compatible: $\nabla_{\alpha} g_{\mu\nu} = 0$

3.5.1 Christoffel Connection

These properties are not essential to all theories of gravity, but they will be treated here as certain. Together, they yield a unique connection on which general relativity is based, known as the **Christoffel Connection**. This connection can be derived by the following method:

1. First, take three cyclic permutations of the metric-compatible connection: $\nabla_{\alpha} g_{\mu\nu} = 0, \nabla_{\mu} g_{\nu\alpha} = 0, \nabla_{\nu} g_{\alpha\mu} = 0$
2. Expand these using the definition of the covariant derivative acting on a type $\binom{0}{2}$ tensor. The expansion for the first permutation behaves then as

$$0 = \nabla_{\alpha} g_{\mu\nu} = \partial_{\alpha} g_{\mu\nu} - \Gamma^{\lambda}_{\alpha\mu} g_{\lambda\nu} - \Gamma^{\lambda}_{\alpha\nu} g_{\mu\lambda}. \quad (Equation 1) \tag{3.18}$$

3. This should be easily generalizable to the other two required derivatives, so that it is also seen that

$$\begin{aligned} 0 &= \partial_{\mu} g_{\nu\alpha} - \Gamma^{\lambda}_{\mu\nu} g_{\lambda\alpha} - \Gamma^{\lambda}_{\mu\alpha} g_{\nu\lambda}; \qquad (Equation 2) \\ 0 &= \partial_{\nu} g_{\alpha\mu} - \Gamma^{\lambda}_{\nu\alpha} g_{\lambda\mu} - \Gamma^{\lambda}_{\nu\mu} g_{\alpha\lambda}. \qquad (Equation 3) \end{aligned} \tag{3.19}$$

4. First subtract equation 2 from equation 1. Due to metric compatibility, both of these terms are required to be 0, so their difference will clearly be the same. This leads to the value

$$\begin{aligned} 0 &= [\partial_\alpha g_{\mu\nu} - \Gamma^\lambda_{\alpha\mu} g_{\lambda\nu} - \Gamma^\lambda_{\alpha\nu} g_{\mu\lambda}] - [\partial_\mu g_{\nu\alpha} - \Gamma^\lambda_{\mu\nu} g_{\lambda\alpha} - \Gamma^\lambda_{\mu\alpha} g_{\nu\lambda}] \\ &= \partial_\alpha g_{\mu\nu} - \Gamma^\lambda_{\alpha\mu} g_{\lambda\nu} - \Gamma^\lambda_{\alpha\nu} g_{\mu\lambda} - \partial_\mu g_{\nu\alpha} + \Gamma^\lambda_{\mu\nu} g_{\lambda\alpha} + \Gamma^\lambda_{\mu\alpha} g_{\nu\lambda} \end{aligned} \tag{3.20}$$

5. Note that the last term, when the torsion-free property of the connection coefficient is applied along with the metric tensor symmetry, can be rewritten $\Gamma^\lambda_{\mu\alpha} g_{\nu\lambda} = \Gamma^\lambda_{\alpha\mu} g_{\lambda\nu}$. This can be seen to be equivalent to the second term such that they will cancel out. Doing this and then subtracting equation 3, we get

$$\begin{aligned} 0 &= \partial_\alpha g_{\mu\nu} - \Gamma^\lambda_{\alpha\nu} g_{\mu\lambda} - \partial_\mu g_{\nu\alpha} + \Gamma^\lambda_{\mu\nu} g_{\lambda\alpha} \\ &= \partial_\alpha g_{\mu\nu} - \Gamma^\lambda_{\alpha\nu} g_{\mu\lambda} - \partial_\mu g_{\nu\alpha} + \Gamma^\lambda_{\mu\nu} g_{\lambda\alpha} - [\partial_\nu g_{\alpha\mu} - \Gamma^\lambda_{\nu\alpha} g_{\lambda\mu} - \Gamma^\lambda_{\nu\mu} g_{\alpha\lambda}] \\ &= \partial_\alpha g_{\mu\nu} - \Gamma^\lambda_{\alpha\nu} g_{\mu\lambda} - \partial_\mu g_{\nu\alpha} + \Gamma^\lambda_{\mu\nu} g_{\lambda\alpha} - \partial_\nu g_{\alpha\mu} + \Gamma^\lambda_{\nu\alpha} g_{\lambda\mu} + \Gamma^\lambda_{\nu\mu} g_{\alpha\lambda} \end{aligned} \tag{3.21}$$

6. Note that by applying the torsion-free and symmetry of the metric tensor as before, the second and second to last terms are seen to be similar, since $\Gamma^\lambda_{\nu\alpha} g_{\lambda\mu} = \Gamma^\lambda_{\alpha\nu} g_{\mu\lambda}$. Then, cancelling these terms leaves the expression

$$\begin{aligned} 0 &= \partial_\alpha g_{\mu\nu} - \partial_\mu g_{\nu\alpha} + \Gamma^\lambda_{\mu\nu} g_{\lambda\alpha} - \partial_\nu g_{\alpha\mu} + \Gamma^\lambda_{\nu\mu} g_{\alpha\lambda} \\ &= \partial_\alpha g_{\mu\nu} - \partial_\mu g_{\nu\alpha} - \partial_\nu g_{\alpha\mu} + 2\Gamma^\lambda_{\nu\mu} g_{\alpha\lambda} \end{aligned} \tag{3.22}$$

7. This can be rearranged to isolate the connection coefficient on a side by it self as

$$2\Gamma^\lambda_{\nu\mu} g_{\alpha\lambda} = \partial_\mu g_{\nu\alpha} + \partial_\nu g_{\alpha\mu} - \partial_\alpha g_{\mu\nu} \tag{3.23}$$

8. Multiplying through by a factor of $\frac{g^{\alpha\beta}}{2}$, the left hand side becomes

$$2\Gamma^{\lambda}_{\nu\mu} g_{\alpha\lambda}(\frac{g^{\alpha\beta}}{2}) = \Gamma^{\lambda}_{\nu\mu}\delta^{\beta}_{\lambda} = \Gamma^{\beta}_{\nu\mu} \tag{3.24}$$

Adjusting some of the indices on the right hand side due to symmetry, one arrives at a nice, final form of the Christoffel connections,

$$\Gamma^{\beta}_{\nu\mu} = \frac{1}{2} g^{\alpha\beta}(\partial_{\nu} g_{\mu\alpha} + \partial_{\mu} g_{\alpha\nu} - \partial_{\alpha} g_{\nu\mu}). \tag{3.25}$$

3.6 Parallel Transport

However, the notion of the change of general tensorial objects across a manifold is not yet solidified. To properly discuss this, recall that tensors in flat spacetime do not change as they are moved across the manifold- its Cartesian components are simply constant. While not an absolute truth for all tensors by any means, this is a distinguishing feature of curves that should be highlighted. Moving a tensor along a path while keeping it constant is known as **parallel transport**. The metric, when the covariant derivative is forced to be metric compatible, is a perfect example of a tensor that is parallel transported.

With the concept of parallel transport in place, the covariant derivative can be defined as the change of a vectors components compared to if the vector were parallel transported there. In such a case the vector has the same components it did before, and a comparison is easy to make. However, one must be careful when speaking of the orientation of the final vectors components. While working in flat spacetime, it was all fine and dandy to move a vector in any which direction to reach another point. However, in curved spacetime, the path one takes is absolutely crucial to the orientation of the parallel transported vector. This is most easily examined by considering the parallel transport of a vector Figure 2, first in flat spacetime, and then

in curved spacetime.

It will be nice to examine this concept a little further before proceeding. In particular, we wish to fix the orientation of the vectors in the vector space, V_P as it is moved along the curve $x(\lambda)$. To this end, define a **covariant directional derivative** analogous to the directional derivative, $\frac{d}{d\lambda} = \frac{dx^\mu}{d\lambda}\frac{\partial}{\partial x^\mu}$ in flat spacetime. It should be clear that the covariant derivative must replace the partial derivative in curved space to get the relation

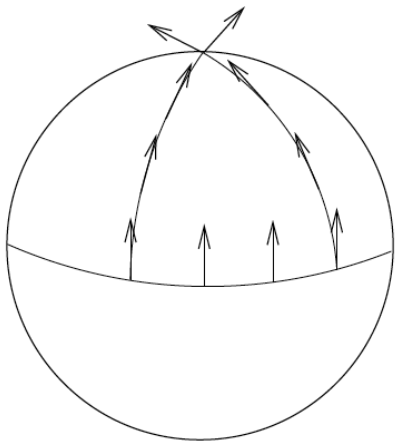

Fig. 2.: How vectors behave when parallel transported along paths on the surface of a sphere. The two resulting final vectors will have different orientations depending on their path through spacetime.

$$\frac{D}{d\lambda} = \frac{dx^\mu}{d\lambda}\nabla_\mu. \tag{3.26}$$

With this in mind, the parallel transport of a type $\binom{n}{m}$ tensor T is defined as the covariant directional derivative being zero, as

$$0 = \frac{dx^\mu}{d\lambda}\nabla_\mu T_{\alpha_1\ldots\alpha_m}{}^{\beta_1\ldots\beta_n} \tag{3.27}$$

Applying this to a vector u^α, it can be seen that a vector is parallel transported according to the relation

$$\begin{aligned} 0 &= \frac{dx^\mu}{d\lambda}\nabla_\mu u^\alpha \\ &= \frac{dx^\mu}{d\lambda}(\partial_\mu u^\alpha + \Gamma^\alpha_{\mu\nu}u^\nu) \\ &= \frac{dx^\mu}{d\lambda}\partial_\mu u^\alpha + \frac{dx^\mu}{d\lambda}\Gamma^\alpha_{\mu\nu}u^\nu \\ &= \frac{dx^\mu}{d\lambda}\frac{\partial}{\partial x^\mu}u^\alpha + \frac{dx^\mu}{d\lambda}\Gamma^\alpha_{\mu\nu}u^\nu \end{aligned} \tag{3.28}$$

Using the chain rule to simplify the derivative in the first term yields

$$0 = \frac{du^\alpha}{d\lambda} + \Gamma^\alpha_{\mu\nu}\frac{dx^\mu}{d\lambda}u^\nu. \tag{3.29}$$

3.6.1 Geodesics

If one narrows their vision further, and focuses only on the curves that have covariantly constant tangent vectors, a group of particularly important geometric structures is formed. Consider, again, a curve $x(\lambda)$ as described in the preceding section. The vector of interest in this case is going to be the tangent vector to the curve. Making the substitution $u^\alpha = \frac{dx^\alpha}{d\lambda}$ into Eq. (3.29), one arrives at the **geodesic equation**:

$$0 = \frac{d}{d\lambda}\frac{dx^\alpha}{d\lambda} + \Gamma^\alpha_{\mu\nu}\frac{dx^\mu}{d\lambda}\frac{dx^\nu}{d\lambda}. \tag{3.30}$$

A **geodesic** are the curved-space generalization of a straight line, being the shortest path between points in spacetime, and as such, their importance cannot be understated. It should be clear that in context of flat spacetime, when the connection coefficients vanish, this becomes $0 = \frac{d^2x^\mu}{d\lambda^2}$, which is the usual straight line in a Cartesian system. This points to the fact that this is a proper generalization into curved spacetime.

It should be noted that in considering timelike paths, parallel transport of the tangent vectors to a curve $x^\mu(\lambda)$ actually constrains the parameterization, λ, of the curve to one associated with that of proper time, τ, by the relation $\lambda = a\tau + b$, for some constants a and b. An alternative derivation of the geodesic equation can be achieved by varying timelike paths between stationary points on a manifold and finding the shortest path. This method should be familiar to anyone who has taken a graduate level mechanics course. Such a derivation gives a proper look at why the

parameterization of the curve must be constrained to proper time, though it will not be done here. This method also leads to connection coefficients which are precisely that of the Christoffel connection. See [1] for more information.

Geodesics are particularly important in their description of the movement of unaccelerated test particles through spacetime as a result of the geometry of the manifold. This will be shown to lead to the manifestation of the gravitational force in the coming chapters. For a timelike path, the parameter in Eq.(3.30) undergoes the transformation $\lambda \mapsto \tau$, such that the geodesic equation is written as

$$0 = \frac{d}{d\tau}\frac{dx^\alpha}{d\tau} + \Gamma^\alpha_{\mu\nu}\frac{dx^\mu}{d\tau}\frac{dx^\nu}{d\tau}, \tag{3.31}$$

or by writing it directly using the directional covariant derivative, i.e., the first relation in Eq. (3.28), where $u^\alpha = \frac{dx^\alpha}{d\tau}$, one finds

$$\begin{aligned} 0 &= \frac{dx^\mu}{d\tau}\nabla_\mu\frac{dx^\alpha}{d\tau} \\ &= U^\mu\nabla_\mu U^\alpha \end{aligned} \tag{3.32}$$

where in the second line, the substitution for the four-velocity $U^\mu = \frac{dx^\mu}{d\tau}$ has been made.

This can also be rewritten in terms of the four momentum, by multiplying through both sides of the equation by the squared mass, as

$$\begin{aligned} 0 &= m^2U^\mu\nabla_\mu U^\alpha \\ &= (mU^\mu)\nabla_\mu(mU^\alpha) \\ &= p^\mu\nabla_\mu p^\alpha \end{aligned} \tag{3.33}$$

This expression is enlightening as it highlights the motion of inertial bodies, i.e., that time-like test particles in free fall move in the direction that their momentum is oriented.

For null-like geodesics, it should be clear that the proper time will no longer be an appropriate parameterization. One could make this deduction on nomenclature alone, but to be technical, this is because there is no notion of proper time on these paths. Nonetheless, it is still possible to define the geodesic equation of null vectors in terms of the parameter, λ. If a curve $x(\lambda)$ satisfies the geodesic equation for the parameter λ, it will also be such for any related affine parameter by the transformation $\lambda \mapsto a\lambda + b$. It should be noted that any of these affine parameters can be chosen, though they will lead to different constructions for continuing the null-like path. It is thus conventional to choose the normalized parameter, λ, along the path such that the rate of change of the curve with respect to the parameter is equal to the momentum four-vector as

$$p^\alpha = \frac{dx^\alpha}{d\lambda} \tag{3.34}$$

This in particular will be important to the topic of this thesis, as it applies to the motion of photons in particular. An expression for the photons energy, as seen from a reference frame with velocity U^μ is then given by

$$E = p_\alpha U^\alpha \tag{3.35}$$

This equation also applies to those curves which are time-like, where the momentum is instead defined as $p_\alpha = mU_\alpha$. Returning mentally to earlier concepts of gravitation, it should be noted that for time-like paths in particular, this energy is only the energy of the particle as a product of inertia. There is no broad curved space generalization of the idea of a gravitational potential energy.

3.7 Curvature Tensor Structures

Recall the path a vector follows as it is parallel transported on a manifold determines its orientation at its final point. This is an important descriptor of how

the curved space behaves "between" these two points, i.e. how paths curve between two points. As such, it will greatly simplify the language of the manifold to create tensorial objects that codify this curvature.

3.7.1 Riemann Curvature Tensor

To get to this point, consider the figure, where there are two points with two separate path combinations connecting them. Let there be a vector $v^\alpha \in V_p$. Taking its covariant derivative first along the path A^μ and then the path B^ν, at point q yields the new vector $\nabla_\nu \nabla_\mu v^\alpha$. Evaluated at the proper points along the path, this new tensor gives the change of the vector relative to if it had been parallel transported (which would have been zero). One can do the same along the opposite path- taking the covariant derivative first along A^μ and then B^ν. This yields the vector $\nabla_\mu \nabla_\nu v^\alpha$, which if you've been following will be different than the first result we achieved, since the covariant derivatives do not commute.

This being the case, notice that by taking the difference between the resulting vectors, one arrives at the commutator of the covariant derivatives acting on the vector v_α

$$\begin{aligned}[\nabla_\nu, \nabla_\mu] v^\alpha &= (\nabla_\nu \nabla_\mu - \nabla_\nu \nabla_\mu) v^\alpha \\ &= \nabla_\nu \nabla_\mu v^\alpha - \nabla_\nu \nabla_\mu v^\alpha\end{aligned} \tag{3.36}$$

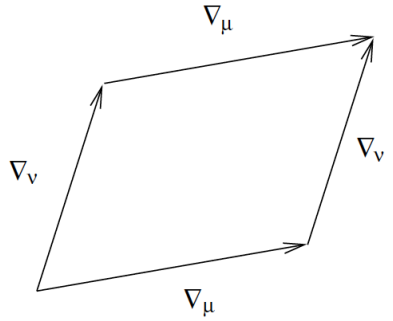

Fig. 3.: A setup of an infinitesimal loop created by the commutator of covariant derivatives, used to distinguish the curvature on a manifold

This commutator describes the difference in a vector being parallel transported by one route (i.e., first curve A then curve B) as opposed to moving it along an inverted route (i.e., B then A). Expanding the first

term above,

$$\begin{aligned}
\nabla_\nu \nabla_\mu v^\alpha &= \nabla_\nu(\partial_\mu v^\alpha + \Gamma^\alpha_{\mu\beta} v^\beta) \\
&= \partial_\nu(\partial_\mu v^\alpha + \Gamma^\alpha_{\mu\beta} v^\beta) + \Gamma^\alpha_{\nu\rho}(\partial_\mu v^\rho + \Gamma^\rho_{\mu\beta} v^\beta) - \Gamma^\rho_{\nu\mu}(\partial_\rho v^\alpha + \Gamma^\alpha_{\rho\beta} v^\beta) \\
&= \partial_\nu(\partial_\mu v^\alpha) + \partial_\nu(\Gamma^\alpha_{\mu\beta} v^\beta) + \Gamma^\alpha_{\nu\rho}\partial_\mu v^\rho + \Gamma^\alpha_{\nu\rho}\Gamma^\rho_{\mu\beta} v^\beta \\
&\quad - \Gamma^\rho_{\nu\mu}\partial_\rho v^\alpha + \Gamma^\alpha_{\rho\beta} v^\beta) \\
&= \partial_\nu\partial_\mu v^\alpha + (\partial_\nu \Gamma^\alpha_{\mu\beta}) v^\beta + \Gamma^\alpha_{\mu\beta}\partial_\nu(v^\beta) + \Gamma^\alpha_{\nu\rho}\partial_\mu v^\rho + \Gamma^\alpha_{\nu\rho}\Gamma^\rho_{\mu\beta} v^\beta \\
&\quad - \Gamma^\rho_{\nu\mu}(\partial_\rho v^\alpha + \Gamma^\alpha_{\rho\beta} v^\beta)
\end{aligned} \tag{3.37}$$

This is easily generalizable to the second term in Eq. (3.36) by interchanging the indices μ, ν on the covariant derivatives as

$$\begin{aligned}
\nabla_\mu \nabla_\nu v^\alpha &= \partial_\mu\partial_\nu v^\alpha + (\partial_\mu \Gamma^\alpha_{\nu\beta}) v^\beta + \Gamma^\alpha_{\nu\beta}\partial_\mu(v^\beta) + \Gamma^\alpha_{\mu\rho}\partial_\nu v^\rho + \Gamma^\alpha_{\mu\rho}\Gamma^\rho_{\nu\beta} v^\beta \\
&\quad - \Gamma^\rho_{\mu\nu}(\partial_\rho v^\alpha + \Gamma^\alpha_{\rho\beta} v^\beta)
\end{aligned}$$

Subtracting this second equation from the first, by focusing on coefficients of the vector v^α and its derivatives, one finds that

$$\begin{aligned}
[\nabla_\nu, \nabla_\mu] v^\alpha &= (\partial_\nu\partial_\mu - \partial_\mu\partial_\nu) v^\alpha + (\Gamma^\alpha_{\nu\rho}\partial_\mu - \Gamma^\alpha_{\mu\rho}\partial_\nu) v^\rho \\
&\quad + (\partial_\nu \Gamma^\alpha_{\mu\beta} + \Gamma^\alpha_{\mu\beta}\partial_\nu + \Gamma^\alpha_{\nu\rho}\Gamma^\rho_{\mu\beta} - \partial_\mu \Gamma^\alpha_{\nu\beta} - \Gamma^\alpha_{\nu\beta}\partial_\mu - \Gamma^\alpha_{\mu\rho}\Gamma^\rho_{\nu\beta}) v^\beta \\
&\quad + \Gamma^\rho_{\mu\nu}(\partial_\rho v^\alpha + \Gamma^\alpha_{\rho\beta} v^\beta) - \Gamma^\rho_{\nu\mu}(\partial_\rho v^\alpha + \Gamma^\alpha_{\rho\beta} v^\beta) \\
&= (\Gamma^\alpha_{\nu\rho}\partial_\mu - \Gamma^\alpha_{\mu\rho}\partial_\nu) v^\rho + (\Gamma^\rho_{\mu\nu} - \Gamma^\rho_{\nu\mu})(\partial_\rho v^\alpha + \Gamma^\alpha_{\rho\beta} v^\beta) \\
&\quad + (\partial_\nu \Gamma^\alpha_{\mu\beta} + \Gamma^\alpha_{\mu\beta}\partial_\nu + \Gamma^\alpha_{\nu\rho}\Gamma^\rho_{\mu\beta} - \partial_\mu \Gamma^\alpha_{\nu\beta} - \Gamma^\alpha_{\nu\beta}\partial_\mu - \Gamma^\alpha_{\mu\rho}\Gamma^\rho_{\nu\beta}) v^\beta
\end{aligned} \tag{3.38}$$

In the last term here, it will be necessary to interchange the dummy indices ρ and β.

Doing so and factoring again yields the expression

$$\begin{aligned}[\nabla_\nu, \nabla_\mu]v^\alpha &= (\Gamma^\rho_{\mu\nu} - \Gamma^\rho_{\nu\mu})(\partial_\rho v^\alpha + \Gamma^\alpha_{\rho\beta}v^\beta) \\ &+ (\Gamma^\alpha_{\nu\rho}\partial_\mu - \Gamma^\alpha_{\mu\rho}\partial_\nu + \partial_\nu\Gamma^\alpha_{\mu\rho} + \Gamma^\alpha_{\mu\rho}\partial_\nu \\ &+ \Gamma^\alpha_{\nu\beta}\Gamma^\beta_{\mu\rho} - \partial_\mu\Gamma^\alpha_{\nu\rho} - \Gamma^\alpha_{\nu\rho}\partial_\mu - \Gamma^\alpha_{\mu\beta}\Gamma^\beta_{\nu\rho})v^\rho\end{aligned} \tag{3.39}$$

Note that in the second term, the terms with partial derivatives acting on the vector components v^ρ cancel each other out, leaving only the expression

$$\begin{aligned}[\nabla_\nu, \nabla_\mu]v^\alpha &= (\Gamma^\rho_{\mu\nu} - \Gamma^\rho_{\nu\mu})(\partial_\rho v^\alpha + \Gamma^\alpha_{\rho\beta}v^\beta) \\ &+ (\partial_\nu\Gamma^\alpha_{\mu\rho} + \Gamma^\alpha_{\nu\beta}\Gamma^\beta_{\mu\rho} - \partial_\mu\Gamma^\alpha_{\nu\rho} - \Gamma^\alpha_{\mu\beta}\Gamma^\beta_{\nu\rho})v^\rho\end{aligned} \tag{3.40}$$

One then defines the **Riemann Curvature Tensor** to be the factor of the first term,

$$R^\alpha{}_{\rho\nu\mu} = \partial_\nu\Gamma^\alpha_{\mu\rho} - \partial_\mu\Gamma^\alpha_{\nu\rho} + \Gamma^\alpha_{\nu\beta}\Gamma^\beta_{\mu\rho} - \Gamma^\alpha_{\mu\beta}\Gamma^\beta_{\nu\rho} \tag{3.41}$$

This tensor is clearly antisymmetric in the indices μ and ν. The last term in Eq.(3.40), contains the factor, $2\Gamma^\rho_{[\nu\mu]} = \Gamma^\rho_{\nu\mu} - \Gamma^\rho_{\mu\nu}$, known as the torsion tensor- an antisymmetric type $\binom{1}{2}$ tensor. However, this will always disappear with the Christoffel connection which has been described for the purpose at hand. It is only mentioned here to point out that this commutator of covariant derivatives should not be explicitly taken as a definition of the Riemann Curvature tensor, as part of this derivation has been assumed on a particular connection. Because the covariant derivative of a tensor is itself a tensor, taking two covariant derivatives of a tensor will also yield a tensor. The difference between two tensors will also be tensorial, so it should be no surprise that the above expression behaves as a tensor.

One can generalize this derivation in order to find that the action of the commu-

tator of covariant derivatives on a tensor T behaves as

$$[\nabla_\nu, \nabla_\mu]T^{\alpha_1\cdots\alpha_m}_{\beta_1\cdots\beta_n} = -2\Gamma^\rho_{[\nu\mu]} + R^{\alpha_1}_{\rho\nu\mu}T^{\rho\cdots\alpha_m}_{\beta_1\cdots\beta_n} + \cdots + R^{\alpha_m}_{\rho\nu\mu}T^{\rho\cdots\alpha_m}_{\beta_1\beta_n} + R^\rho_{\beta_1\nu\mu}T^{\alpha_1\cdots\alpha_m}_{\rho\cdots\beta_n} + \cdots + R^\rho_{\beta_n\nu\mu}T^{\alpha_1\cdots\alpha_m}_{\beta_1\cdots\rho} \tag{3.42}$$

3.7.2 Extensions of Curvature

The Riemann curvature tensor is an extremely powerful tool for calculations due to the fact it has a handful of symmetries which greatly reduces the number of independent components. The symmetries in particular will be highlighted here; the reader is encouraged to read further about deriving the number of independent components in [1]. A number of new symmetries pop up when one restricts the connection defining the curvature to the Christoffel connection, as is the standard procedure in general relativity. These symmetries are more easily reconciled by first lowering all of the Riemann tensor indices as $R_{\alpha\beta\mu\nu} = g_{\alpha\lambda}R^\lambda{}_{\beta\mu\nu}$.

Then the immediate symmetries of this tensor are as follows:

1. $R_{\alpha\beta\mu\nu} = -R_{\beta\alpha\mu\nu}$
2. $R_{\alpha\beta\mu\nu} = -R_{\alpha\beta\nu\mu}$
3. $0 = R_{\alpha\beta\mu\nu} + R_{\alpha\mu\nu\beta} + R_{\alpha\nu\beta\mu}$

One can get the **Ricci tensor** by contracting the first and third indices according to

$$R_{\mu\nu} = R^\alpha{}_{\mu\alpha\nu} = g^{\alpha\beta}R_{\beta\mu\alpha\nu} \tag{3.43}$$

By the symmetries given above, it should be clear that this is the only independent contraction that can be made on this tensor. The Ricci tensor can then in turn be contracted over, to yield the **Ricci Scalar**

$$R = R^\alpha{}_\alpha = g^{\mu\alpha}R_{\mu\alpha} \tag{3.44}$$

These objects, the Ricci scalar and tensor, contain all of the information about the possible traces one can take over the curvature tensor. The trace free parts of the metric can then be decomposed to form the **Weyl Tensor**, though we will not need this detail further. It is an interesting subject in its own right, as it is invariant under conformal transformations. However, again, this will not be covered here and for further reading see [1].

Consider next the covariant derivative of the curvature tensor evaluated in locally Lorentz coordinates. In such a coordinate system, we will only need to consider the partial derivative term. Substituting the relevant expressions for the curvature tensor and the Christoffel connections. Working in local Lorentz coordinates, it will be appropriate to drop terms in the curvature components that have first order derivatives of the metric as factors. The first step will be to get the curvature itself expressed in terms of the metric. Starting with the expansion,

$$\begin{aligned} R_{\beta\rho\nu\mu} &= g_{\beta\alpha}R^{\alpha}{}_{\rho\nu\mu} \\ &= g_{\beta\alpha}(\partial_\nu\Gamma^\alpha_{\mu\rho} - \partial_\mu\Gamma^\alpha_{\nu\rho} + \Gamma^\alpha_{\nu\beta}\Gamma^\beta_{\mu\rho} - \Gamma^\alpha_{\mu\beta}\Gamma^\beta_{\nu\rho}) \end{aligned} \tag{3.45}$$

note that the Christoffel connections of particular interest will be of the form

$$\Gamma^\alpha_{\mu\rho} = \frac{1}{2}g^{\alpha\tau}(\partial_\mu g_{\rho\tau} + \partial_\rho g_{\tau\mu} - \partial_\tau g_{\mu\rho}). \tag{3.46}$$

It can then be seen that the last two terms in the curvature expression will reduce to 0, since these will contain first order metric derivatives will all go to zero in the neighboring flat space. The first two terms will contain some first order derivatives of the metric, but these will not be dropped until they are reached. Thus,

$$R_{\beta\rho\nu\mu} = g_{\beta\alpha}(\partial_\nu\Gamma^\alpha_{\mu\rho} - \partial_\mu\Gamma^\alpha_{\nu\rho}) \tag{3.47}$$

Only one of these terms will need to be considered, as these will be the same upon

switching the μ, ν indices in the second term. With this in mind, the first term expands as

$$\begin{aligned}\partial_\nu \Gamma^\alpha_{\mu\rho} &= \partial_\nu[\frac{1}{2} g^{\alpha\tau}(\partial_\mu g_{\rho\tau} + \partial_\rho g_{\tau\mu} - \partial_\tau g_{\mu\rho})] \\ &= \frac{1}{2}[(\partial_\nu g^{\alpha\tau})(\partial_\mu g_{\rho\tau} + \partial_\rho g_{\tau\mu} - \partial_\tau g_{\mu\rho}) \\ &\quad + g^{\alpha\tau}\partial_\nu(\partial_\mu g_{\rho\tau} + \partial_\rho g_{\tau\mu} - \partial_\tau g_{\mu\rho})]\end{aligned} \tag{3.48}$$

where the first term will be dropped as it only contains factors that are first partial derivatives of the metric. Thus, this leaves only

$$\partial_\nu \Gamma^\alpha_{\mu\rho} = \frac{1}{2}[g^{\alpha\tau}\partial_\nu(\partial_\mu g_{\rho\tau} + \partial_\rho g_{\tau\mu} - \partial_\tau g_{\mu\rho})] \tag{3.49}$$

Then, this is easily generalizable to both of the terms in the curvature expression, so that

$$\begin{aligned}R_{\beta\rho\nu\mu} = g_{\beta\alpha}\frac{1}{2}[&g^{\alpha\tau}\partial_\nu(\partial_\mu g_{\rho\tau} + \partial_\rho g_{\tau\mu} - \partial_\tau g_{\mu\rho}) \\ &- g^{\alpha\tau}\partial_\mu(\partial_\nu g_{\rho\tau} + \partial_\rho g_{\tau\nu} - \partial_\tau g_{\nu\rho})]\end{aligned} \tag{3.50}$$

Taking partial derivatives to commute with one another, it should be easy to see the first terms within the parentheses on either line will cancel one another. Thus, this simplifies further with this step and by contracting over the index α. Then,

$$\begin{aligned}R_{\beta\rho\nu\mu} &= \frac{1}{2} g_{\beta\alpha} g^{\alpha\tau}[\partial_\nu(\partial_\rho g_{\tau\mu} - \partial_\tau g_{\mu\rho}) - \partial_\mu(\partial_\rho g_{\tau\nu} - \partial_\tau g_{\nu\rho})] \\ &= \frac{1}{2}\delta^\tau_\beta[\partial_\nu(\partial_\rho g_{\tau\mu} - \partial_\tau g_{\mu\rho}) - \partial_\mu(\partial_\rho g_{\tau\nu} - \partial_\tau g_{\nu\rho})] \\ &= \frac{1}{2}[\partial_\nu\partial_\rho g_{\beta\mu} - \partial_\nu\partial_\beta g_{\mu\rho} - \partial_\mu\partial_\rho g_{\beta\nu} + \partial_\mu\partial_\beta g_{\nu\rho}]\end{aligned} \tag{3.51}$$

Then, finally, one can get the covariant derivative of the Riemann curvature tensor in locally inertial coordinates.

$$\begin{aligned}\nabla_\lambda R_{\beta\rho\nu\mu} &= \partial_\lambda R_{\beta\rho\nu\mu} \\ &= \frac{1}{2}\partial_\lambda[\partial_\nu\partial_\rho g_{\tau\mu} - \partial_\nu\partial_\tau g_{\mu\rho} - \partial_\mu\partial_\rho g_{\tau\nu} + \partial_\mu\partial_\tau g_{\nu\rho}]\end{aligned} \tag{3.52}$$

Note that even though we have chosen a particular coordinate system, this fact will generalize everywhere on a manifold due to the tensorial nature of this derivative. Then, one can take the cyclic permutation of the first 3 indices, λ, β, ρ to yield the Bianchi Identity, though only the identity itself will be given here.

$$0 = \nabla_\lambda R_{\beta\rho\mu\nu} + \nabla_\rho R_{\lambda\beta\mu\nu} + \nabla_\beta R_{\rho\lambda\mu\nu} \tag{3.53}$$

3.7.3 Einstein Tensor

Suppose then that one examines Eq. (3.53) further by contracting twice with the metric components $g^{\lambda\mu}$ and $g^{\nu\rho}$. This yields the relation

$$\begin{aligned} 0 &= g^{\nu\rho} g^{\lambda\mu} [\nabla_\lambda R_{\beta\rho\mu\nu} + \nabla_\rho R_{\lambda\beta\mu\nu} + \nabla_\beta R_{\rho\lambda\mu\nu}] \\ &= g^{\nu\rho} [\nabla^\mu R_{\beta\rho\mu\nu} + \nabla_\rho R^\mu{}_{\beta\mu\nu} + \nabla_\beta g^{\lambda\mu} R_{\rho\lambda\mu\nu}] \\ &= g^{\nu\rho} [\nabla^\mu R_{\beta\rho\mu\nu} + \nabla_\rho R^\mu{}_{\beta\mu\nu} - \nabla_\beta g^{\lambda\mu} R_{\lambda\rho\mu\nu}] \\ &= g^{\nu\rho} [\nabla^\mu R_{\beta\rho\mu\nu} + \nabla_\rho R^\mu{}_{\beta\mu\nu} - \nabla_\beta R^\mu{}_{\rho\mu\nu}] \end{aligned} \tag{3.54}$$

Then, contracting over the curvature components finds the expression

$$0 = g^{\nu\rho} [\nabla^\mu R_{\beta\rho\mu\nu} + \nabla_\rho R_{\beta\nu} - \nabla_\beta R_{\rho\nu}] \tag{3.55}$$

The action of the second metric then behaves as

$$\begin{aligned} 0 &= g^{\nu\rho} [\nabla^\mu R_{\beta\rho\mu\nu} + \nabla_\rho R_{\beta\nu} - \nabla_\beta R_{\rho\nu}] \\ &= \nabla^\mu g^{\nu\rho} R_{\beta\rho\mu\nu} + \nabla^\nu R_{\beta\nu} - \nabla_\beta R^\nu{}_\nu \\ &= \nabla^\mu g^{\nu\rho} R_{\rho\beta\nu\mu} + \nabla^\nu R_{\beta\nu} - \nabla_\beta R \\ &= \nabla^\mu R_{\beta\mu} + \nabla^\nu R_{\beta\nu} - \nabla_\beta R \end{aligned} \tag{3.56}$$

The dummy indices of the first two terms μ and ν can be interchanged in order to combine these terms to yield

$$0 = 2\nabla^{\mu} R_{\beta\mu} - \nabla_{\beta} R \tag{3.57}$$

This can be rewritten then as

$$0 = \nabla^{\mu} R_{\beta\mu} - \frac{1}{2}\nabla^{\mu} g_{\beta\mu} R = \nabla^{\mu}(R_{\beta\mu} - \frac{1}{2} g_{\beta\mu} R) \tag{3.58}$$

The tensor in parentheses on the far right hand side of this equation is then defined as the **Einstein Tensor**,

$$G_{\beta\mu} = R_{\beta\mu} - \frac{1}{2} g_{\beta\mu} R, \tag{3.59}$$

so that the twice contracted Bianchi identity can be written as just $\nabla^{\beta} G_{\beta\mu} = 0$.

3.8 Geodesic Deviation

The effects of curvature on a manifold show themselves through the Riemann curvature tensor in a number of different applications. One particularly important discussion that induces the use of this tensor is the calculation of the geodesic deviation. It has been mentioned previously, in curved spacetime, that moving the same vector along different paths of a manifold. It should be expected, then, that these resulting vectors cross at some point in a way that they are no longer oriented identically. To quantify this, it will be necessary to consider the curvature tensor introduced above. This will be necessary for the purpose at hand as this describes how test particles are affected by the passing of metric perturbations - i.e. gravitational waves.

It will be useful to examine geodesics which are initially parallel in order to determine their evolution as a function of the parameter, λ. In particular, we wish to determine how the spacing between two geodesics change as one continues down

the two curves. With this in mind, consider a collection of one-parameter geodesics, $\gamma_s(t)$, which do not cross, where s denotes the curve in the collection and t is an affine parameter on each curve. Assume that the curves are in increasing order in their index s. These curves make up a 2 dimensional manifold embedded into some arbitrary higher manifold, M, with coordinates chosen to be s and t. The surface made by these coordinates consists of the points $x^\mu(s,t) \in M$.

From the image it can be seen that along the curves, we have a simple choice of tangent vectors along the curves, defined by the family

$$T^\mu = \frac{\partial x^\mu}{\partial t} \tag{3.60}$$

This particular derivative defines the tangent vector on the manifold M at x^μ for some value t along some fixed curve $\gamma_{s_0}(t)$. Furthermore, we can define the separation vector between any two geodesics as

$$S^\mu = \frac{\partial x^\mu}{\partial s}. \tag{3.61}$$

This derivative then gives the change in relative position on the manifold M at x^μ between one geodesic $\gamma_{s_0}(t_0)$ and anotherr $\gamma_{s_1}(t_0)$ in the family $\gamma_s(t)$ for some fixed t_0.

One can now define the notion of the instantaneous change of the separation vector as it moves along the geodesic. Note that the change of the tangent vector will be zero since only geodesics are in question. Then, the only covariant derivative it makes sense to take will be that of S^μ in the direction of the tangent vector T^ν. Thus,

$$V^\mu = T^\nu \nabla_\nu S^\mu \tag{3.62}$$

This expression then gives the relative velocity of geodesics. Furthermore, the relative acceleration of the geodesics can be defined by again taking the covariant derivative

in the direction of the tangent vector. This yields

$$A^\mu = T^\nu \nabla_\nu V^\mu \tag{3.63}$$

One could also calculate the relative acceleration of some path away from a geodesic by taking the directional derivative of the tangent vector itself, from which one would get instead the expression, $a^\mu = T^\nu \nabla_\nu T^\mu$, which should be straightforward. It can be shown fairly easily that the components of the commutator of the basis vectors S and T yields the expression

$$[S,T]^\mu = S^\rho \nabla_\rho T^\mu - T^\rho \nabla_\rho S^\mu = 0, \tag{3.64}$$

where since the basis vectors have been adapted to the coordinate system at hand, their commutator goes to 0. Thus, it is found $S^\rho \nabla_\rho T^\mu = T^\rho \nabla_\rho S^\mu$. Replacing this for a definition of the velocity such that $V^\mu = S^\rho \nabla_\rho T^\mu$, the acceleration can now be calculated. It is found that

$$\begin{aligned} A^\mu &= T^\nu \nabla_\nu (S^\rho \nabla_\rho T^\mu) \\ &= T^\nu (\nabla_\nu S^\rho)(\nabla_\rho T^\mu) + T^\nu S^\rho \nabla_\nu (\nabla_\rho T^\mu) \\ &= S^\nu (\nabla_\nu T^\rho)(\nabla_\rho T^\mu) + T^\nu S^\rho \nabla_\nu (\nabla_\rho T^\mu). \end{aligned} \tag{3.65}$$

Noting then that the commutator of two covariant derivatives is related to the curvature by $\nabla_\mu \nabla_\nu - \nabla_\nu \nabla_\mu = R^\alpha{}_{\beta\mu\nu}$, this can be written instead as

$$\begin{aligned} A^\mu &= S^\nu (\nabla_\nu T^\rho)(\nabla_\rho T^\mu) + T^\nu S^\rho (R^\mu{}_{\beta\nu\rho} T^\beta + \nabla_\rho \nabla_\nu T^\mu) \\ &= S^\nu (\nabla_\nu T^\rho)(\nabla_\rho T^\mu) + T^\nu S^\rho \nabla_\rho \nabla_\nu T^\mu + T^\nu S^\rho R^\mu{}_{\beta\nu\rho} T^\beta. \end{aligned} \tag{3.66}$$

Applying the Leibniz product rule to the second term according to the relation

$$T^\nu \nabla_\rho \nabla_\nu T^\mu = \nabla_\rho (T^\nu \nabla_\nu T^\mu) - (\nabla_\rho T^\nu)(\nabla_\nu T^\mu) \tag{3.67}$$

, the relative acceleration is seen to simplify as

$$\begin{aligned} A^{\mu} &= S^{\nu}(\nabla_{\nu}T^{\rho})(\nabla_{\rho}T^{\mu}) + S^{\rho}[\nabla_{\rho}(T^{\nu}\nabla_{\nu}T^{\mu}) \\ &\qquad - (\nabla_{\rho}T^{\nu})(\nabla_{\nu}T^{\mu})] + T^{\nu}S^{\rho}R^{\mu}{}_{\beta\nu\rho}T^{\beta} \\ &= S^{\nu}(\nabla_{\nu}T^{\rho})(\nabla_{\rho}T^{\mu}) + S^{\rho}\nabla_{\rho}(T^{\nu}\nabla_{\nu}T^{\mu}) \\ &\qquad - S^{\rho}(\nabla_{\rho}T^{\nu})(\nabla_{\nu}T^{\mu}) + T^{\nu}S^{\rho}R^{\mu}{}_{\beta\nu\rho}T^{\beta} \\ &= T^{\nu}S^{\rho}R^{\mu}{}_{\beta\nu\rho}T^{\beta}. \end{aligned} \tag{3.68}$$

In the second to last line, the first and third terms are seen to cancel, while the second term contains the expression $T^{\nu}\nabla_{\nu}T^{\mu}$, which for geodesics are known to disappear. Thus, one arrives at this last line, known as the geodesic deviation equation. It can then be seen that the relative acceleration of two neighboring geodesics is directly proportional to the curvature. Furthermore, this acceleration itself can be interpretted physically as the appearance of gravitational tidal forces.

CHAPTER 4

GENERAL RELATIVITY

General relativity is most concerned with the behavior on manifolds which are metric-compatible and torsion-free. These specific properties have been shown to correlate in particular with the Christoffel connection. This will be used exclusively from here on out. The abstraction of a manifold which has been built up thus far must now be peeled back in order to consider the consequences of this framework. The main components of gravitation that will be encountered and need to be decoded with the tools of differential geometry are:

1. How spacetime curvature manifests as gravity

2. How momentum and energy change the spacetime geometry.

This, as one can imagine, has many consequences- all of which we will be unable to cover in the span of this thesis. Thus, we try to remain brief in this chapter. For more information on the full implications of GR, see [1] [19] [18], and the like.

4.1 The Equivalence Principle(s)

The primary motivation of general relativity, though we have not mentioned it explicitly thus far, is the equivalence principle. In particular, we now wish to consider the Einstein Equivalence Principle (EEP), which states that in small enough regions of spacetime, basic physics reduces to that of flat spacetime, making the gravitational field unobservable. This, in essence, is the physical equivalent of the manifolds defined earlier, which reduced to $\mathbb{R}^n$ in the local neighborhood of a point.

To actually make the transition, one must apply the minimal coupling principle,

which essentially states that if one takes a valid measurement of physics in a Lorentz frame, one can assert that this measurement will be the same in curved space at some point, as it should look locally Lorentz. In the established framework, if an expression can be derived for a physical observable in local Lorentz spacetime, one must only make the transformations

$$\eta_{\mu\nu} \mapsto g_{\mu\nu}; \qquad \partial_\mu \mapsto \nabla_\mu$$

to generalize this to curved manifolds.

A prime example in the standard graduate text is the stress energy tensor $T_{\alpha\beta}$ discussed previously in the context of flat spacetime. Recall that this tensor contained all the density-flux relations of mass-energy and momentum, and that it was required to ultimately be conserved. While the flux across some surface in curved space is more complex, it turns out that it can be done with the right positioning. Thus, in curved spacetime this law should still apply, and to make this transition one simply makes the transformation

$$\partial_\mu T^{\mu\nu} \mapsto \nabla_\mu T^{\mu\nu}. \tag{4.1}$$

From there, the connection coefficients, once acquired, along with the concept of parallel transport, are capable of doing all the heavy lifting of how this behaves across curved spaces. Intuitively, due to the method of construction of the Christoffel connections in the context of GR, this same information is also inherently contained in the metric, albeit in a different form. This principle thus generates the ability to calculate in curved space in the same way one would in flat space. Furthermore, this can be verified against the Newtonian predictions for the behavior of the gravitational field (i.e., the connection, the metric, etc) in its weak field limit, with which it is found to agree.

4.2 Einstein's Equations

Having now discussed how matter couples and responds to the geometry of spacetime, the inverse must be considered. It has long been known that mass creates gravity- early cosmological calculations involved the mass of both bodies bound to one another by a gravitational force. With this in mind, note that the density of mass-energy as seen by observers with velocity v^α is the scalar

$$\rho = v^\alpha T_{\alpha\beta} v^\beta \tag{4.2}$$

This mass energy density is expected to be the source of gravity. However, as seen here the stress energy tensor must be the coordinate independent object which induces changes in the geometrical structure. This now generalizes to the curved space relation $\nabla_\alpha T_{\mu\nu} = 0$, which in turn satisfies a conservation of energy-momentum law.

The goal now is to construct an equality that on one side, has this stress-energy tensor describing how the fields are generated by the mass energy density. On the other side of the equation, it is desired that there is another symmetric, divergence-free tensor which actually characterizes gravity itself. To appropriately characterize geometry it should be constructed purely of the geometrical objects which were discussed throughout the previous chapter (i.e., the metric, christoffel connections, the curvature tensor and its traces).

To ensure that this tensor gives a consistent picture of the spacetime curvature, enforce the properties:

1. The tensor vanishes in flat spacetime

2. The tensor is constructed from the Riemann curvature tensor and the metric, and from nothing else

3. The tensor be specifically linear in the Riemann tensor,

4. Again, that this be a rank 2 symmetric tensor and divergence free

It can be shown that the unique tensor satisfying all of these properties simultaneously is in fact the Einstein tensor, $G_{\mu\nu}$. This will simply be taken for granted here. Simply equating these tensors and their components would assume to much about the ratio between these two objects. This far, they have been kept very distinct from one another in the discussion. As such, when building this equality, a constant of proportionality κ will be introduced, and then solved for under limiting conditions. Then, this leaves the component relation

$$G_{\mu\nu} = \kappa T_{\mu\nu} \tag{4.3}$$

To get the value for κ, consider a perfect fluid in the limit of Newtonian gravity. The limiting conditions on general relativity to get Newtonian mechanics require obsevation of this perfect fluid in a weak-field, time-independent, low velocity state. Recall that a perfect fluid then has a stress energy tensor of the form

$$T_{\mu\nu} = (\rho + p)U_\mu U_\nu + p g_{\mu\nu} \tag{4.4}$$

In this expression, the pressure, p, can be neglected as this quantity is negligible for velocities not approaching the speed of light. Therefore, this expression is better approximated in this limit as

$$T_{\mu\nu} = \rho U_\mu U_\nu, \tag{4.5}$$

which is more accurately the stress energy of ideal dust, but alas. Nonetheless, even if this is the stress energy of ideal dust, it would be nice for this ideal dust to still be representative of some massive body in the manifold.

Working in the rest frame of this massive body, the relative velocity vector component U^α can be expressed as only having a time component, $U^i = 0$ for latin indices representing the spatial components, as i=1,2,3. In the weak field limit, the metric should be expressed as some perturbation about flat spacetime,according to the relation given in preceding section. However, it has already been assumed that the energy density ρ, and as such,by previous arguments, the local space should be expected to reduce to the linear theory described by the metric in the preceding section, $g_{\mu\nu} = \eta_{\mu\nu} + h_{\mu\nu}$

Therefore by the construction of this system, the only covariant components of the metric which need to be considered as the Lorentzian metric of flat space, $g_{00} = -1$. Then, the covariant component(s) of the velocity can be found by enforcing the normalization connection, $g_{\mu\nu}U^\mu U^\nu = -1$. Only the timelike components need to be considered, since only U^0 is nonzero. Thus, it can be seen that $-1 = g_{00}U^0U^0 = (-1)(U^0)^2$.

Then, it should be clear that the approximation at hand takes the form $U^0 = 1$. By the metric component, the covariant form of this vector is just $U_0 = g_{00}U^\alpha = -1$. Then, it should be easy to look back at the current expressin for the stress energy tensor, and see that the only nonzero component in this limit is $T_{00} = \rho$. It should also be clear from this fact that the trace of this stress energy tensor will behave as

$$T = g^{\mu\nu}T_{\mu\nu} = g^{00}T_{00} = -\rho, \tag{4.6}$$

since the contravariant metric component here will just be that of flat space in this limit, as has been mentioned.

Return to equation which was constructed to relate mass energy density to the curvature. Let the left hand side of the equation be expanded so that it is expressed in terms of the metric $G_{\alpha\beta}$, the Ricci tensor,$R_{\alpha\beta}$, and the Ricci curvature scalar, R.

Thus, this equation should be expressed as

$$R_{\mu\nu} - \frac{1}{2}Rg_{\mu\nu} = \kappa T_{\mu\nu} \tag{4.7}$$

Note then that contracting both sides of the equation by multiplying through a factor of $g^{\mu\nu}$, the left hand side becomes

$$\begin{aligned} g^{\mu\nu}(R_{\mu\nu} - \frac{1}{2}Rg_{\mu\nu}) &= g^{\mu\nu}R_{\mu\nu} - \frac{1}{2}Rg_{\mu\nu}g^{\mu\nu} \\ &= R^{\mu}{}_{\mu} - \frac{1}{2}R(4) = -R \end{aligned} \tag{4.8}$$

and the right hand side can be written using the standard definition of the trace as T, such that one finds the relation $-R = \kappa T$. Substitute this back into Eq. (4.7) to find it rewritten instead as

$$R_{\mu\nu} + \frac{1}{2}(\kappa T)g_{\mu\nu} = \kappa T_{\mu\nu}, \tag{4.9}$$

which is rearranged to yield instead,

$$R_{\mu\nu} = \kappa T_{\mu\nu} - \frac{1}{2}(\kappa T)g_{\mu\nu} \tag{4.10}$$

Then, to calculate R_{00} substitution of the stress energy component $T_{00} = \rho$, its trace $T = -\rho$, and the derived relevant metric component, $g_{00} = -1$ yields

$$\begin{aligned} R_{00} &= \kappa\rho - \frac{1}{2}\kappa(-\rho)(-1) \\ &= \kappa\rho - \frac{1}{2}\kappa\rho \\ &= \frac{1}{2}\kappa\rho. \end{aligned} \tag{4.11}$$

Then, this expression relates derivatives of the metric to the stress-energy tensor- giving a good representation of how the energy in a given space changes the metric

around it. As such, it would be nice to expand this term on the left out. Then, note

$$R_{00} = R^{\alpha}{}_{0\alpha 0} = \partial_\alpha \Gamma^\alpha_{00} - \partial_0 \Gamma^\alpha_{\alpha 0} + \Gamma^\alpha_{\alpha\lambda}\Gamma^\lambda_{00} - \Gamma^\alpha_{0\lambda}\Gamma^\lambda_{\alpha 0} \tag{4.12}$$

The last two terms are second order in the christoffel connections, but it should be noted that all of the terms which arise from these will be first order derivatives of the metric. Then, these two terms can be dropped as they will certainly go to zero. The second term is a time derivative, and since the metric is approximately constant in this limit, the christoffel connection will be also.

Thus, this term can be dropped, and the first term can be contracted over, giving a time derivative in it's first term where $\alpha = 0$. As such, this term can be ignored from the beginning, so that only the spatial components need to be considered. This can then be expanded using the definition of the christoffel connection as

$$\begin{aligned} R_{00} &= \partial_i \Gamma^i_{00} \\ &= \partial_i (\frac{1}{2} g^{i\rho})[\partial_0 g_{0\rho} + \partial_0 g_{\rho 0} - \partial_\rho g_{00}] \\ &= \frac{1}{2}\partial_i g^{i\rho}[-\partial_\rho g_{00}] \\ &= -\frac{1}{2}(g^{i\rho}\partial_i\partial_\rho) g_{00} \\ &= -\frac{1}{2}(g^{ij}\partial_i\partial_j) g_{00} \end{aligned} \tag{4.13}$$

where the time derivatives have been dropped as they appear, including the one contained in the partial derivative ∂_ρ.

Now, to a certain level of approximation in this calculation, it was possible to say that the metric component $g_{00} = -1$. However, now it would nice to be more precise by applying the full perturbation $g_{00} = -1 + h_{00}$. Then, also noting that the operator $g^{ij}\partial_i\partial_j)$ is just the Laplacian, ∇^2, in euclidean coordinates, this expression simplifies

to

$$R_{00} = -\frac{1}{2}\nabla^2 h_0 0 \tag{4.14}$$

Note the constant background flatness from the metric disappears upon taking the derivative here. Returning to the definition from section 1 of this chapter, $h_0 0 = 2\Phi$, this leaves the relation

$$R_{00} = \frac{1}{2}\kappa\rho = -\nabla^2\Phi. \tag{4.15}$$

where this must, in our limiting condition, be the relativistic generalization of the poisson equation.

As such, the definition $\kappa = 8\pi$, where the gravitational constant G is set equal to 1 to avoid confusion with the trace of the Einstein tensor. This leads to **Einstein's field equations**, which are the fundamental equations governing the theory of general relativity

$$G_{\mu\nu} = 8\pi T_{\mu\nu}. \tag{4.16}$$

These equations have been tested extensively in the past century, and are still held to be experimentally valid. Many of these experiments are important discussions in their own right for observing the power of the theory. One of the most recent validations, of course, is the topic of this thesis; gravitational waves. With Einstein's field equations in hand, this bear of a topic can now be appropriately poked at.

CHAPTER 5

GRAVITATIONAL RADIATION

With a better understanding of the role matter plays into spacetime curvature, as it is governed by Einstein's equations, one can then shift the vision to the small perturbations about the metric. This is particularly important as it will give us a simpler set of governing equations, from which gravitational waves can easily be derived. The best approach to accomplish this is by considering a weak field situation in which spacetime is assumed to be almost flat, as in the weak field discussion of the last chapter. However, this time, it would be nice to generalize the solution to include time-dependencies and the un-restricted motion of particles. This chapter summarizes information from [1] [19].

5.1 The Linearized Theory of Gravity

With the weak field situation in mind, the choice of new metric will be the same which was considered last chapter,

$$g_{\mu\nu} = \eta_{\mu\nu} + h_{\mu\nu}; \qquad |h_{\mu\nu}| << 1 \tag{5.1}$$

This can be substituted into the Einstein field equations, which, from Eq. (4.2) is, $G_{\mu\nu} = 8\kappa T_{\mu\nu}$. Expanding using the definitions

$$G_{\mu\nu} = R_{\mu\nu} - \frac{1}{2} g_{\mu\nu} R \tag{5.2}$$

and

$$R_{\mu\nu} = R^{\alpha}{}_{\mu\alpha\nu} = \Gamma^{\alpha}_{\nu\mu,\alpha} - \Gamma^{\alpha}_{\alpha\mu,\nu}, \tag{5.3}$$

Note that in the Ricci tensor, the terms that are second order in the connection coefficients have been dropped, since they contain only terms that are first order derivatives in the metric. Then, one finds that the left hand side of Einstein's field equations simplify as

$$\begin{aligned} G_{\mu\nu} &= R_{\mu\nu} - \frac{1}{2} g_{\mu\nu} R \\ &= R_{\mu\nu} - \frac{1}{2} g_{\mu\nu} R \\ &= R_{\mu\nu} - \frac{1}{2} g_{\mu\nu} g^{\rho\beta} R_{\rho\beta} \\ &= \Gamma^{\alpha}_{\nu\mu,\alpha} - \Gamma^{\alpha}_{\alpha\mu,\nu} - \frac{1}{2} g_{\mu\nu} g^{\rho\beta} (\Gamma^{\sigma}_{\beta\rho,\sigma} - \Gamma^{\sigma}_{\sigma\rho,\beta}) \end{aligned} \tag{5.4}$$

The connection coefficients may be linearized independently. Recalling the definitions for metric compatible coordinates and substituting in the new metric definition, we find that

$$\begin{aligned} \Gamma_{\alpha\mu\nu} &= \frac{1}{2}(g_{\alpha\mu,\nu} + g_{\alpha\nu,\mu} - g_{\mu\nu,\alpha}) \\ &= \frac{1}{2}(\partial_\nu g_{\alpha\mu} + \partial_\mu g_{\alpha\nu} - \partial_\alpha g_{\mu\nu}) \\ &= \frac{1}{2}(\partial_\nu(\eta_{\alpha\mu} + h_{\alpha\mu}) + \partial_\mu(\eta_{\alpha\nu} + h_{\alpha\nu}) - \partial_\alpha(\eta_{\mu\nu} + h_{\mu\nu})) \\ &= \frac{1}{2}(\partial_\nu h_{\alpha\mu} + \partial_\mu h_{\alpha\nu} - \partial_\alpha h_{\mu\nu}) \\ &= \frac{1}{2}(h_{\alpha\mu,\nu} + h_{\alpha\nu,\mu} - h_{\mu\nu,\alpha}) \end{aligned} \tag{5.5}$$

Then, the appearance of the connection coefficients in EQ are of the form

$\Gamma^{\alpha}_{\mu\nu,\alpha} - \Gamma^{\alpha}_{\mu\alpha,\nu}$. Using the above definition, this difference simplifies as

$$\begin{aligned}
\Gamma^{\alpha}_{\mu\nu,\alpha} - \Gamma^{\alpha}_{\mu\alpha,\nu} &= g^{\alpha\tau}(\Gamma_{\tau\mu\nu,\alpha} - \Gamma_{\tau\alpha\mu,\nu}) \\
&= g^{\alpha\tau}(\partial_{\alpha}\Gamma_{\tau\mu\nu} - \partial_{\nu}\Gamma_{\tau\alpha\mu}) \\
&= g^{\alpha\tau}(\partial_{\alpha}[\frac{1}{2}(h_{\tau\mu,\nu} + h_{\tau\nu,\mu} - h_{\mu\nu,\tau})] \\
&\quad - \partial_{\nu}[\frac{1}{2}(h_{\tau\alpha,\mu} + h_{\tau\mu,\alpha} - h_{\mu\alpha,\tau})]) \\
&= \frac{1}{2}g^{\alpha\tau}(h_{\tau\mu,\nu\alpha} + h_{\tau\nu,\mu\alpha} - h_{\mu\nu,\tau\alpha} - h_{\tau\mu,\alpha\nu} - h_{\tau\alpha,\mu\nu} + h_{\mu\alpha,\tau\nu})
\end{aligned} \tag{5.6}$$

The first and fourth terms will cancel, at which point the new form of the metric may be substituted, and terms not to first order in $h_{\mu\nu}$, can be dropped.

$$\Gamma^{\alpha}_{\mu\nu,\alpha} - \Gamma^{\alpha}_{\mu\alpha,\nu} = \frac{1}{2}\eta^{\alpha\tau}(h_{\tau\nu,\mu\alpha} - h_{\mu\nu,\tau\alpha} - h_{\tau\alpha,\mu\nu} + h_{\mu\alpha,\tau\nu}). \tag{5.7}$$

In linearized theory, the indices of $h_{\mu\nu}$ are raised and lowered using the flat spacetime metric $\eta_{\mu\nu}$, and as such this difference simplifies to

$$\begin{aligned}
\Gamma^{\alpha}_{\mu\nu,\alpha} - \Gamma^{\alpha}_{\mu\alpha,\nu} &= \frac{1}{2}(h^{\alpha}{}_{\nu,\mu\alpha} - h_{\mu\nu,\alpha}{}^{\alpha} - h_{\alpha}{}^{\alpha}{}_{,\mu\nu} + h_{\mu\alpha,\nu}{}^{\alpha}) \\
&= \frac{1}{2}(h^{\alpha}{}_{\nu,\mu\alpha} - h_{\mu\nu,\alpha}{}^{\alpha} - h_{,\mu\nu} + h_{\mu\alpha,\nu}{}^{\alpha})
\end{aligned} \tag{5.8}$$

Therefore,

$$\begin{aligned}
G_{\mu\nu} &= \frac{1}{2}(h^{\alpha}{}_{\nu,\mu\alpha} - h_{\mu\nu,\alpha}{}^{\alpha} - h_{,\mu\nu} + h_{\mu\alpha,\nu}{}^{\alpha}) \\
&\quad - \frac{1}{2}g_{\mu\nu}g^{\alpha\beta}(\frac{1}{2}(h^{\sigma}{}_{\beta,\alpha\sigma} - h_{\alpha\beta,\sigma}{}^{\sigma} - h_{,\alpha\beta} + h_{\alpha\sigma,\beta}{}^{\sigma})) \\
&= \frac{1}{2}(h^{\alpha}{}_{\nu,\mu\alpha} - h_{\mu\nu,\alpha}{}^{\alpha} - h_{,\mu\nu} + h_{\mu\alpha,\nu}{}^{\alpha}) \\
&\quad - \frac{1}{2}(\frac{1}{2})g_{\mu\nu}\ (h^{\sigma\alpha}{}_{,\alpha\sigma} - h_{,\sigma}{}^{\sigma} - h_{,\alpha}{}^{\alpha} + h_{\alpha\sigma,}{}^{\alpha\sigma})
\end{aligned} \tag{5.9}$$

It does not take much to show that $-h^{\alpha\sigma}{}_{,\alpha\sigma}andh_{\alpha\sigma}{}^{,\alpha\sigma}$ are the same. The same is also true for $h_{,\alpha}{}^{\alpha}$ and $h_{,\sigma}{}^{\sigma}$, trivially.

$$G_{\mu\nu} = \frac{1}{2}(h^{\alpha}{}_{\nu,\mu\alpha} - h_{\mu\nu,\alpha}{}^{\alpha} - h_{,\mu\nu} + h_{\mu\alpha,\nu}{}^{\alpha}) - \frac{1}{2}g_{\mu\nu}(h_{\alpha\sigma}{}^{,\alpha\sigma} - h_{,\alpha}{}^{\alpha}) \tag{5.10}$$

Finally, this equation must be linearized as before.

$$G_{\mu\nu} = \frac{1}{2}(h^{\alpha}{}_{\nu,\mu\alpha} - h_{\mu\nu,\alpha}{}^{\alpha} - h_{,\mu\nu} + h_{\mu\alpha,\nu}{}^{\alpha}) - \frac{1}{2}g_{\mu\nu}(h_{\alpha\sigma}{}^{,\alpha\sigma} - h_{,\alpha}{}^{\alpha}) \tag{5.11}$$

This is further simplified by defining $\bar{h}_{\mu\nu} = h_{\mu\nu} - \frac{1}{2}\eta_{\mu\nu}h$. Noting that the trace $\bar{h}$ is given by

$$\begin{aligned} \bar{h} &= \eta^{\mu\nu}\bar{h}_{\mu\nu} \\ &= \eta^{\mu\nu}(h_{\mu\nu} - \frac{1}{2}\eta_{\mu\nu}h) \\ &= h - \frac{1}{2}(4)h \\ &= -h \end{aligned} \tag{5.12}$$

According to this relation, the definition of $\bar{h}$ can be transformed to yield the relation $\bar{h}_{\mu\nu} = h_{\mu\nu} + \frac{1}{2}\eta_{\mu\nu}\bar{h}$. Thus it is found that

$$h_{\mu\nu} = \bar{h}_{\mu\nu} - \frac{1}{2}\eta_{\mu\nu}\bar{h} \tag{5.13}$$

These relations can be applied to the definition of $G_{\mu\nu}$ to yield the following.

$$\begin{aligned} G_{\mu\nu} &= \frac{1}{2}(\eta^{\alpha\tau}(\bar{h}_{\nu\tau} - \frac{1}{2}\eta_{\nu\tau}\bar{h})_{,\mu\alpha} - (\bar{h}_{\mu\nu} - \frac{1}{2}\eta_{\mu\nu}\bar{h})_{,\alpha}{}^{\alpha} + \bar{h}_{,\mu\nu} + (\bar{h}_{\mu\alpha} - \frac{1}{2}\eta_{\mu\alpha}\bar{h})_{,\nu}{}^{\alpha}) \\ &\quad - \frac{1}{2}\eta_{\mu\nu}((\bar{h}_{\alpha\sigma} - \frac{1}{2}\eta_{\alpha\sigma}\bar{h})^{,\alpha\sigma} + \bar{h}_{,\alpha}{}^{\alpha}) \\ &= \frac{1}{2}(\eta^{\alpha\tau}(\bar{h}_{\nu\tau} - \frac{1}{2}\eta_{\nu\tau}\bar{h})_{,\mu\alpha} - (\bar{h}_{\mu\nu} - \frac{1}{2}\eta_{\mu\nu}\bar{h})_{,\alpha}{}^{\alpha} + \bar{h}_{,\mu\nu} + (\bar{h}_{\mu\alpha} - \frac{1}{2}\eta_{\mu\alpha}\bar{h})_{,\nu}{}^{\alpha} \\ &\quad - \eta_{\mu\nu}(\bar{h}_{\alpha\sigma} - \frac{1}{2}\eta_{\alpha\sigma}\bar{h})^{,\alpha\sigma} - \eta_{\mu\nu}\bar{h}_{,\alpha}{}^{\alpha}) \\ &= \frac{1}{2}(\eta^{\alpha\tau}\bar{h}_{\nu\tau,\mu\alpha} - \frac{1}{2}\eta^{\alpha\tau}\eta_{\nu\tau}\bar{h}_{,\mu\alpha} - \bar{h}_{\mu\nu,\alpha}{}^{\alpha} + \frac{1}{2}\eta_{\mu\nu}\bar{h}_{,\alpha}{}^{\alpha} + \bar{h}_{,\mu\nu} \\ &\quad + \bar{h}_{\mu\alpha,\nu}{}^{\alpha} - \frac{1}{2}\eta_{\mu\alpha}\bar{h}_{,\nu}{}^{\alpha} - \eta_{\mu\nu}\bar{h}_{\alpha\sigma}{}^{,\alpha\sigma} + \frac{1}{2}\eta_{\mu\nu}\eta_{\alpha\sigma}\bar{h}^{,\alpha\sigma} - \eta_{\mu\nu}\bar{h}_{,\alpha}{}^{\alpha}) \end{aligned} \tag{5.14}$$

Raising and lowering indices appropriately, this can be further simplified.

$$\begin{aligned} G_{\mu\nu} &= \frac{1}{2}(\bar{h}_{\nu}{}^{\alpha}{}_{,\mu\alpha} - \frac{1}{2}\delta^{\alpha}_{\nu}\bar{h}_{,\mu\alpha} - \bar{h}_{\mu\nu,\alpha}{}^{\alpha} + \frac{1}{2}\eta_{\mu\nu}\bar{h}_{,\alpha}{}^{\alpha} + \bar{h}_{,\mu\nu} \\ &\quad + \bar{h}_{\mu\alpha,\nu}{}^{\alpha} - \frac{1}{2}\bar{h}_{,\nu\mu} - \eta_{\mu\nu}\bar{h}_{\alpha\sigma}{}^{,\alpha\sigma} + \frac{1}{2}\eta_{\mu\nu}\bar{h}_{,\alpha}{}^{\alpha} - \eta_{\mu\nu}\bar{h}_{,\alpha}{}^{\alpha}) \\ &= \frac{1}{2}(\bar{h}_{\nu}{}^{\alpha}{}_{,\mu\alpha} + (1 - \frac{1}{2} - \frac{1}{2})\bar{h}_{,\mu\nu} - \bar{h}_{\mu\nu,\alpha}{}^{\alpha} + (-1 + \frac{1}{2} + \frac{1}{2})\eta_{\mu\nu}\bar{h}_{,\alpha}{}^{\alpha} \\ &\quad + \bar{h}_{\mu\alpha,\nu}{}^{\alpha} - \eta_{\mu\nu}\bar{h}_{\alpha\sigma}{}^{,\alpha\sigma}) \\ &= \frac{1}{2}(\bar{h}_{\nu}{}^{\alpha}{}_{,\mu\alpha} - \bar{h}_{\mu\nu,\alpha}{}^{\alpha} + \bar{h}_{\mu\alpha,\nu}{}^{\alpha} - \eta_{\mu\nu}\bar{h}_{\alpha\sigma}{}^{,\alpha\sigma}). \end{aligned} \tag{5.15}$$

Then, using this the weak field equations are found to take the form,

$$16\kappa T_{\mu\nu} = \bar{h}_{\nu}{}^{\alpha}{}_{,\mu\alpha} - \bar{h}_{\mu\nu,\alpha}{}^{\alpha} + \bar{h}_{\mu\alpha,\nu}{}^{\alpha} - \eta_{\mu\nu}\bar{h}_{\alpha\sigma}{}^{,\alpha\sigma} \tag{5.16}$$

One important property of the weak field equations is that it is always possible to find a gauge transformation which forces $h^{\mu\alpha}{}_{,\alpha} = 0$ [19]. This gauge condition yields the linearized field equations,

$$16\kappa T_{\mu\nu} = -\bar{h}_{\mu\nu,\alpha}{}^{\alpha} \tag{5.17}$$

Before proceeding, it should be noted that the stress-energy tensor in Eq.(5.17) needs to also be considered in the weak field limit. It should not be surprising that the momentum and energy contained in a weak field situation will be small. For the goal at hand, only the vacuum equations $R_{\mu\nu} = 0$ will be needed, which is due to the condition $T_{\mu\nu} = 0$. Therefore, the linearized field equations in vacuum are simply

$$0 = \bar{h}_{\mu\nu,\alpha}{}^{\alpha} = \partial^{\alpha}\partial_{\alpha}\bar{h}_{\mu\nu}. \tag{5.18}$$

5.1.1 Gauge Transformations

A quick aside should be made on gauge transformations before proceeding, as this will be an important notion in how gravitational waves are chosen to be viewed.

It was mentioned in passing that "gauge conditions" could always be found to force the partial derivative of the metric perturbation to disappear. It should be noted this fact implies that the metric chosen to consider the weak-field previously is not in fact unique!

A gauge transformation can be thought of as an infinitesimal coordinate transformation [19] which leaves the system and its observables apparently unchanged. One could always change lorentz frames locally, but because the metric is not truly local, even changing coordinate systems. nearby will result in the perturbations taking a different form in the new frame. To consider this a bit deeper, a bit more precision would be nice.

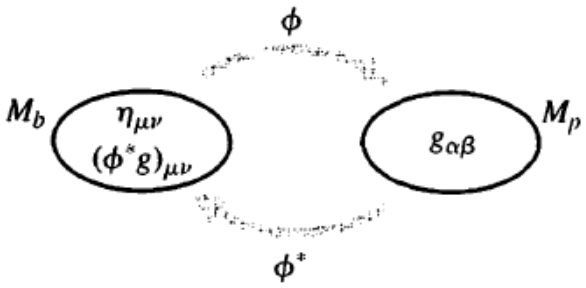

Fig. 4.
The pullback of the metric to a background spacetime

Suppose then that there are two spacetimes, M_b and M_p. Let M_b be the spacetime with the background metric, $\eta\mu\nu$, and equip this manifold with coordinates x^μ. On the other hand, let M_p describe the spacetime containing the full metric, $g_{\alpha\beta}$, which, after constructing the curvature tensors and connections, is a valid solution to Einstein's equations. Let this physical spacetime be armed with the coordinates y^α. Suppose there exists a diffeomorphism between these two spacetimes, ϕ. Then, the transition which we modeled in the previous section through the linearization of einstein's equations is in fact the diffeomorphism $\phi : M_p \mapsto M_b$. This, in general, permits the mapping of tensors between these two coordinate systems. In particular, the interest here is in retaining the metric tensor, and thus the validity of the constructions of Einstein's equations, as these tensorial objects are mapped from M_p to

M_b (Fig. 4.

In particular, it would be nice to redefine the metric $g_{\alpha\beta}$ on the background spacetime by taking the **pullback** of the metric $(\phi^* g)_{\mu\nu} \in M_b$. Doing such will in fact retain the Einstein equation solvability of the metric, due to the fact that diffeomorphism require an inverse map to be properly defined. In doing so, one can then have some well defined notion of the physical perturbation in the background spacetime by the relation

$$h_{\mu\nu} = (\phi^* g)_{\mu\nu} - \eta_{\mu\nu} \tag{5.19}$$

With this in mind, it will be in fact necessary to restrict our consideration above strictly to those where $h_{\mu\nu}$ is small, which was enforced earlier but had not yet been for the purpose hand. By this requirement, a space has been created on which the linear theory can be analyzed. Furthermore, the relation created above, along with the smallness condition on $h_{\mu\nu}$, ensures that it will be a solution to the linearized equations on the background spacetime. This still leaves a number of diffeomorphisms, i.e. solutions to the system of equations, as there are plenty of perturbations that can exist below some arbitrary smallness threshold. Thus, it is necessary to examine further and impose gauge conditions, which in essence allows for a unique coordinate system for the perturbations to be viewed from.

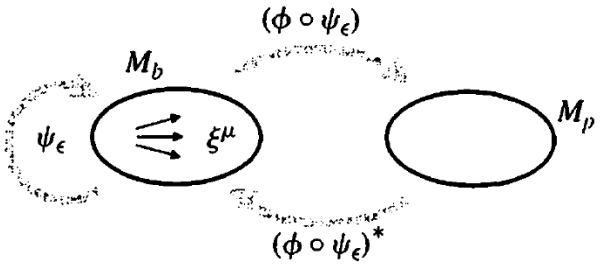

Fig. 5.
A mapping between the full metric and the coordinate transformations allowing for the proper conditions on the perturbation.[1]

Consider a vector field $\chi^\mu(x) \in M_b$ which generates a single parameter collection

of diffeomorphisms, ψ_ϵ, from M_b back onto itself. If ϕ is a diffeomorphism which yields a sufficiently small pertubation, as described above, then for some sufficiently small ϵ, $(\phi \circ \psi_\epsilon)$ will also be a diffeomorphism between M_b and M_p that generates a sufficiently small perturbation, though it will take on some different value. Then, in turn, define a collection of perturbations defined by this diffeomorphism as

$$h^{(\epsilon)}_{\mu\nu} = (\phi \circ \psi_\epsilon)^*(g)_{\mu\nu} - \eta_{\mu\nu} = [\psi^*_\epsilon(\phi^*(g))]_{\mu\nu} - \eta_{\mu\nu} \tag{5.20}$$

It can then be shown by substitution of the previously defined metric pullback that this equation simplifies down into the form

$$h^{(\epsilon)}_{\mu\nu} = h_{\mu\nu} + \epsilon\mathcal{L}_\epsilon\eta_{\mu\nu}, \tag{5.21}$$

where $\mathcal{L}_\epsilon$ is the Lie derivative discussed in chapter 3. It can be shown, see [1], that the Lie derivative of the metric in the direction of some vector field χ_μ can be written as $\mathcal{L}_\chi g_{\mu\nu} = 2\nabla_{(\mu}\epsilon_{\nu)}$. This will carry over to the background metric, $\eta_{\mu\nu}$, at hand. Furthermore, in this case the covariant derivative must be translated back to a partial derivative, and the perturbation becomes

$$h^{(\epsilon)}_{\mu\nu} = h_{\mu\nu} + 2\epsilon\partial_{(\mu}\epsilon_{\nu)}. \tag{5.22}$$

This gives the gauge transformation, which represents "the change in the perturbation under an infinitesimal diffeomorphism"[1]. By utilizing this gauge transformation, one can, without loss of generality in our previous derivation, change the coordinate system without losing physical meaning. This is analogous to the invariance of the Lorentz gauge described earlier for electromagnetism in special relativity, which left the field strength tensor invariant. For the gauge transformation of linearized theory, as described here for weak field situations of general relativity, it can be shown that the resulting invariant property is the Riemannian curvature (and thus the physical

spacetime),

$$\delta R^{\alpha}{}_{\beta\mu\nu} = 0. \tag{5.23}$$

5.2 The Transverse Traceless Gauge

The particular gauge transformation for the observation of gravitational waves is that into the transverse traceless (TT) gauge. This will actually be in addition to the gauge conditions imposed during the linear theory derivation. In order to see the necessity of this, consider the linearized field equations which were found previously,

$$0 = \bar{h}_{\mu\nu,\alpha}{}^{\alpha} = \partial^{\alpha}\partial_{\alpha}\bar{h}_{\mu\nu}. \tag{5.24}$$

The simplest solution to these field equations is the plane wave solution with constant amplitude $A_{\mu\nu}$ and wave vector k_{α}

$$\bar{h}_{\mu\nu} = Re[A_{\mu\nu}exp(ik_{\alpha}x^{\alpha})] \tag{5.25}$$

The amplitude and wave vectors are restricted by the conditions that the wave vector is null, i.e., $k_{\alpha}k^{\alpha} = 0$, and that it is orthogonal to the amplitude, i.e., $A_{\mu\nu}k^{\nu} = 0$. The time component of the wave four vector is the frequency, ω, of the wave. To ensure the vector is null, the frequency must be related to the spatial components by

$$\omega^2 = \delta^i_j k_i k^j. \tag{5.26}$$

Furthermore, this wave will propogate with the speed of light. Note that by the symmetry of the metric perturbations, it must be the case that $A_{\mu\nu}$ is also symmetric. Therefore, in 4 dimensions it will have 10 independent components. Furthermore, by the orthogonality condition imposed above between the wave vector and the amplitude, the independence of 4 more components is lost, leaving 6 independent components.

It will not be shown in this thesis, but it can be taken for granted that the solutions to the nonlinearized field equations of general relativity have only 2 independent components. In linearizing the field equations, one should expect to find the same number of independent components, which is clearly not the case.

Furthermore, it should also be noted that one could introduce an arbitrary plane-wave vector field which generates a gauge transformation. This would arbitrarily change four of the independent components of $A_{\mu\nu}$, which would eliminate the need for discussing gauge transformations at all earlier. To remedy this, one can in fact find a specific gauge to work in- the *transverse traceless gauge*.

Choose a global reference frame with four-velocity u^α, which is appropriate for the near vacuum conditions being considered. Then, one can impose the conditions that

$$A_{\mu\nu}u^\nu = 0; \qquad A^\mu{}_\mu = 0. \tag{5.27}$$

These two conditions together eliminate 4 more independent components, leaving a solution in which the amplitude has 2 independent components, as desired. The gauge is thus fixed by the 8 constraints $0 = A_{\mu\nu}u^\nu = A^\mu{}_\mu = A_{\mu\nu}k^\nu$, and the two independent components physically manifest as the degrees of freedom of the plane wave. This latter statement will be further examined in the next section. For now, turn attention to the constraints on the amplitude of the plane wave. It would be better to instead examine this situation from a static Lorentz frame, i.e., only $u^0 = 1$ is nonzero. Then, these properties are

1. Only spatial components are nonzero: $h_{\mu 0} = 0$
2. Spatial components divergence free: $\partial_j h_{jk} = 0$
3. Spatial components are trace-free: $h^k{}_k = 0$

Therefore, the metric perturbation components have the properties of a TT tensor. The term transverse means that this tensor is both purely spatial and divergence free, i.e., wave face is orthogonal to direction of propagation. Any symmetric tensor satisfying these constraints is known as a *transverse-traceless tensor*, for the reasons which should be clear. Another way of saying all this is that the TT gauge is that in which $h_{\mu\nu}$ reduces to a TT tensor. For calculations done in this gauge, the metric is referred to notationally by $h^{TT}_{\mu\nu}$.

Before proceeding, consider how some of the key geometric components behave. The christoffel connections themselves will disappear on the space, since it globally lorentz, but will take the form they had in the EQ. when found in derivatives. Furthermore, recall the expression for the curvature which was found in the derivation of the bianchi identity,

$$R_{\alpha\beta\mu\nu} = \frac{1}{2}[g_{\alpha\nu,\beta\mu} + g_{\beta\mu,\alpha\nu} - g_{\alpha\mu,\beta\nu} - g_{\beta\nu,\alpha\mu}] \tag{5.28}$$

Then, this can be generally linearized by making the substitution for the metric in the TT gauge, so that

$$R_{\alpha\beta\mu\nu} = \frac{1}{2}[h^{TT}_{\nu\alpha,\beta\mu} - h^{TT}_{\beta\nu,\alpha\mu} - h^{TT}_{\mu\alpha,\beta\nu} + h^{TT}_{\beta\mu,\alpha\nu}] \tag{5.29}$$

It is important to note that only time derivatives of quantities will remain. As such, it can be seen that the index pairings on each term must be $(1)\beta = 0, \mu = 0$; (2) $\rho = 0, \mu = 0$; $(3)\beta = 0, \nu = 0$; and $(4)\rho = 0, \nu = 0$; respectively. Furthermore, only the spatial components of the perturbation will be retained in this gauge. This gives a number of underlying conditions.

Then, due to the high number of symmetries in the Riemann curvature tensor, one can simplify this expression greatly by considering it in cases. In fact, it can be seen that the only nonzero components are those in which one of the four cases above

applies. To simplify this consider first the case $\alpha = 0$, where the above becomes

$$\begin{aligned} R_{0\beta\mu\nu} &= \frac{1}{2}[h^{TT}_{\nu 0,\beta\mu} - h^{TT}_{\beta\nu,0\mu} - h^{TT}_{\mu 0,\beta\nu} + h^{TT}_{\beta\mu,0\nu}] \\ &= \frac{1}{2}\eta^{00}[-h^{TT}_{\beta\nu,0\mu} + h^{TT}_{\beta\mu,0\nu}] \end{aligned} \tag{5.30}$$

Consider then the indices μ and ν. It is important to note that only one of these terms will remain at the same time, as if both these indices are 0, both terms will have non spatial perturbations- which are 0 in the gauge. Again, by the symmetries of the curvature tensor, only one of these cases need to be considered, as they will just be additive inverses of one another. Then, this expression can be generalized by fixing further $\nu = 0$ and forcing μ and β to be purely spatial indices, one finds

$$R_{0jk0} = \frac{1}{2}[-h^{TT}_{j0,0k} + h^{TT}_{jk,00}] = \frac{1}{2}h^{TT}_{jk,00}. \tag{5.31}$$

Furthermore, with the curvature symmetries in mind, it should be clear that this solution can be in turn generalized into the solutions $R_{0jk0} = \frac{1}{2}h^{TT}_{jk,00} = -R_{0jk0} = R_{0k0j} =$

In turn, the case where α is some spatial component should also be considered. This leaves the curvature tensor in the form

$$\begin{aligned} R_{j\beta\mu\nu} &= \frac{1}{2}[h^{TT}_{\nu j,\beta\mu} - h^{TT}_{\beta\nu,j\mu} - h^{TT}_{\mu j,\beta\nu} + h^{TT}_{\beta\mu,j\nu}] \\ &= \frac{1}{2}[h^{TT}_{\nu j,\beta\mu} - h^{TT}_{\mu j,\beta\nu}], \end{aligned} \tag{5.32}$$

Again, due to the divergence-free property of the perturbation, the two divergence terms (second and fourth) will disappear by default. It should further be noted that this is an almost identical pattern to the case $\alpha = 0$, as one should expect from the gauge conditions and the symmetries arising from the curvature tensor. Then, it can be seen that one must again either choose μ or ν to be the index k, but not both, as this would force both terms to disappear. It will be chosen here that $\nu = k$, and thus

it must be the case $\mu = 0$. Finally since only time derivatives should be popping up, it should be clear the only possible value for β is its temporal index, $\beta = 0$. Thus,

$$\begin{aligned} R_{j00k} &= \frac{1}{2}[h^{TT}_{kj,00} - h^{TT}_{0j,0k}] \\ &= \frac{1}{2}h^{TT}_{kj,00} \end{aligned} \tag{5.33}$$

Therefore, one in fact finds the form of the curvature tensor in both cases of α leads to the same result, due to the symmetries of the Riemann curvature tensor. Thus, the nonzero components can simply be written in general as

$$R_{0jk0} = \frac{1}{2}h^{TT}_{jk,00} = \frac{1}{2}\frac{\partial^2}{\partial t^2}h^{TT}_{jk}. \tag{5.34}$$

5.3 Gravitational Waves

Only pure wave solutions can be reduced into the TT gauge, not just general solutions to the linear equations. As per usual, it would be nice to generalize this specific solution to a more general gravitational wave. Luckily, just as in electromagnetism, any gravitational wave can be expressed as some linear combination of these plane waves. If one applies the gauge above to each plane wave in the superposition, the arbitrary wave will also satisfy these conditions, since the gauge conditions are all linear in $h_{\mu\nu}$. This being the case only the spatial components of the arbitrary wave are nonzero also. As such, notice that the 10 field equations in $0 = \partial^\alpha \partial_\alpha h_{\mu\nu}$ reduce to only 6 equations.

$$0 = \partial^\alpha \partial_\alpha h^{TT}_{jk}. \tag{5.35}$$

Then, the obvious question to ask is what influence do gravitational waves have on matter and spacetime geometry? To answer this question, consider the geodesic deviation of two particles as a gravitational wave passes by. Consider particle A

from the reference frame described previously- the comoving frame in which the only nonzero component of the spacetime position is given by $x^0 = t$. This gives the same nonzero four-velocity component of $u^0 = 1$. It should be noted that in the literature, it is often the case that this "proper reference frame" is denoted with a hat on its components, as $x^{\hat{\mu}}$. Then, recall that the geodesic deviation of a four vector was found to take the form

$$A^\mu = T^\nu S^\rho R^\mu{}_{\beta\nu\rho} T^\beta. \tag{5.36}$$

For the current consideration, the basis vector $\mathbf{T}$ will be the four-velocity of the comoving frame. Since there is only one nonzero component of the four-velocity, the above system of equations reduces to

$$\begin{aligned} A^\mu &= u^0 S^\rho R^\mu{}_{00\rho} u^0 \\ &= u^0 S^\rho \eta^{\mu\sigma} R_{\sigma 00\rho} u^0. \end{aligned} \tag{5.37}$$

Then consider the coordinate system which is at play here. The frame has both been described as comoving with particle A and globally Lorentz. It should then be noted that one can always find a TT gauge transformation that moves with this coordinate system, to a good approximation. Thus, the previously derived expression for the curvature can be used. Furthermore, from the previous consideration of the curvature in the TT gauge, it should be clear that the only nonzero cases of the Riemann curvature tensor are those in which the indices σ and ρ are spatial indices. furthermore, imposing the diagonality of the background metric, this expression

simplifies to

$$\begin{aligned} A^j &= u^0 S^k \eta^{jm} R_{m00k} u^0 \\ &= S^k \eta^{jm} R_{m00k} \\ &= \frac{1}{2} S^k \eta^{jm} h^{TT}_{mk,00} \end{aligned} \tag{5.38}$$

Furthermore, the separation vector can just be described by the position of the other particle, which can be referred to as particle B. Only the spatial coordinates will be needed, and so these will be written x^j_B. In general, the vector components A^j reference the relative acceleration of the two geodesics, so that this should be the second derivative of the separation vector with respect to the absolute time. However, in a weak field situation with low enough energy, the absolute time can be approximated as the relative time, t. In the current situation it can be assumed that the mixed tensor components of the metric perturbation are identical to those of the lower indices, since they are both spatial. Then, it is assumed that this raising of indices with the metric does nothing. Most references will keep these spatial indices lowered from this point on and state that all identical indices can be summed over regardless of index placement. Therefore, the above equation is rewritten as

$$\frac{d^2 x^j_B}{dt^2} = \frac{1}{2} h^{TT}_{jk,00}(x^k_B). \tag{5.39}$$

Then, one can enforce the further conditions that the particles are at rest before the wave perturbs the local space. In doing so, it is possible to integrate the equations above to get

$$x^j_B(\tau) = x^k_{B(0)}(\delta_{jk} + \frac{1}{2} h^{TT}_{jk}), \tag{5.40}$$

where the term in parentheses is evaluated at the position of particle A. This gives the oscillations of particle B's location relative to A, as the wave passes by. Consider in

particular a plane wave, it is important to note that if the separation vector is parallel to the direction of the wave, then the particles are unaffected. This in other words says that gravitational waves only oscillate separations which are transverse to its direction. Thus this gauge property is not only an abstract naming, but physically appropriate.

5.3.1 Polarization & Properties

This gives an okay picture of how two particles are affected but what does this say about how the waves affect local spacetime? To consider this, examine the gravitational plane wave propagating along the z-axis as it hits a ring of particles lying in the xy-plane, so that the wave vector can be written as $k_\alpha = (\omega, 0, 0, \omega)$. Then, recall the solution that gave the plane gravitational wave, and substtitute this into the exponential as,

$$\begin{aligned} \bar{h}_{\mu\nu} &= Re[A_{\mu\nu} \exp(ik_\alpha x^\alpha)] \\ &= Re[A_{\mu\nu} \exp(i(k_0 x^0 - k_3 x^3))] \\ &= Re[A_{\mu\nu} \exp(i\omega(t - z))] \end{aligned} \tag{5.41}$$

It can be explicitly shown that the conditions imposed in the tranverse traceless gauge along with the orientation of the setup described here leads to the gravitational plane wave amplitude in matrix form as

$$(A_{\mu\nu}) = \begin{pmatrix} 0 & 0 & 0 & 0 \\ 0 & A_+ & A_\times & 0 \\ 0 & A_\times & -A_+ & 0 \\ 0 & 0 & 0 & 0 \end{pmatrix} \tag{5.42}$$

These components in combination with the frequency ω are capable of giving a

complete picture of the wave behavior. This is because the only independent, nonzero perturbations are now

1. $h_{11}^{TT} = -h_{22}^{TT} = Re[A_+ \exp(i\omega(t-z))]$

2. $h_{12}^{TT} = h_{21}^{TT} = Re[A_\times \exp(i\omega(t-z))]$

A generalized integrated equation of motion was obtained previously (Eq. 5.40), and now the corresponding wave solutions can be substituted in for the two components, $x_N^1(\tau)$, $x_N^2(\tau)$. This yields the oscillations of the Nth particle of the ring

$$\begin{aligned} x_N^1(\tau) &= x_{N(0)}^k(\delta_{1k} + \frac{1}{2}h_{1k}^{TT}) \\ &= x_{N(0)}^1(\delta_{11} + \frac{1}{2}h_{11}^{TT}) + x_{N(0)}^2(\delta_{12} + \frac{1}{2}h_{12}^{TT}) \\ &= x_{N(0)}^1(1 + \frac{1}{2}Re[A_+ \exp(i\omega(t-z))]) \\ &\quad + x_{N(0)}^2\frac{1}{2}Re[A_\times \exp(i\omega(t-z))] \end{aligned} \tag{5.43}$$

and

$$\begin{aligned} x_N^2(\tau) &= x_{N(0)}^k(\delta_{2k} + \frac{1}{2}h_{2k}^{TT}) \\ &= x_{N(0)}^1(\delta_{21} + \frac{1}{2}h_{21}^{TT}) + x_{N(0)}^2(\delta_{22} + \frac{1}{2}h_{22}^{TT}) \\ &= x_{N(0)}^1\frac{1}{2}Re[A_\times \exp(i\omega(t-z))] \\ &\quad + x_{N(0)}^2(1 - \frac{1}{2}Re[A_+ \exp(i\omega(t-z))]). \end{aligned} \tag{5.44}$$

Any gravitational wave can be expressed as a linear combination of these coefficients. It should be noted here that in order to consider a ring of particles, as mentioned, it will ultimately be beneficial to create a characterization to refer back to. In particular, it is nice to draw parallels to the electromagnetic wave in order to resolve some of behaviors of this wave. As such, it is more accurate to say that there exists two independent polarizations of the gravitational wave solutions corresponding to the two independent components A_+ and $A_\times$.

Note that the work being considered in this chapter has done calculations almost exclusively in some form of component notation. However nice this decision has made the calculations, a moment should be taken to consider the linear polarization basis tensors. Notice that by default, the tensor amplitude describing the gravitational wave differs from the vector description of the amplitude of an EM wave in its nature, being type $\binom{0}{2}$ for gravity, and $\binom{0}{1}$ for EM.

In EM, one talks about how a light wave with some polarization vector hits a charged particle at a point in space, resulting in oscillations along a single axis, parallel to the electric field of the wave. However, when speaking of gravitational waves, the tensorial nature leads to the effects being dependent also on the orientation of their separation. This applies specifically to the plane orthogonal to the direction of the wave's propagation, since it has already been seen that

It will become more clear once the position of the particles in a ring are evaluated for the individual, independent components, but for now it will suffice to simply give the definition of the linearly-polarized basis tensors,

$$\mathbf{e}_+ = \mathbf{e}_x \otimes \mathbf{e}_x - \mathbf{e}_y \otimes \mathbf{e}_y, \tag{5.45}$$

and

$$\mathbf{e}_+ = \mathbf{e}_x \otimes \mathbf{e}_y + \mathbf{e}_y \otimes \mathbf{e}_x. \tag{5.46}$$

Then, suppose $A_\times = 0$, so that only the terms with components A_+ remain in the solution. Then, the component solutions above behave as

$$x^1_N(\tau) = x^1_{N(0)}(1 + \frac{1}{2}Re[A_+ \exp(i\omega(t-z))]) \tag{5.47}$$

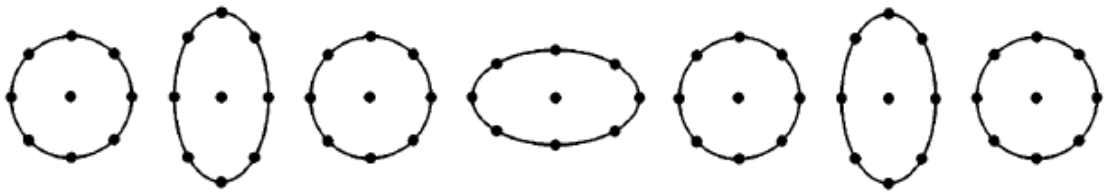

Fig. 6.
The phases of a ring of particles centered on a plus polarized gravitational wave propagating into the page.[1]

and

$$x^2_N(\tau) = x^2_{N(0)}(1 - \frac{1}{2}Re[A_+ \exp(i\omega(t-z))]). \tag{5.48}$$

This gives the first of the linearly polarized states. It can be shown that a ring of 8 particles around the origin will respond to the passing of a linearized gravitational wave by jittering back and forth in a "+" shape. More descriptively particles along the x axis move away from the origin along the x axis, while particles along the y axis move toward the origin along the y axis. The complex exponential in the wave form then ensures that each of these particles bounces back and forth like this. Note, this is in accordance with the the basis tensor described above: particles with a nonzero position component in the direction of the basis vector $\mathbf{e}_x$ is moved in direction which the basis vector $\mathbf{e}_x$ is oriented, and also for the $\mathbf{e}_y$ direction. These oscillations are then shown explicitly in Fig. 6, below.

Then, suppose that $A_+ = 0$ instead in the general component equations. In such a case, it can be seen that the components of the perturbed particles simplify to

$$x^1_N(\tau) = x^1_{N(0)} + \frac{1}{2}x^2_{N(0)}Re[A_\times \exp(i\omega(t-z))] \tag{5.49}$$

and

$$x^2_N(\tau) = \frac{1}{2}x^1_{N(0)}Re[A_\times \exp(i\omega(t-z))] + x^2_{N(0)} \tag{5.50}$$

Fig. 7.
The phases of a ring of particles centered on a times polarized gravitational wave propagating into the page.

In this case, the gravitational wave creates the same "+" pattern in the oscillations of the particles, but as if it had been rotated at an angle of 45 deg, which would instead resemble the shape "×" if the different deformations are imposed on top of one another. The basis tensors in this case should also make appropriate sense now: the relative position of particles with a nonzero (positive) $\mathbf{e}_x$ component are moved in the positive $\mathbf{e}_y$ direction, and vise versa. This leads to the deformation of the ring shown in Figure 7.

Then, it is also important to consider the circularly polarized states. It should be noted that, again, in analogy with electromagnetism, these "circular" waves are the possibly linear combinations of the polarization state tensors. The equations of motion for these equations are those given above for simultaneously nonzero A_+ and $A_\times$. For electromagnetism, these took the form of the left and right circular polarizations,

$$\hat{e}_R = \frac{1}{\sqrt{2}}(\hat{e}_x + i\hat{e}_y); \qquad \hat{e}_L = \frac{1}{\sqrt{2}}(\hat{e}_x - i\hat{e}_y).$$

It should be noted that each of the particles in the ring (and otherwise nearby) will themselves be moved around in small circles, and not rotate entirely around the origin of the coordinate system. This is better seen by the red loop superimposed over particle in the center of the ring.

5.4 Gravitational Wave Energy

To appropriately consider the energy of gravitational waves, one must step outside the realm of linearized theory. The shortwave approximation is beyond the scope of this thesis, but it is encouraged that the reader refer to [19] for more information on this subject if a deeper understanding is desired. It should be noted briefly that the energy of a gravitational field in consideration can not be localized and evaluated with any sort of meaning.

The simplest explanation for this is that the equivalence principle permits one to isolate a region in spacetime in which one cannot detect gravitational fields. This clearly implies an inability to measure any sort of local stress energy tensor, as how would one notice it? This is not to say that it does not exist, but that the equivalence principle forces the curvature here to appear flat, and the laws of physics behave accordingly- as if there were no gravitational field. Similarly, this applies to gravitational waves- one can not localize the energy contained in any one part of a wave. However in asymptotically flat spaces away from a source, volume and surface integrals can be constructed in a manner that allows one to calculate the energy flux over some region. The same can be done for an arbitrary gravitational wave in asymptotically flat space. In this case, one may describe an effective stress energy tensor over some macroscopic region, in the tranverse traceless gauge,

$$T_{\mu\nu}^{(GW)} = \frac{1}{32\pi}\langle h_{jk,\mu}^{TT} h_{jk,\nu}^{TT}\rangle. \tag{5.51}$$

This is gauge invariant and divergence free in vacuum. One important property of the stress energy tensor of a gravitational wave is that it can be shown to contribute to the large scale background curvature- an effect that is overlooked in the linearized

theory derivation. These are related according to

$$G^{(B)}_{\mu\nu} = 8\pi(T^{(GW)}_{\mu\nu} + T^{(matter)}_{\mu\nu} + T^{(otherfields)}_{\mu\nu}) \tag{5.52}$$

This, in turn, cannot be easily put back into the field equations to view the contribution to the large scale curvature, as it leads to the possibility of over counting the contributions of the gravitational wave. The nonzero components of the stress energy of a general linear combination of the possible plane wave, $h_{\mu\nu} = Re[(A_+(e_+)_{\mu\nu} + A_\times(e_\times)_{\mu\nu})\exp(i\omega(t-z))]$ can be shown to take the following form

$$T^{(GW)}_{tt} = T^{(GW)}_{zz} = -T^{(GW)}_{tz} = \frac{1}{2}\omega^2(|A_+|^2 + |A_\times|^2). \tag{5.53}$$

Then, the background radius of the curvature $\mathcal{R}$ is related to the magnitude of the components of the background Riemann tensor by $\frac{1}{\mathcal{R}^2} \sim R^{(B)}_{\alpha\beta\gamma\mu}$. In turn it can be shown that the amplitude of a gravitational wave, $\mathcal{A}$, is related to its average wavelength λ, and the background curvature radius as

$$\mathcal{A} \lesssim \frac{\lambda}{\mathcal{R}} \tag{5.54}$$

This forces the amplitude to be small relative to this scaled wavelength. Now it should be noted that the if the wavelengths are comparable to the magnitude of the curvature components, too much leeway will be given to the amplitude term. In fact this leads to the metric perturbation being significant relative to the background curvature, which is in stark contradiction to the whole linearized theory definition in the first place. In such a case, the concept of a gravitational wave falls apart, and one is once again looking at a generally curved space. Therefore, this condition must be met in order for gravitational waves to be witnessed in the first place.

5.4.1 Multipole Expansion

This means we will typically be thinking about the perturbations from radiation emanated far away its source. In classical theory, if one has an arbitrary moment density describing a source object, such that the potential around the field has an angular dependence. Then, one can describe the potential sufficiently far away from the source using a multipole series expansion of Green's function. If done in an spherical coordinate, this splits the contributions to a field into terms made up of spherical harmonics contributions. Since GR is inherently classical, it can in turn be shown that, from asymptotically flat regions far away, the gravitational field produced by a source is

$$h_{ij} = \frac{2G}{r}\frac{d^2}{dt^2}I_{ij}(t-r) \tag{5.55}$$

This is known as the quadrupole formula, where I_{ij} is a tensor evaluated at t-r. In electromagnetic theory, one makes particular use of the dipole moment to describe variations in the internal polarization states of a material. In this context, the dipole moment physically describes the motion of the center of charge density in response to an existing EM field. However, one does not get this term for gravitational fields, because oscillations of an isolated object's center of mass density violate the conservation of energy (i.e., there would need to be some force outside of the isolated system which is conserving the energy changes resulting from the oscillation).

However, the higher order terms, which each describe specific levels of the mass density's dynamics, are still fair game. In particular, for gravity, the reduced quadrupole moment, I_{ij}, which is the general quadrupole moment tensor given in a

trace free form,

$$I_{jk}(t) = \int \rho(x_j x_k - \frac{1}{3} r^2 \delta_{jk}) d^3x$$

is the first nonvanishing moment of the multipole expansion. As can be seen in the preceding term, if I_{ij} is time-dependent, it is responsible for producing gravitational radiation. Because of the nature of the multipole expansion, quadrupole terms are smaller than dipole terms. As such, gravitational radiation is going to be generally much weaker than the electromagnetic radiation. This can be physically explained by the fact that gravitational waves are produced in the bulk motion of objects, while any accelerating charged particle can produce EM waves. Furthermore, it should be noted that this quadrupole term is not the only one which can arise in the multipole expansion. Certainly, higher order terms are responsible for gravitational radiation as well, and they can arise as a consequence of asymmetric mass distribution, such as with GW190412 [21] and GW190814 [17]. The radiation from the individual multipole terms of quadrupole or higher will take on quite different plane fronts and, in general, will be much weaker than the quadrupole contributions.

5.5 Sources

It is shown in [18] that one can derive the amplitudes of gravitational waves emitted from a variety of sources in terms of this quadrupole tensor. As mentioned, in order to "feel" the effects of a passing gravitational wave, one must be appreciably far from the source. If one is too close, the spacetime is heavily disrupted, on length scales much larger than that of a detector. As such, we wish to briefly discuss the transformation to a TT gauge in which, appreciably far from the source, one gets a nice form of the wave characteristics.

Radiation from a binary system is emitted radially, and so its normal unit vector

describing the direction of its travel can be written as $n^j = x^j/r$ (r is the spherical radial coordinate from some central observation point of the source). Then, at some point in space we wish to define a TT gauge that has a plane transverse to this direction of travel- particularly a wave that is travelling along the z-axis of the TT gauge transformed frame. Then the waveform restrictions imposed previously can be expanded to include $h_{\mu j}n^j = 0$, and then the circularly polarized waveform from a binary system can be shown have nonzero components

$$h_{11} = -h_{22} = -2ml_0^2\omega^2\frac{e^{i\omega(r-t)}}{r} \tag{5.56}$$

and

$$h_{12} = h_{21} = -2iml_0^2\omega^2\frac{e^{i\omega(r-t)}}{r} \tag{5.57}$$

As usual, the real part of these functions are taken to get the appropriate strain at some time t. This is a highly idealized case, in which m describes the mass of a single component of the binary system, and thus the $2m$ factor accounts for the total mass. Furthermore, l_0 describes the distance between the two mass components and ω describes the angular frequency of the orbital. Nonetheless, these are considered to be good approximations for systems in newtonian gravitational fields. The details of the full transformation are given in [18], though it should be noted that this method omits higher order multipoles.

Furthermore, it should be noted that the lifetime of a GW emitted by an inspiralling binary system is relatively short, described by the relation

$$\tau_{GW} = 2.43(\frac{M}{M_\odot})^{-5/3}(\frac{f}{100Hz})^{-8/3}\text{sec} \tag{5.58}$$

for systems describing equally massive components.

As the massive bodies spiral toward one another, the frequency of the orbital

will increase dramatically, before dying off, producing a "chirp". This can be seen to correspond to the masses involved in the system, and so we find that one can generally describe the mass of an object in a binary system by its orbital frequency, $f = \frac{\omega}{2\pi}$, and the life time of it's inspiral. We will find that this the frequency and approximate life time are generally measurable in the modern detector setup. In systems with larger mass asymmetry, where there is more variation of the internal mass-energy density, a more diverse equation will have to be applied to account for things like its eccentricity and the individual behavior of the mass components.

As is the case with EM waves, these waves can be classified in terms of their expected frequencies, corresponding to specific mass-energy density of the source. This will make it easier to visualize which systems will be observable by which detectors later on. While there are not necessarily well-defined analogs to infrared and ultraviolet light in the categorization of the gravitational wave spectrum, there are 4 particular frequency bands of interest in the gravitational wave astronomy[22], which are as follows.

1. **Extremely Low Frequency (ELF) Band**: $10^{-15} - 10^{-18}$ Hz

   This covers gravitational waves that are emitted by primordial quantum fluctuations in the gravitational field. These aim to be detected by their cosmic microwave background imprint.

2. **Very Low Frequency (VLF) Band**: $10^{-7} - 10^{-9}$ Hz

   In this band, gravitational waves are expected to be emitted by processes from the early universe and supermassive BBHs

3. **Low Frequency (LF) Band**: $10^{-4} - 1$ Hz

   This is expected to be able to observe a wide bandwidth range of frequency, in which we expect (a) GWs from supermassive BBHs in the mass range $10^5 - 10^7 M_\odot$;

(b) the early inspiral of smaller objects (such as BHs, NSs, and white dwarfs (WDs) eventual merge with massive black holes, along with (c) even earlier descriptions of the inspirals of binary compact systems than are available from ground systems.

4. **High Frequency (HF) Band**: $1 - 10^4$ Hz

   This includes GWs emitted in the final moments of the merger of binary compact objects, and maybe a few brief seconds of the inspiral just before, depending on the system. At full sensitivity, these are expected to detect some spinning NSs.

Ground based detectors will never achieve a sensitivity outside of the HF band. Thus, in the context of the advanced state LIGO/VIRGO observatories, the most important situations to consider will usually be those of BBHs, BNSs, and NSBHs. In the most recent publication from the LIGO/VIRGO collaboration, the majority of results fall into these categorizations[15].

Black holes can, in theory, take on any given mass above 0, up to the limit of the total matter of the universe. However, this is a somewhat impractical search range to impose on the masses. In particular, we want to consider stellar mass black holes, which at one point were expected to fall in the general range of about $M_{BH} = 2.5 - 20M_{\odot}$ [23]. Similiarly, NSs could be expected to fall in the range from $1.2 - 3.0M_{\odot}$, though the probabilities fall off significantly above $2.0M_{\odot}$. In some early calculations of expected intensity values of GWs observed from binary systems, the masses were often approximated near $m_{NS} \approx 1.4M_{\odot}$ and $m_{BH} \approx 10M_{\odot}$ [22]. However, since observation of the first GW, we have detected systems that appear to have high confidence mass probabilities near $M_{BH} = 30M_{\odot}$. In consideration of this, calculations determined the expected stellar mass black hole upper limit should be adjusted to around $40M_{\odot}$ [24], which was the general search range for the O3A detection run [17].

CHAPTER 6

GRAVITATIONAL WAVE DETECTORS

We now wish to consider gravitational waves as they are observed by an experimenter here on earth. The entire discussion presented thus far has been entirely in terms of the classical theory of general relativity. It is has been mostly computational, yet tied into the essence of the physical spacetime behavior. Gravitational waves are very finicky, hence the elaborate construction which one must apply to conclude their existence in the first place (which was still up for debate long after their initial proposal). Thus, it should be no surprise that laying the requirements to detect them has been no small task.

This chapter aims to serve multiple purposes. First, we give a brief overview of Michelson interferometry, and then detail the setup of the LIGO/VIRGO collaboration. This includes an overview of the modifications required for a simple Michelson interferometer to reach a sensitivity capable of detecting strain from gravitational waves in general.

Then, the detector's output signal is described in order to get a feel for the signal parameters and the ways in which it is interpreted. This will build up the knowledge base required to consider the recent data from the detectors in the next chapter. We then aim to use this information along with the immense literature from the past decade, to consider the nature of modern day detectors. Finally, we conclude with the advanced upgrades made in the transition to the detector states used in the most recent observing run, O3A.

6.1 Michelson Interferometry

The primary means of detection driving the field is the interferometer [1], which, in general, uses the coherence (and decoherence) of light to measure minute changes in distance to some surface. At it's core, an interferometer splits a laser beam, of wavelength λ, so that two paths are created, directed down two orthogonal arms, with one path in the direction of the original beam, and one in some perpendicular direction. One of these beams is directed at some fixed reference mirror, which reflects the first beam back toward the beam splitter. The second beam is directed at another reflective surface, which is at rest in some starting position, and returned to the beam splitter. When the two waves interfere as they recombine, they induce some pre-defined phase shift in the linear superposition that is the new wave.

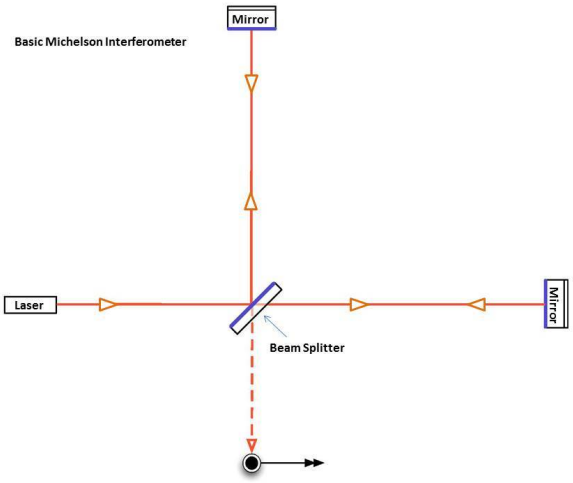

Fig. 8.
The simple working mechanism behind a basic michelson interferometer

After the beams are recombined, they are sent to a photodetector, which collect the light to determine the phase of the incoming light wave. Then, as the second mirror is moved, this phase shift will fluctuate between decoherence and coherence, indicating a change in the surface position being covered by the wave face. This characterizes the general nature of an interferometer, but things behave a little differently when a gravitational wave passes, which causes the arm lengths, and the shape of the waveform itself to morph. One can no longer talk about

a fixed reference mirror, and so the design must be changed slightly. These advanced decisions are discussed in more detail shortly. The general setup of the interferometer is shown in the Fig. 8

6.2 The LIGO-VIRGO Collaboration

The LIGO-VIRGO collaboration (LVC) is the state of the art technology of gravitational wave observatories to this date. The two LIGO observatories are located in Hanford, Washington, USA and Livingston, Lousisian, USA, while the VIRGO facility is outside of Pisa, Italy. All 3 locations in the collaboration went through an initial phase in which design sensitivities were tested over the course of science runs [25]. After these science runs, upgrades to the interferometers were made to transition them into their "advanced" states, aLIGO and aVIRGO[2] [3]. Here we consider the observatories at the time of their upgrades to their advanced states.

6.2.1 LIGO

The aLIGO detectors deserve the bulk of the attention, as these detectors are the most sensitive piece in this collaboration. The Hanford and Livingston sites each run a single aLIGO detector. These two detectors are the most developed to date, and in joint operation with one another, were capable of detecting the first ever gravitational waves observed by the scientific community [12]. What follows in this section is a summary of the detector setup given in the initial publication.

The LIGO detectors are Michelson interferometers that have had advanced modifications applied in order to achieve a sufficient sensitivity to the strain effects of a gravitational wave. The orthogonal arms of are made of 1.2 diameter tubes that are 4 km long. At both ends of each arm are mirrors designed to behave as test masses, forming Fabry-Perot cavities in the arms, designed to increase the storage time of the

laser, and in effect lengthening the arms. These mirrors, suspended by pendulums, undergo differential changes in their position when a gravitational wave passes nearby. This effectively changes the length of the arms in the detectors corresponding to the orientation and phase of the passing wave.

The changes in the length of the arms, L_x and L_y correspond to the dimensionless strain amplitude of the gravitational wave, h, according to the relation

$$\Delta L = \delta L_x - \delta L_y = h(t)L \tag{6.1}$$

The differential changes of the arms has an effect on the phases of the two traveling waves as described before. In this way, the phase of the optical signal reaching the photodiode is directly proportional to the strain of a passing gravitational wave. In the case of LIGO and VIRGO, the standard is to set up the pendulum mirrors such that when at rest, the two beam phases are in decoherence upon returning to the beam splitter [13]. Thus, when there are no local spacetime perturbations, no light reaches the photodiode. The main enhancements required to reach the sensitivity requirements involve amplification and recycling of the laser and overall signal. These techniques are meant to maximize the quality of the phase shift signals that are reaching the photodiode- to most accurately interpret the strain felt along the length of the arms. In particular, the modifications are as follows:

1. **Partially transmitting, power recycling mirrors at input arm.**

   This produces a resonant buildup of laser light in the interferometer, increasing the laser light incident on the beam splitter from 20W to 700W.

2. **Resonant optical cavities formed by test mirrors in arms.**

   This modification magnifies the phase differences between the two beams by a factor of 300. This increases the laser light in the arms to about 100kW each.

3. **Partially transmitting, signal recycling mirrors at output node.**
   This broadens the bandwidth of the signal from the arm cavities in order to optimize extraction of the signal.

These adjustments cumulatively have a huge improvement on data quality and precision in high frequency strain amplitude oscillations through the reduction of photon shot noise. Further enhancements were made to ensure low displacement noise of test masses, corresponding to other frequency ranges of interest.

Low frequency data was clouded by seismic disturbances, while intermediate frequency noise arose mostly from thermal excitation. To reduce the impact of the former, test masses were suspended from seismic isolation platforms at the end of a quadruple pendulum chain. This provided the incoming signal up to 10 orders magnitude of freedom from ground noise above frequencies of 10 Hz.

The thermal noise was then reduced by using fused silica fibers for the suspension and pendulum systems. The thermal noise from the test masses themselves were reduced by using 40 kg fused silica substrates with dielectric optical coating. The general diagram description of the LIGO detectors is shown in Fig. 9. This is shown with diagram labels for the highest possible laser output, which is constrained to reduce optical noise.

Additional systematic disturbances were eliminated by mounting all the components in the detector to vibration isolation stages in vacuum, with the exception of the laser. The tubes making up the arms were pressurized to predetermined constraints to control optical phase fluctuations as the result of Rayleigh scattering. Finally servo motors control the alignment of the optical components of the arms, to keep the laser light in resonance as it is in the cavities.

The detector output is calibrated to the strain response of the mirror test masses

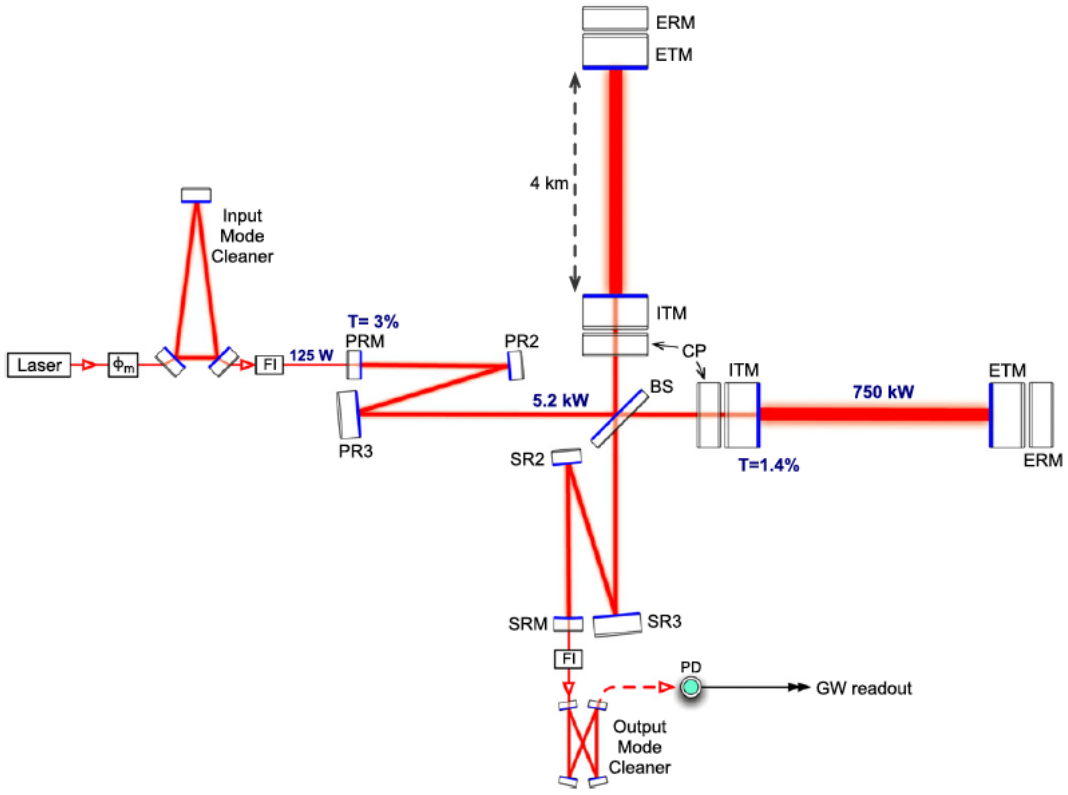

Fig. 9.
Schematic diagram of the LIGO's advanced modifications, displaying the Fabry-Perot cavities in the arms (where the power is greatly increased), along with the power (PRM) and signal recycling mirrors (SRM) [2].

by introducing a calibration laser. This calibration laser continuously monitors the system to validate the current position of the mirrors, to some predefined degree of certainty. The pressure of photons from laser pulses at selected frequency is used to induce the motion of the test masses, which is in turn used to calculate the intensity changes of the laser as they are perturbed. Furthermore, the overall detector response was simulated in early science runs by using this calibration laser to inject a simulated waveform.

Finally, each detector is equipped with seismometers, accelerometers, microphones, magnetometers, radio receivers, weather sensors, power monitors, and a cosmic ray detector designed to monitor the status of the detectors as they are influenced by these

environmental fluctuations. The time at each detector is synchronized to a GPS clock and accurate to within 10 microseconds- this is verified by the use of an atomic clock and secondary GPS at each observatory. This information takes up a huge amount of data space, upwards of 10^5 channels of information from the noise sources alone.

Detector validation requires extensive analyses of these detectors to ensure no significant parts of the waveform arise as the result of instrumentation. A valid result will yield analysis that (in the case of some specific data) shows that no external disturbances would be large enough to contribute significantly to the detected waveform. This factor determines the false alarm rate of a system, which will be discussed further later. Much of the data received at the detector output is laced with noise of particular signatures, making them easy to distinguish and remove from the signal[26].

The design factors listed above give the aLIGO detectors their highest sensitivities over the frequency range 100-300 Hz, which is 3-5 times more sensitive than the Initial LIGO setups. In observation of systems with lower frequencies, the sensitivity improvement is almost 10x greater than the initial setup at frequencies below 60 Hz.

6.2.2 VIRGO

We now change the focus to consider the setup of the VIRGO detector, located near the town of Pisa, Italy. Though the initial construction and initial science runs match the timelines of LIGO, this detector was not at full design sensitivity when LIGO began its observing runs in 2015 [3]. As such, it was required to undergo further upgrades before going online in collaboration with LIGO. We here consider the setup of the Advanced VIRGO (aVIRGO) detector as it stood in 2015.

The general setup of VIRGO bears a close resemblance to LIGO- a Michelson interferometer with advanced modifications to reach the required sensitivity. These

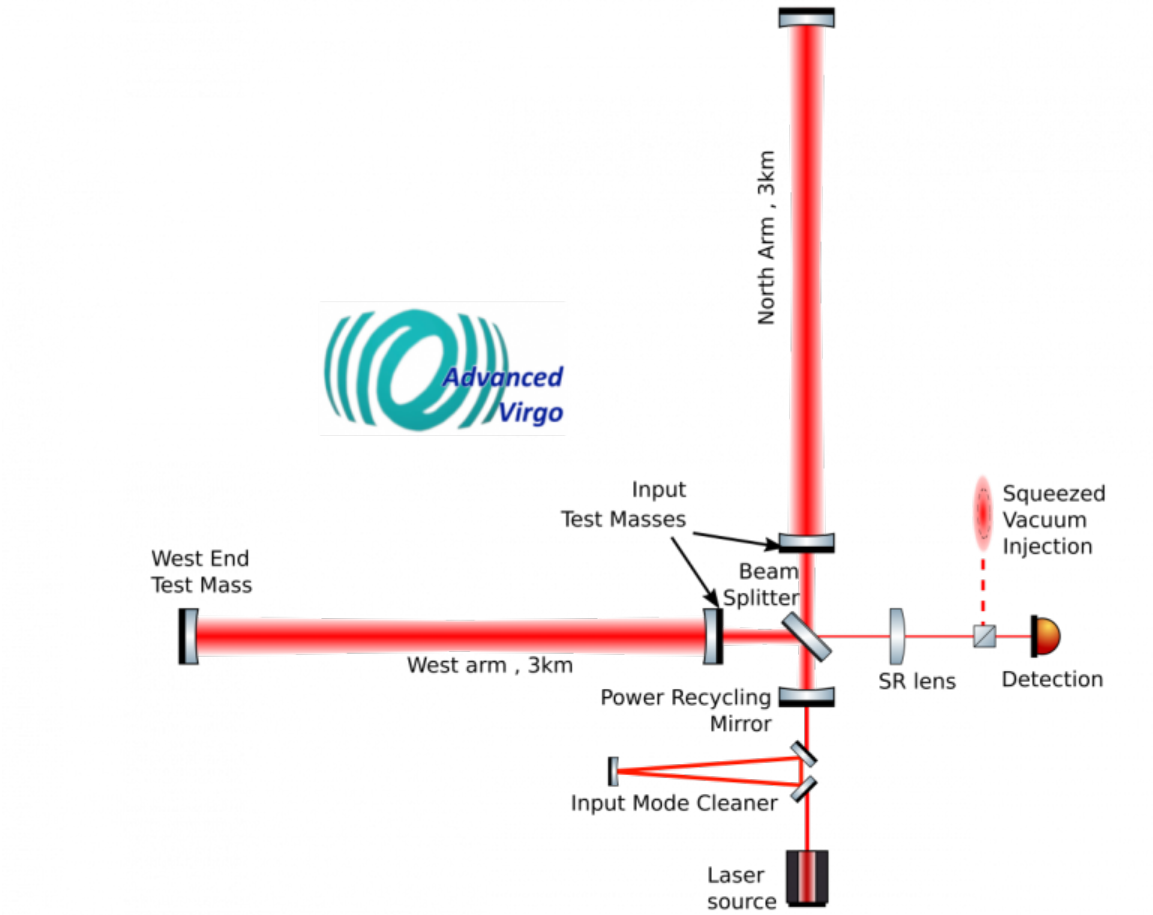

Fig. 10.: A schematic representation of the VIRGO detector.[3]

similarities can be seen in comparing the nature of the diagram in Fig 10 to 9. However, there of course will be some differences. For instance, VIRGO's interferometer scheme uses 3 km arms, both containing Fabry-Perot cavities made from 42 kg test mass mirrors [3]. This system in particular uses a 7-tier pendulum suspension for the masses from metallic material. The setup includes signal and power recycling methods akin to those described for the aLIGO detector. The tuning of the signal recycling mirrors allows for optimization of search methods by changing the shape of the sensitivity curve.

As of the final stages of the aVIRGO upgrade[3], the detector was still using the initial VIRGO laser 60 W of power, though there were already plans to install a high powered 200 W laser. Some of the techniques applied to enhance sensitivity in the aVIRGO detector include the increase of beam size, control of optical alignment, an improved system for vibration isolation, and control of environmental parameters. The laser beam's spot size was increased to reduce thermal noise fluctuations in the mid frequency range due to the mirror coating [27]. Optical losses are avoided by using low-loss and absorption coatings on the mirror of test masses. Furthermore, diaphragms are suspended near the mirror to avoid the accidental backscattering of light.

The payload system was upgraded to account for the installment of heavier test masses, due to the sensitivity of a 7 part pendulum and the surrounding support needs. Furthermore, to properly account for vacuum states in the arm chambers, cryogenic chambers were installed at the ends near the mirrors. Much of the experimental validation and systematic tuning process of aVIRGO is similar to that of aLIGO. Even more so, the validation of the detector ability of aLIGO made it easier for troubleshooting and systematic adjustments in the aVIRGO detector. At the time of publication of [3], the expected design sensitivity range of VIRGO were described by the maximum BNS (1.4 $M_\odot$ each) and BBH ($30M_\odot$ each) inspiral ranges at approximately 140Mpc and 1Gpc, respectively.

6.2.3 Collaboration

Finally, when all three detectors are operational and combined to transfer data between them, the precision of results goes through the roof. These three observatories are designed to undergo simultaneous searches, boosting likelihood of detection in the case of other detectors being offline. This is even more noticeable in the 11 results of

the first two runs when compared to the 39 observations in 03A. This is the result of this run having the highest detector online rate by far, with all 3 detectors running simultaneously at least 44.5% of the time, and 2 detectors running 81.9% of the time. This is in comparison to run O2, in which 2 detectors were running only 46.4% of the overall run, while 1 detector was in use for 75.6% of the run [15].

VIRGO was not added until the last month of this run, on August 1, 2017. The first detection using all 3 detectors was made on August 14th, 2017 [28], just 3 days before the detection of the first BNS [29]. The addition of the VIRGO detector data helped greatly in identifying this relatively low energy system [26]. This was a huge step up in data quality even without the most recent upgrades. For one, it allowed for the orientation of a passing gravitational wave to be determined by considering the minuscule difference in origin time of the waves first perturbation at each detector[17]. Furthermore, this gives insight into the phase evolution of the wave far beyond what was previously attainable [28].

6.3 Signal Detection and Comprehension

We then turn attention to the way a signal is actually perceived as it is detected. The general "pure" signal from a gravitational wave can be written as a superposition of its polarization states [5]

$$h = A_+ h_+ + A_\times h_\times, \tag{6.2}$$

where the factors of h_+ and h_+ contain a description of the wave in terms of its frequency and wave vector (i.e., they are the exponential factors in our previous treatment of gravitational waves). The effects of such a passing wave are dependent on the orientation of the detector, consistent with the fact that there are no perturbations parallel to the direction of the wave's propagation. The output signal of a working

detector, $s(t)$, is then generally expressible in the form

$$s(t) = n(t) + h(t), \tag{6.3}$$

where n(t) is the noise of the signal. If there is no strain felt by the detector, then $h(t)$ will be zero, and the output signal will be just noise. Furthermore, if these fall below the acceptable sensitivity range, predefined by some signal-to-noise ratio (SNR) cutoff, the signal will be much more difficult to extract. Besides this signal description of the strain, there are a few parameters defining detector sensitivity as well as the loudness of sources.

Signal theory requires quite a bit of Fourier Analysis to transition between time and frequency dependent functions. The nature of this math will not be exhibited in full here, as it requires substantial pre-treatment that is not anywhere near the scope of this thesis. Instead we note simply that the Fourier transform of a signal $h(t)$ into the frequency space is given by the relation

$$\tilde{x} = \{\{x(t)\}(f) = \int_{-\infty}^{\infty} dt x(t) \exp -2\pi i f t \tag{6.4}$$

and the noise power spectral density (PSD) defined by

$$\langle \tilde{n}(f)\tilde{n}^*(f')\rangle = \frac{1}{2}\delta(f - f')S_n(f) \tag{6.5}$$

The noise PSD is capable of fully characterizing the noise in the detector under the assumption that the noise is Gaussian and stationary, which can be made. The angular bracket represent an average over many noise realizations. Due to the nature of the detector and signal, there will only be one realization. As such, a time average over stationary stochastic noise is sufficient [5]. Then, with this in mind we jump straight to a general governing relation for each of the 3 main signal parameterizations:

1. **Characteristic Noise**, $h_c(f)$

   This is designed to give a signal parameterization describing the integral over the accumulated signal, boosting the SNR in the case the instantaneous amplitude of the true signal h is orders of magnitude below the noise value. The characteristic equations of this parameterization are

$$|h_c(f)|^2 = 4f^2|\tilde{h}(f)|^2 \tag{6.6}$$

   and

$$|h_n(f)|^2 = fS_n(f) \tag{6.7}$$

2. **Root Power Spectral Density (PSD)**, $\sqrt{S_n(f)}$

   From the form of the noise power spectral density defined above, one can define a similar quantity for the signal power spectral density,

$$\langle \tilde{h}(f)\tilde{h}^*(f')\rangle = \frac{1}{2}\delta(f-f')S_h(f). \tag{6.8}$$

   . Then, the root PSD is expressed as

$$\sqrt{S_h(f)} = h_c(f)f^{-1/2} = 2f^{1/2}|\tilde{h}(f)|, \tag{6.9}$$

   with the corresponding root noise PSD

$$\sqrt{S_n(f)} = h_n(f)f^{-1/2}. \tag{6.10}$$

   Both of these quantities have units of $\mathrm{Hz}^{-1/2}$. The root noise PSD is frequently encountered in the literature to represent the known strain noise at a detector. The noise root PSD in particular is consistently used in noise evaluation at the detectors in almost every LVC publication stumbled upon so far.

3. **Energy Density**

   The energy density of the system can actually be parameterized using the Isaacson stress energy tensor defined in the previous chapter, given by the averaging derivatives of the perturbations $h_{\mu\nu}$ over several periods. In doing so and looking at the energy density, one derives an integral representation, which is taken over the full frequency range. The integrand of this expression defines the spectral energy density, given in units of energy per unit spatial volume per unit frequency,

   $$S_E(f) = \frac{\pi c^2}{4G} f^2 S_h(f) \tag{6.11}$$

   This can also be calculated as it applies to the noise signal. The general notational standard of cosmological studies is to use a dimensionless quantity describing the energy density per logarithmic frequency interval, normalized to the critical density of the universe

   $$\Omega_{GW}(f) = \frac{f S_E(f)}{\rho_c c^2}. \tag{6.12}$$

We will not work explicitly with any of these expressions, though it is beneficial to understand how the signal corresponds to the physical aspects of the system. We will certainly see the parameter description by the PSD. The 2 figures here display the detector sensitivities in terms of the characteristic strain and root PSD, where areas are shaded to indicate the areas in which one expects to detect compact binaries, followed by the 3 standard data plots that are usually included in the LVC detection publications after the data is released to the public [28].

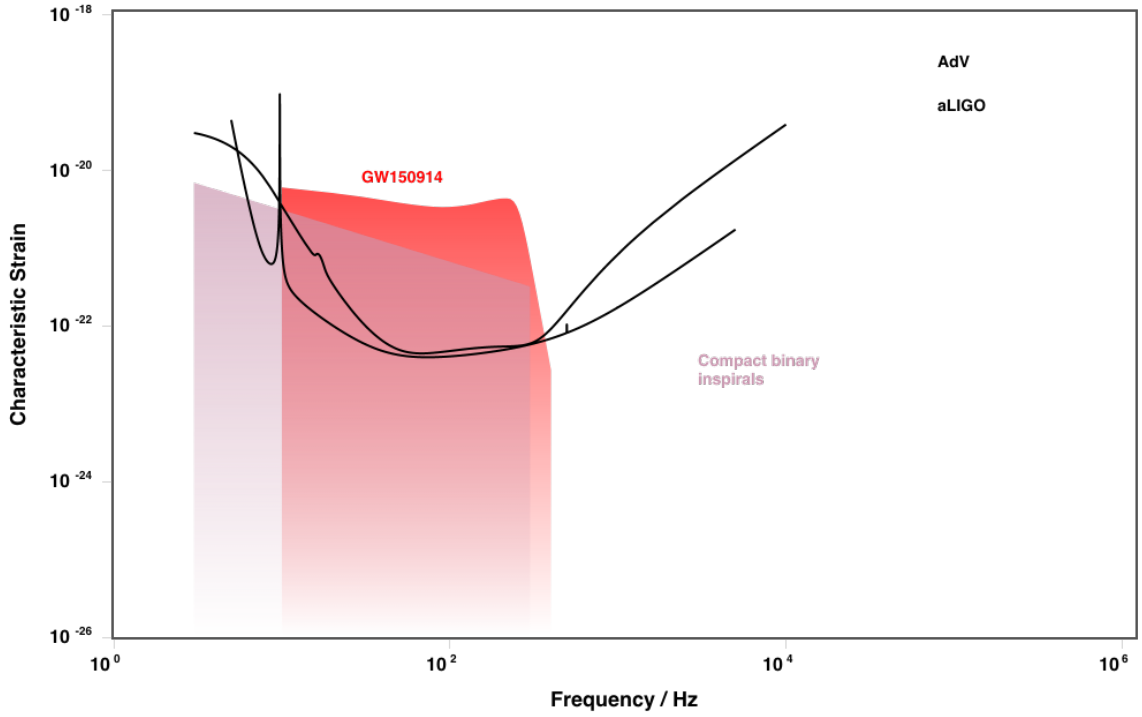

Fig. 11.: Plot of the Characteristic Noise Strain at the aLIGO and aVIRGO (AdV) detectors. [4]. The likelihood of detections may be assessed by considering the colored area of expected source parameters on a log-log scale by an "eye integration" technique[5].

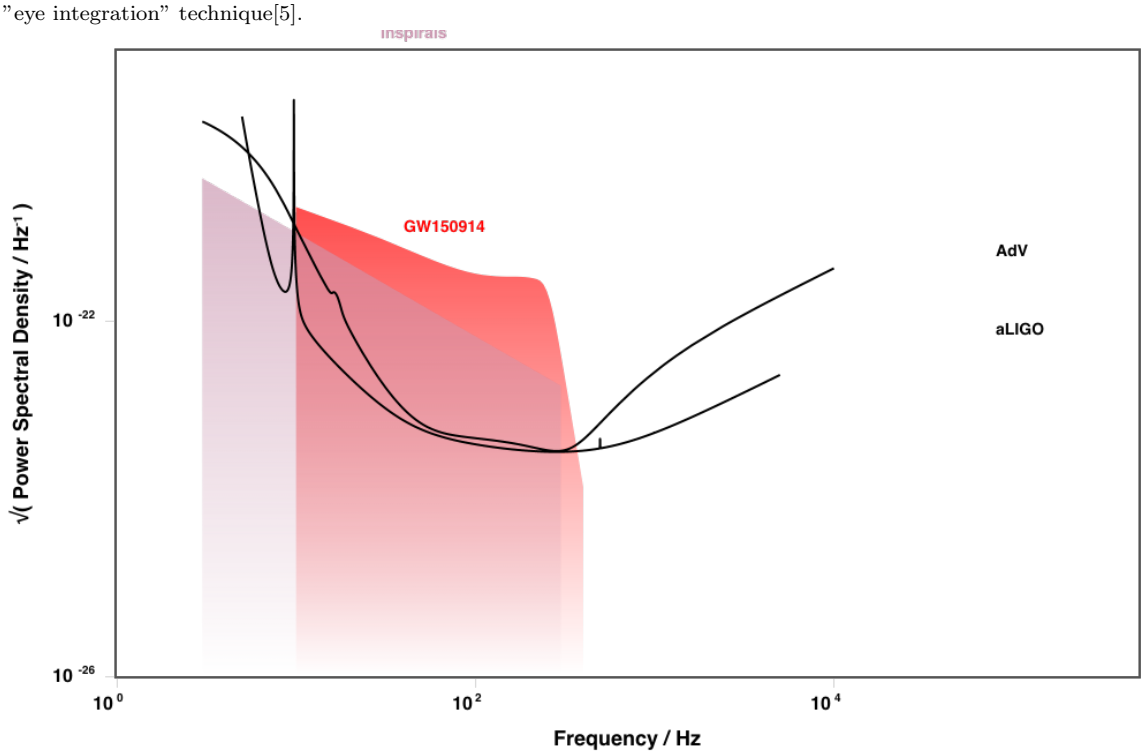

Fig. 12.: Plot of the Root Power Spectral Density at the aLIGO and aVIRGO (AdV) detectors. [4]

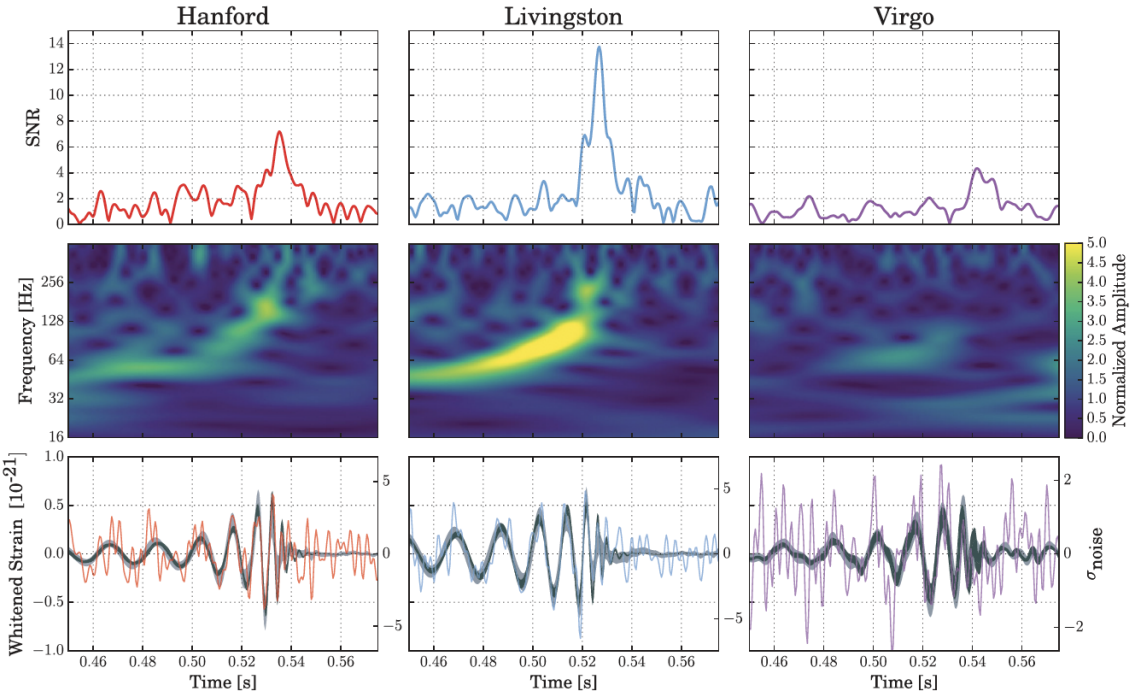

Fig. 13.: Plot of the SNR, the Energy Density, and a cleaned-up version of the characteristic strain which were measured in the detection of GW170814, the first detection with all 3 detectors in operation.

6.3.1 Source Parameters

We should also touch on the matter of data analysis and hypothesis formation in modern detection. Initially, the BW signals of a binary at a single detectors were expected to be determinable through the 4 parameters (i) amplitude, (ii) chirp mass, (iii) time, (iv) phase [30]. However, as the state of technology and gravitational wave theory has advanced, the waveforms were capable of being solved numerically with the addition of extra parameters, for well-defined waveform "families." The parameters governing the system from which a signal is detected will end up being determined by comparison with well-understood waveforms. These waveform models are organized into specific physical categories defining system dynamics such as those with and without both spin and precession. These models produce time or frequency dependent numerical solutions of waveform signals when given the necessary parameterized

inputs.

In particular, each studied waveform is given a vector input that describes its parameter space, which generally includes at least the following 9 parameters [31]

1. **Component Masses**, m_1, m_2.

   The "mass plane" between these parameters can be reparameterized to be represented instead by the *chirp mass*,$\mathcal{M}$ and *mass ratio*, q, which are less correlated, making this particular space easier to sample over.

   $$\mathcal{M} = (m_1 m_2)^{\frac{3}{5}} (m_1 + m_2)^{\frac{-1}{5}}; \qquad q = \frac{m_1}{m_2} \tag{6.13}$$

   The chirp mass corresponds to the "chirp" described previously as the frequency of the inspiral increases.

2. **The Luminosity Distance to Source**, d_L

   A measure of the relative brightness of an object that is determined by the path deviation of the light on its way to earth through curvature, redshifting, etc.

3. **The right ascension and declination of source**, α, δ

   Astronomical coordinates specifying an event's location with longitude and latitude coordinates on a sphere centered around the earth.

4. **The inclination angle**, ι

   The angle between the system's orbital angular momentum and the line of sight.

5. **The polarisation angle**, ψ.

   A description of the orientation of the orbital's momentum vector projection onto the sky plane.

6. **Arbitrary Reference Time**, t_c

   Such as the time of coalescence.

7. **The orbital phase of binary at t_c, ϕ_c**

Note that with the exception of the strain amplitude, a direct measurement by the detector, these parameters contain perfect analogs to those described in 1993. However, the first paper [30] is concerned with detections from single interferometers. Once the LVC was established, the use of 3+ detectors gave the ability to determine the sky location and expected distance of a system. This, in turn, allowed for the addition of parameters to this space describing the relative orientation of the system.

For our purposes, we only need to be aware that these parameters govern the underlying waveform templates that are matched to incoming data in a detector. A parameter space as defined above is needed to describe a circular binary consisting of 2 point mass objects without spin. To include spin, one must also introduce to the model, the dimensionless spin magnitudes of the components, $a_i = \frac{|s_i|}{m_i^2}$, along with two angles corresponding to each spin, specifying orientation with respect to the initial inclination angle. To fully describe the matter effects of a system, an equation of state (EOS) is necessary, though this is not always an achievable task.

After comparing the generated waveform of many models to the waveform detected, one is capable of deducing most likely parameters. This involves varying the parameters and underlying assumptions of a general waveform family to find a closest match. If a close enough match is found for a GW signal that can be separated from the noise signals, the signal is sent along the search pipeline for closer analysis. These parameters can be then appropriately decomposed into an understanding of the physical nature of this system (i.e., these can be compared to well known parameter ranges from which the objects in the system are deduced). With a strong enough signal, these models can determine the source parameters with high precision and accuracy. However, the overall accuracy of the detection will be based on the cumulative exploration of

solutions in the field of numerical relativity (NR).

6.4 Design Sensitivity

Having covered the general setup of the detector's advanced states, we now explore briefly the adjustments that were made for their most recent observing run, O3A [15]. This will lead us to the first real discussion of the design sensitivity during this run. The magic number for noise threshold in a system was 10^{-21} as detection methods were coming to fruition. This is the expected amount of strain that was expected to be felt by the interferometer arms in a wave by a high-frequency system

The operating power of the aLIGO detectors between the second and third runs were greatly improved by an increase in the input laser power at both the Hanford and Livingston sites. Furthermore, more circulating power was added by replacing the test mass mirrors in both facilities (Hanford and Livingston) with lower scattering mirrors. This helped improve sensitivities for high frequency systems. Beam diaphragms such as the one described in aVIRGO upgrades were also installed in the LIGO detectors to reduce scattered light.

VIRGO was only involved in 2 detections before also receiving some major upgrades between the runs. One of the major upgrades was the replacement of the metal wire suspensions for the test masses with silica-fused fibers, as was already the case for LIGO. HF noise was corrected by improved suspension of the external laser injection bench, reducing beam jitter and improving seismic disturbance. Furthermore, small upgrades in the control strategies of the suspensions were also made to improve sensitivities below 30 Hz. Some of the upgrades were applied to all 3 facilities, such as the installation of squeezed light states at the output detector, resulting in increased sensitivity in the HF range.

The median BNS inspiral detection range for the Hanford and Livingston LIGO

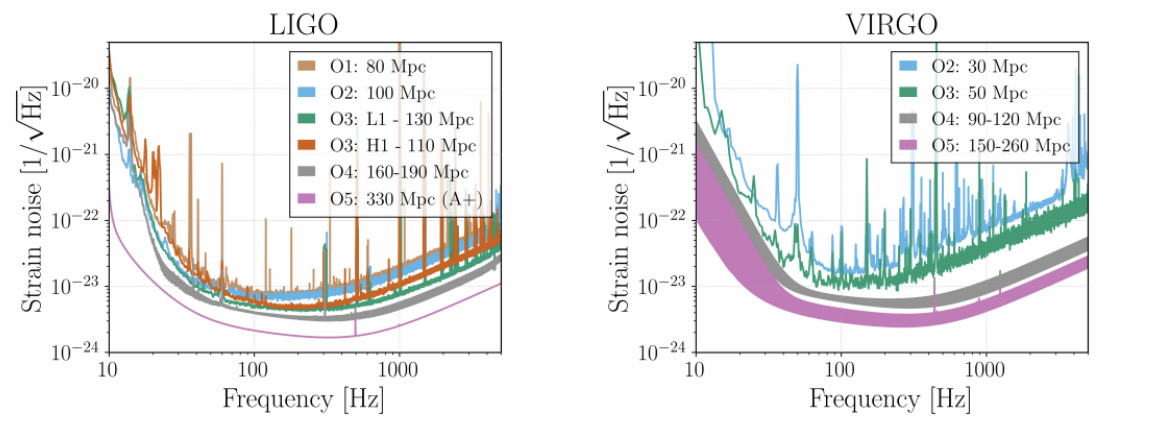

Fig. 14.: The strain noise of the aLIGO and aVIRGO detectors at various expected milestones

sites increased from 66 and 88 Mpc, respectively, to 108 and 135 Mpc. For the aVIRGO detector, the median BNS inspiral increased from 26 Mpc to 45 Mpc at the start of the 3rd observing run. These values define the median distance in which one expects to have the sensitivity to measure The previous and projected sensitivity curves of the detectors during future observing runs is given in the figure above.

.

CHAPTER 7

GW190814

In the first two observing runs, only 11 confirmed events were detected by LIGO. Many of these were binary black hole (BBH) systems, while one was a binary neutron star (BNS) system [14]. In the first half of the third observing run alone (April 1, 2019 - October 1, 2019), a total of 39 systems had already been detected [15]. One system yielded what is assumed to be the second detected BNS coalescence, with two NSs with masses in the range $m_{NS} = 1.46 - 1.87\ M_{\odot}$ under expected spin conditions [16]. This BNSC detection was determined to have the largest chirp and total mass of any BNS to date, though this is stated alongside the fact that these objects may yet be determined to be black holes.

A particularly interesting detection, GW190521, was determined to be produced by a BBH with a total mass of $150M_{\odot}$ [32], implying with 99% credibility that the primary black hole in the system was at least 65 solar masses. This result was the first to implicate a black hole being in the upper mass gap, between $65 - 120M_{\odot}$ [32]. Another system which has been heavily emphasized in the literature is GW190412[21], which contained the first conclusively asymmetric BBH, having a mass ratio of $q = 0.28^{+0.12}_{-0.07}$. Such an asymmetry in the mass distribution results in detectable radiation contributions from multipole terms other than the standard quadrupole [21]. This detection opened up new discussion on the expected explorable binary system populations.

Months later, gravitational radiation was detected from a source that had even more asymmetry in its masses. In fact, the system was found to be asymmetrical to the point that the nature of the secondary component mass has yet to be fully

concluded. The secondary mass was first observed to fall into the "lower mass gap" of $2.5 - 5M_{\odot}$ where previous EM observations had found a particular lack of BHs and NSs in the galaxy [33]. After undergoing proper waveform analysis, GW190814 was determined to have been produced by the mass components $M_1 = 23.2^{+1.1}_{-1.0}M_{\odot}$ and $M_2 = 2.59^{+0.08}_{-0.09}M_{\odot}$, resulting in a mass ratio of $q = .112^{+0.009}_{-0.008}$ [17]. The first of these is certainly a black hole, while the second has been put through consideration as both a black hole and a NS, though not through any more exotic assumptions.

Early studies lean in the direction that the system is in fact a BBH, though this can not be entirely confirmed in the current framework of the known parameter space. In either case, it is an astronomical event of great interest, as it is an extreme of the collection of direct astronomical observations, i.e., it will most likely be the smallest black hole detected to date. This observation will hopefully lead to expansion of the explored parameter space, and thus make it easier for planned detectors in the future to analyze systems with lower energy.

7.1 Detection

On August 14, 2019, there were only 2 detectors in the LVC that were in a fully operational mode: the Livingston LIGO detector and VIRGO. The Hanford based LIGO detector was undergoing a routine upgrade at the time, but was still taking in some data at a nominal state. This data ended up being worthwhile when matched with the results from the fully operational detectors, and was used in subsequent analysis. At 21:11:00 UTC, a loud event was identified in a matched-filter search algorithm for coalescing binaries [17] from banks of modeled gravitational waveforms. The time-frequency analysis of the strain data for the 3 observatories is given in Fig 15.

One of the immediate notifications sent out to the scientific community indicated that at least one of the mass components falls into the lower mass gap, $3 - 5M_{\odot}$. Comparing the arrival time of the wave at all 3 detectors yields the ability to estimate the location of the system [17]. Upon initial detection the system's location was constrained to a sky area of 38 deg^2, about 220-330 Mpc away. This was updated a few hours later to 23 deg^2 and 215-325 Mpc, respectively. This update came with the new classification of a neutron star-black hole (NSBH), meaning that the secondary mass was now expected to be less than 3 solar masses. Follow-up searches across the EM spectrum and neutrino observations yielded no counterpart candidates [34]. These low-latent analyses, though nice, do not give the full picture of the wave and data must be further processed to eliminate noise and get better parameter constraints.

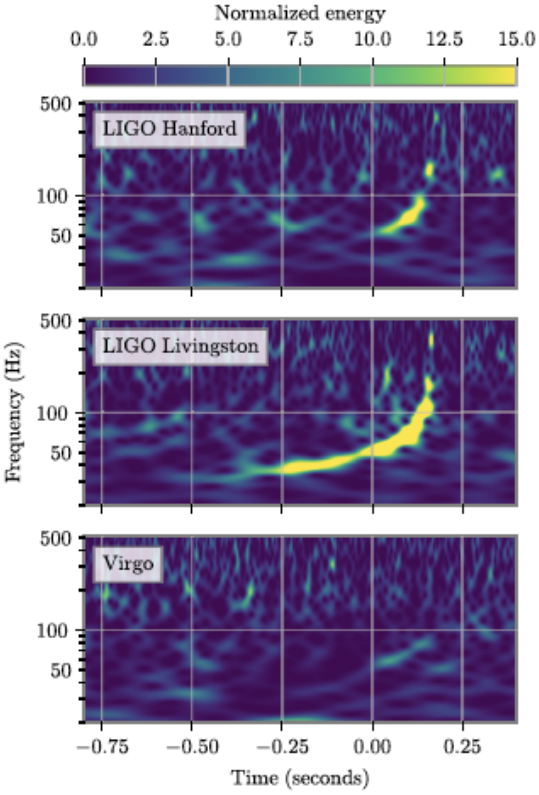

Fig. 15.
The normalized energy plotted on its time-frequency curve

The significance of the input was calculated once the parameter data had been properly refined. Well-defined algorithms are used to estimate the noise background of a waveform, generating the likelihood of the event being due to a statistical error. This false alarm rate (FAR) is given in terms of the years per each event. After a procedure designed to yield an unbiased average of the noise over course of the observing run, the FARs for GW190814, for two different algorithms, GSTLAL and PYCBC, were found to be less than 1 per 10^5 yr and less than 1 per 4.3×10^4 yr. This indicates

that any waveform of this form (given all of its parameters) was highly likely to be the result of an actual system, and not systematically driven noise.

7.2 Waveform Analysis

The physical parameters of the system are inferred though a Bayesian analysis of the waveform collected by the detector. This uses prior knowledge of events with related conditions to assess the conditions of an event at hand. In particular, the waveform collected by the detectors is compared to state of the art waveforms modeled similar to that of the detected data (i.e. similar signal frequency, intensity, etc.) [35] as determined by the low latent analyses. From these waveforms and their similarities, one (or rather one's machine) is capable of deducing the likelihood of the binary system's individual properties, such as tidal deformability, the component masses, spin, and orbital precession, etc. These probability values are referred to as the posteriors of the system's parameters.

The incoming data is assumed to be noise-free during some interval in which there is a nonzero power spectral density (i.e., there is characteristic strain). At this point the model waveform is inserted for comparison. This "zero-noise realization" of the detection is statistically equivalent to a waveform with many random Gaussian fluctuations being averaged over a long period of time[36] [37]. Here, the time interval of the data chosen for use in analysis of GW190814 was about 16 seconds near the time of detection[17].

To test for possible systematic errors, the same analysis is done, instead choosing the model waveforms generated by numerical relativity, with signal parameters similar to GW190814, as mock signals. From this, one deduces the source properties with the same methods described above[36]. No evidence was found for systematic bias in the recovery of the system parameters relative to usual statistical errors in estimation.

However, these models are inherently limited by the current availability of high quality data to provide a strong basis for waveform models of certain systems, resulting in less understanding of the parameter space coverage of some numerical solutions.

It was discussed previously that in the 3rd run, a frequency sensitivity as low as 10Hz could be measured in the LIGO detectors. Though there was no evidence of instrumental or environmental disturbances in the primary detector at LIGO Livingston, the usual scattered light noise at low frequency was encountered. The data from LIGO Livingston was also clouded by further noise from a local thunderstorm at the time, requiring the low-end frequency cutoff to be shifted up to 30 Hz to achieve a usable signal. This data was ran through Bayesian analysis under both the two possible assumptions that it was a BBH and a NSBH, the choice of which comes from the physical interpretation of the deduced parameters.

The model waveforms chosen for the BBH analysis were based off effective-one body(EOBNR) and phenomenological (Phenom) approaches. There were about 300 usable cycles at frequencies above 20 Hz, from which source properties could be deduced with well defined parameters. These models each produced distinct, similar posteriors in which there exists a peak probability for each parameter. The Bayes factor is used to compare the likelihood of the results found by two competing assumptions in the model. For the parameters estimated by the models EOBNR and Phenom, this Bayesian factor is 1. This tells us the models produce similar results, and thus can be averaged over without giving too much variation in the parameters. The averaged system parameters corresponding to those in the previous chapter (give or take) are given by the first table below, including the SNR ratios both at each detector and cumulatively.

The waveform parameter space of NSBHs has not been explored as extensively as that of BBHs. As such, to model these waveforms, the same BBH models were

Table 1.: The averaged deduced parametters from the waveform model families EOBNR and Phenom [17]

Primary Mass, m_1	$23.2^{+1.1}_{-1.0}M_\odot$	Secondary Mass, m_2	$2.59^{+0.08}_{-0.09}M_\odot$
Chirp Mass, $\mathcal{M}$	$6.09^{+0.06}_{-0.06}M_\odot$	Mass Ratio, q	$0.112^{+0.009}_{-0.008}$
Total Mass, M_{TOT}	$25.8^{+1.0}_{-0.9}M_\odot$	Remnant Mass, M_R	$25.6^{+1.1}_{-0.9}M_\odot$
Constraint on Primary Spin, χ_1	$\chi_1 \leq 0.07$	Final Spin, χ_F	$0.28^{+0.02}_{0.02}$
Luminosity Distance, d_L	241^{+41}_{-45} Mpc	Inclination Angle, ι	$0.8^{+0.3}_{-0.2}$ rad
LIGO Livingston SNR	$22.18^{+.10}_{-.17}$	LIGO Hanford SNR	$10.7^{+0.1}_{-0.2}$
VIRGO SNR	$4.2^{+0.2}_{-0.6}$	Cumulative SNR	$25.0^{+0.1}_{-0.2}$

applied after being supplemented with the proper tidal effects. There is literature to suggest that the system as an NSBH would merge prior to any noticeable tidal effects. The assumptions of the model yielded an uninformative, wide ranging posterior distribution describing the would be NSs tidal deformability. This is a potential effect of Bayesian statistics that leads to insignificant posteriors. This tells us that these models can not decipher the significant matter effects of the signal that are required to sufficiently describe the system as a NSBH. As such, the Bayesian analysis on this system[17] was done as if it were a BBH, and we will proceed through this discussion with the results from these particular analyses.

7.3 Properties

The binary system was found to have the greatest mass asymmetry of any gravitational wave observed to date, with a mass ratio $q = 0.112^{+0.009}_{-0.008}$ [17]. The frequency evolution of the system allowed for a tight constraint on the chirp mass of the system. The mass of the larger object in the system is found to be $m_1 = 23.2^{+1.1}_{-1.0}M_\odot$, which makes it easy to deduce that it is most likely a black hole, consistent with the lack of EM counterparts from the system. The generated posteriors of the mass

parameters are given in Fig 16.

The magnitude and orientation of the spin in a system provide further insight into the origins of the binary. The effective spin parameter, describing the amount of spin perpendicular to the orbital plane, is $\chi_{\rm eff} = 0.002^{+0.060}_{-0.061}$.

The system GW190814 was found to have an orbital precession $\chi_P = 0.04^{+0.04}_{-.01}$, which is the closest precession to zero detected in the small sample size of the LVC. This describes the amount of significant spin in the orbital plane. However, a Bayes factor of 0.5 was computed for the ratio of precessing to non-precessing models, showing no evidence in favor of spin precession in the model. Thus, the effective precession parameter is constrained to $\chi_P \leq 0.07$.

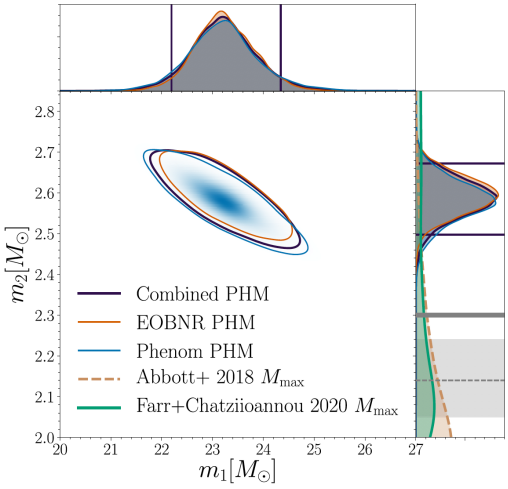

Fig. 16.
The mass posterior space, in which the most likely magntiudes of the two components are compared to each other. Along the top and right sides are the probability densities corresponding to the individual parameter spaces.

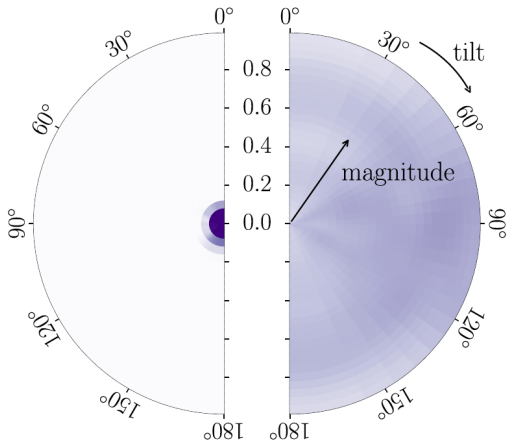

Fig. 17.
A plot of the posterior probabilities of the spin components of the system. The purple shaded areas indicate regions of high probability for both the spin and magnitude.

Furthermore, this precession has the smallest estimated variation of any binary system observed by the LVC so far. While in general, the system is found to have near-zero precession and the models show no favor for using the precessing models, they are found to yield much tighter constraints on the secondary mass estimation. Thus, they are still used as a prior assumption in analysis, where the models are assumed to have isotropically distributed spin components.

The asymmetric mass distribution of the system implies that the larger mass component is going to dominate the effective spin contributions to the system. Due to the constraints on the orbital precession and the effective spin parameter, the spin of the primary mass in the system is constrained to the upper bound $\chi_1 \leq 0.07$. The spin posteriors are given in Fig. 17, with the primary mass shown on the left and the secondary mass on the right, where deviations from uniform shading indicate a spin property.

As mentioned, the spin of the primary mass is tightly constrained in the purple shaded area. The orientation deduced was unchanged from the information given in the model assumptions, indicating that the signal gave no true information on the actual orientation. The spin magnitude and orientation of the smaller object is seen to be unconstrained, producing posteriors that are similar to the assumptions of the model.

Finally, the black hole remnant after the merger was analyzed as if it were definitively a BBH. NR calibrated fits to the system are used to infer a remnant with mass $M_R = 25.6^{+1.1}_{-0.9} M_\odot$ with spin $\chi_R = 0.28^{+0.02}_{-0.02}$. This spin is lower than previous mergers, consistent with the asymmetry of the mass components. This merger is indicated in the figure above, for comparison with other astronomical events up to this date.

7.3.1 Secondary Mass Component

The less massive object in the binary system is deduced to have a mass in the range $2.50 - 2.67 M_\odot$. Though the initial flag with the detection notification specified the binary system as a NSBH, this was only because of the assumed existence of a $2.5 - 5.0 M_\odot$ lower mass gap observed in BHs and NSs. This is present in some

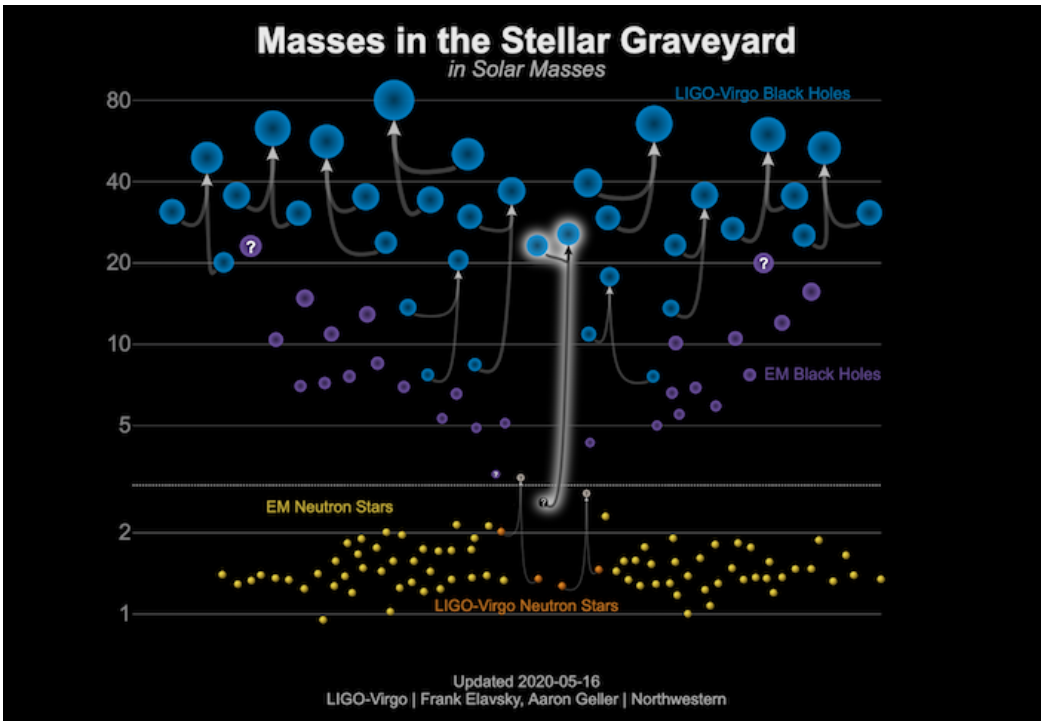

Fig. 18.
A graphic to visualize the compact binaries observed in total thus far, with the merger of GW190814 highlighted

population models [33], as the result of a lack of detections in this mass range. The assumed existence of this mass gap for black holes can be found programmed into quite a few waveform models[38], even though there is belief that they are purely products of the population models not having detections in this range (a good belief). These are the models used as filters against the incoming signal to find matches without much analysis. This is unfortunate, as it could lead to foregone conclusions of the nature of this component after only a brief analysis of the signal. There has been much discussion on the nature of this object in the literature, as a NS, as a BH, and even as a NS pulsar [39]. We assume moving forward that it is either a NS or a BH, and leave the more complex assumptions for those getting their doctorates in cosmology somewhere.

Though a precise categorization has yet to be determined, this would either be

the most massive NS or the least massive BH observed to date. The lack of EM counterparts, the high asymmetry, indistinguishable tidal signatures, and low spin-induced quadrupole effects all leave this matter inconclusive. While the parameter space has not yet been explored in full, the possible nature of the mass can be explored by comparison to the literature to identify possible candidates that match the known physical properties of the system. Here, we consider some of the estimates on the mass ranges of NSs and BHs in an attempt to, at the very least, skew likelihood in favor of one system over another.

The merger corresponding to GW170817 [29], with mass $M_{\mathrm{GW170817}} = 2.74^{+0.04}_{0.01} M_{\odot}$, is suggested to have left a black hole remnant. This suggests that NSs may not be capable of sustaining tidal forces from a mass of such magnitude, collapsing at some inherent upper limit below this mass value. The TOV (Tolman-Oppenheimer-Volkoff) limit, when first established numerically, generally recognized the maximum mass of the NS between $2.2 - 2.9 M_{\odot}$ [40]. Recently, the sample events available from recent detections has led to the estimation of expected BNS populations that have forced an adjustment to $M_{NSMAX} \leq 2.6 M_{\odot}$[41], while for cold NSs the limit is much smaller, generally accepted around $M_{\mathrm{COLD\ NS\ MAX}} \leq 2.3 M_{\odot}$[42].

In terms of purely observational constraints, on the other hand, the most massive known NS detected within a pulsar is of mass $M_{\mathrm{PULSAR\ NS}} = 2.27^{+0.17}_{-0.15} M_{\odot}$ [43]. From this point of view, it seems unlikely that the secondary mass is a neutron star, even if it must violate the assumed mass gap of some population models.

In some EOS of nuclear theory, there are nonrotating NSs for which the limit is theoretically estimated to reach upwards of 3.0. This was considered but was expected to lead to measurable tidal deformation in the NS, which was not observed. Thus, the notion was dropped. Further attempts were made to determine a likely EOS, $p = p(\rho)$ as if it were a NS, with little success.

It should be noted that deciding on a category to fit this binary system into creates an issue due to the inability to rely on this particular parameter space when looking at waveform models. There have not been any systems yet that resemble this system, and thus they have had no need to model its many parameter variations and their effects numerically to account for all possible states. The discovery of the two mass asymmetric compact binaries in this half of the observing run is expected to force more focus on calculating accurate waveform models for such mass distributions. Furthermore, the possibility of this being an exotic stellar object was not explored at all in the original paper, thus leaving many possibilities still up in the air.

7.3.2 Higher Order Multipoles

The high mass asymmetry present in the system produces a signal which provides significant evidence for higher order multipoles. In fact, the Bayesian factors used in determining the posteriors show stronger support for the existence of higher order multipoles than the support for a simple quadrupolar radiation. Measurements of these can yield greater system constraints on the system's deduced parameters, as each multipole moment higher than the quadrupole moment has a unique angular dependence. Evidence of higher order multipoles were also explored in the case of GW190412[21].

These are interesting physical effects in their own regard and deserve to be explored a little further. The contributions of the higher order multipole moments scales as the mass ratio q moves away from 1- i.e., the more skewed the mass symmetry is, the greater the multipole contribution to the energy and thus the waveform. For a general field, the multipole radiation can be expressed as some spherical harmonics

expansion, according to the relation

$$\Phi(\mathbf{r}) = \sum_{m=0}^{\infty} \sum_{k=-m}^{m} C_m^k Y_m^k(\theta, \phi) \tag{7.1}$$

where $Y_m^k(\theta, \phi)$ are the spherical harmonics functions and the parameters (θ, ϕ) denote the angular orientation relative to the source. The factor C_m^k is a constant term that depends on the scalar density (such as the mass density) that generates the field. If rewritten appropriately,

$$\Phi(\mathbf{r}) = \Phi_{\text{mono}} + \Phi_{\text{dipole}} + \Phi_{\text{quadrupole}} + \Phi_{\text{octupole}} + ..., \tag{7.2}$$

gives the general definition of each of these multipole terms corresponding to the m index in the spherical harmonics expansion. While the ideal of a gravitational potential is not explicitly defined in curved spacetime, one can generalize this derivation to find the expansion for the gravitational field perturbations far way from a source corresponding to the metric $h_{\mu\nu}$. This will not be done here but it is in this way that one reaches the multipole representations of the gravitational field.

The means of derivation of this equation lead to constraints on the indices (m, n) naturally, such that n takes on integer values between $-m$ and m. The dipole states, which describe EM polarization, are defined by $m = 1$, while the quadrupole states are defined by $m = 2$ The higher order $(m > 2)$ solutions of spherical harmonics naturally have more angular dependence. This corresponds to GWs that are "beaming" off the compact system in the orbital plane, with additional multipole order increases effectively narrowing the width of the wave.

In particular, the comparison of the original waveform models (EOBNR/Phenom) to their counterpart families including higher order multipole (EOBNR PHM/Phenom PHM), the Bayesian factors show the strongest support ($\log_1 0\mathcal{B} \approx 9.6$) for a model in

which the (3,3) multipole exists along with the (2,2) multipole. The higher order multipoles observed in this system are further evidenced by exploring time-frequency tracks. This method is further detailed in [21].

We show here the simulated physical appearance of these beams in the last 10s of the merger, as they are shown in the simulation of GW190814 [6]. The images used here can be found at `https://www.aei.mpg.de/263744/gw190814` or from image captures of the video simulation. The simulation covers the last 160 orbits of the binary inspiral, and assumes they are both black holes with the masses defined by the relevant posteriors. This is consistent with the data from the frequency range above 20Hz in the detection of GW190814.

The simulation uses results combined between the waveform families SEOBNRv4HM and numerical relativity simulations. The colors in the images represent the real part of the GW strain, though for visualization purposes the radial inverse scaling of radiation is removed, so that the waves do not die off and render the simulation useless. In particular, the waves shown have colors that correspond to the multipole solutions $l = 2, 3, 4, 5$, the m index in each case is considered for $m = \pm l$.

The individual modes are normalized to their respective maximum amplitude, where brighter colors indicate stronger radiation (strain) within the mode itself. In the

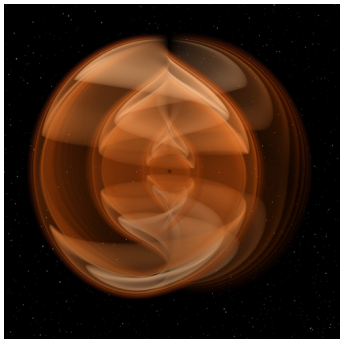

(a) Quadrupolar contribution [6]

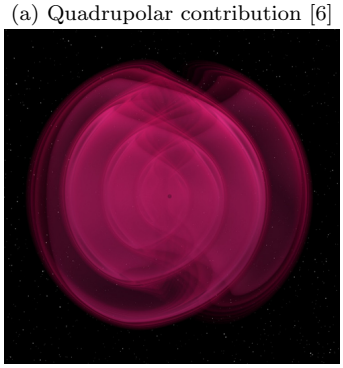

(b) Octupolar contribution [6]

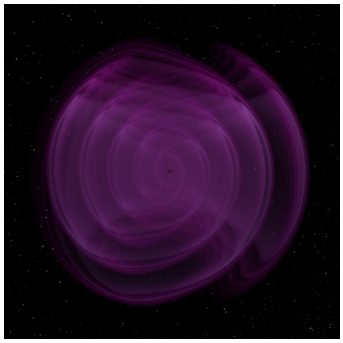

(c) Hexadecupolar contribution [6]

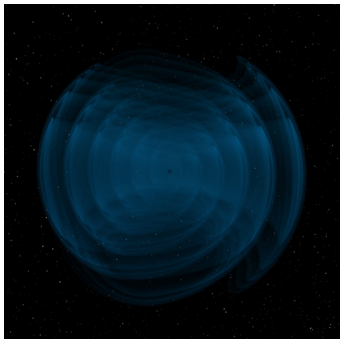

(d) 32-polar contribution [6]

Fig. 19.: The scaled radiation contributions from the first 4 terms in the multipole expansion as seen in the simulation in [6]

simulation itself there is also a side panel which displays the simulated total contribution from the system all at once, though this image will not be looked at here. The simulated radiation from the quadrupolar contributions are shown first in Fig 19(a). These contributions have dominated the discussion in the literature until the asymmetric mass detections this year. Here the heavy warping around the system is clear. As the frequency increases, (Fig. 20), the contributions from the multipole moments become brighter, displaying the increased energy density as the massive objects get closer together. One may notice the increased energy density that is beginning to develop in center of the system from the quadrupole contributions. The higher order multipoles are shown beneath the quadrupole in order (b) octupole moment (c)hexadecupole moment (d) 32-pole moment. The variation in angular dependence can be seen from the shape of the waveforms.

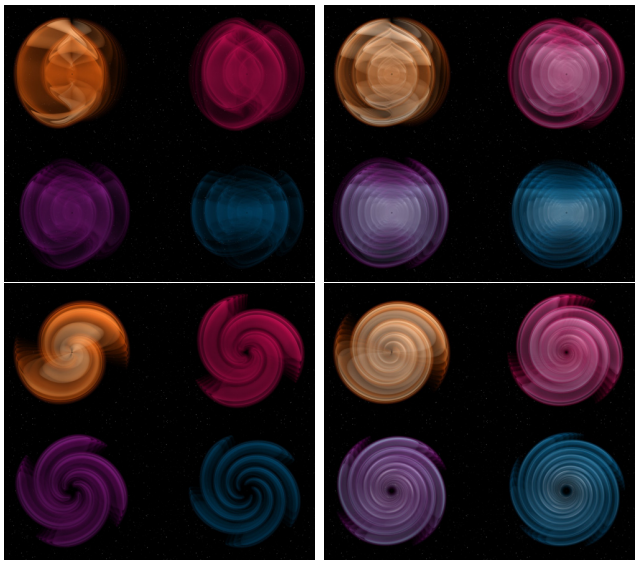

Fig. 20.: The simulated distinct contributions from the multipole moments both early in the inspiral (first column) and close to the merger (second column). The top row shows the system from a side view, while the bottom row shows the images perpendicular to its orbital plane [6].

The final .7 seconds of the simulation were calculated with NR to demonstrate the horizons of the ringdown with identical mass ratio (Fig 21. We see the apparent change in magnitude of the lower order multipoles, including the 32-pole contribution, increasing relatively as the objects join together. The calculation of this simulation deviates from the original waveform, but is still an accurate initial guess in the case that the system at hand is indeed a BBH.

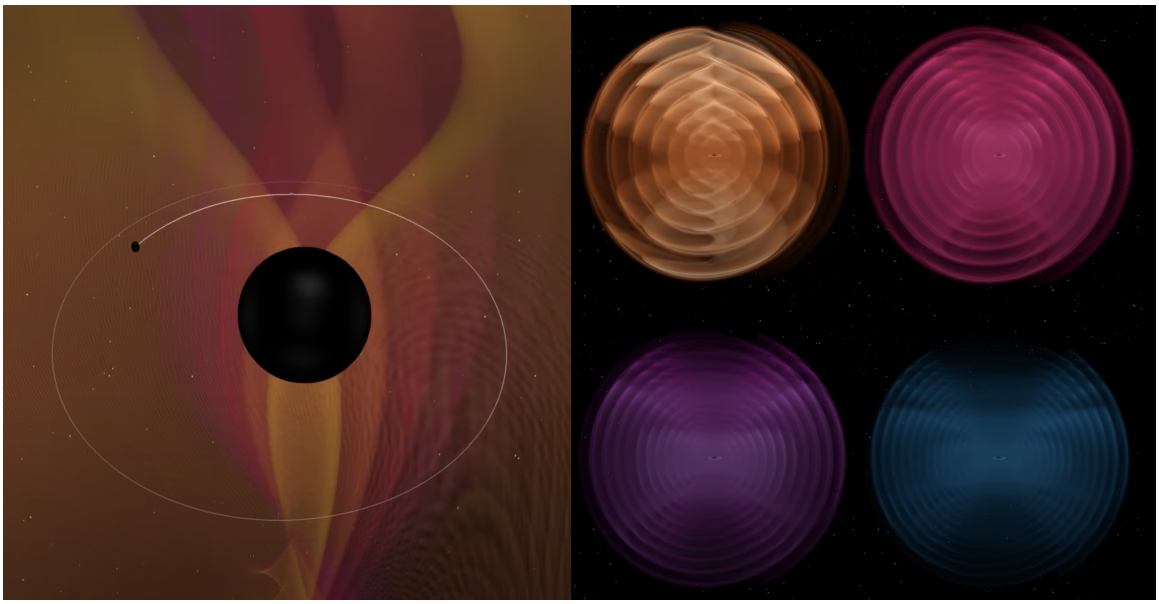

Fig. 21.: On the left, the final seconds of the merger simulation are shown, with masses appropriately scaled. On the right, again the contributions from each multipole term just moments before the merger.

7.3.3 Tests of GR

The large mass asymmetry provides a nice event to probe the robustness of the strong field theory of general relativity. Multiple tests with the assumed posteriors were performed, allowing for this new parameter space to be explored in NR.

1. **A consistency test of the signal reconstruction.**

   This analysis is done by removing the shape of the most like CB waveforms to analyze 4s of residual data near the merger. This helps to give a realization of the noise PSD from which non-Gaussian and non-stationary noises can be determined through analysis [44]. If the non-Gaussian noises are found to be insignificant compared to the original waveform, it shows evidence of a true signal, and thus verifying the expectations of GR. This test in particular showed no evidence of general deviations from GR.

2. **Test of the spin-induced quadrupole moments**]

The spin-induced multipole moments of a Kerr black hole are completely described by its spin angular momentum and mass, according to the no-hair conjecture. One can define a scalar value corresponding to the quadrupole moment tensor, $Q = -\kappa a^2 m^3$, for a single compact object, where Kerr BHs have $\kappa = 1$ and NSs have $\kappa = [2 - 14]$. This in particular describes the variations of the spin-induced quadrupole moment.

In assuming that both objects are both black holes we shall have $\kappa_1 = \kappa_2 = 1$, which is a degenerate system. The parameter $\kappa_s = (\kappa_1 + \kappa_2)/2$ is then deduced from the GW signal. For BBHs, this parameter should be equal to 1. The program was fed the a priori interval $[0, 500]$, and though there was a small increase in likelihood near $\kappa_s = 0$, the output returned nonzero posteriors over most of the interval.

- This indicates the results are consistent with GR if GW190814 generated by a BBH source, as we have assumed. This still does not rule out any consistency if the waveform is generated by other sources, leaving this open as a possibility.

3. **Parameterized test of source's ability to generate waveform**

   An aligned spin EOB waveform without higher order multipoles is used to model wave generation from an evolving source with identical parameter priors as the deduced posteriors. In this source model the Post-Newtonian coefficients describing the early orbit inspiral [45]. These models are varied from their GR predicted values in an attempt to find a better fit for the model. These coefficients showed no deviation from their standard values in GR.

In summary, the overall GW signal is concluded to be consistent with GR and the expected description of a CB merger.

CHAPTER 8

FUTURE

In the future, it is extremely likely that systems similar GW190814 will be detected. Hopefully the detection of GW190814 allows for an expanded exploration of the parameter space before that time. We believe furthermore that the noise at aLIGO Livingston, along with the reduced state of operation at aLIGO Handford, led to suboptimal detections of the system below 30 Hz. In the frequency range below this imposed cutoff, it should be possible to get a better understanding of the early dynamics of compact binary's evolutions [22]. This could lead to earlier "follow up" searches for EM counterparts, and if detected early enough in the inspiral, this could translate into a better determination of the component's individual properties.

Thus, it would be beneficial to make detections that allow us to understand what is happening in the lower frequency range, and thus earlier on in the evolution of the orbital. Though aLIGO and aVIRGO are expected to reach design sensitivities as low as 10 Hz in the coming years, we wish to briefly consider the design of some of the ground based detectors which may help add extra layers of consideration to the data.

One proposal that has received funding and is currently in the design stage is the Einstein Telescope [46]. This has still not begun construction, and is site-planning but its design is interesting enough to warrant some discussion. The plan is to build it underground in such a way that isolates it from seismic noise much more efficiently than the LVC detectors. Furthermore, it is a triangular interferometer, designed to have an arm length of 10 km. The interferometer is expected to reach close to the LF band border at 1 Hz. This can be seen in Fig 22, which is seen to penetrate

the frequency-strain area covered by compact binary inspirals. This will give a nice collection of data to be analyzed in the coming decades.

However, as mentioned, putting this system online is still a ways off. Fortunately, in the meantime, the field of gravitational wave astronomy still has something to look forward to from Tokyo. KAGRA, having started observing runs in February 2020, is expected to be pushing toward its design sensitivity soon which is projected to be near that of aLIGO and aVIRGO [47]. This will be the first ever fully operational underground gravitational wave observatory. This 3 km arm interferometer will use much of the same advanced techniques make modifications to the Michelson setup, along with cryogenic chambers surrounding the test masses themselves. This setup will simultaneously eliminate noise and thermal noises that aLIGO and aVIRGO cannot, leading to the expected sensitivity of KAGRA being particularly lower (from a characteristic strain perspective) than aLIGO and aVIRGO near the low frequency edges of its broadband.

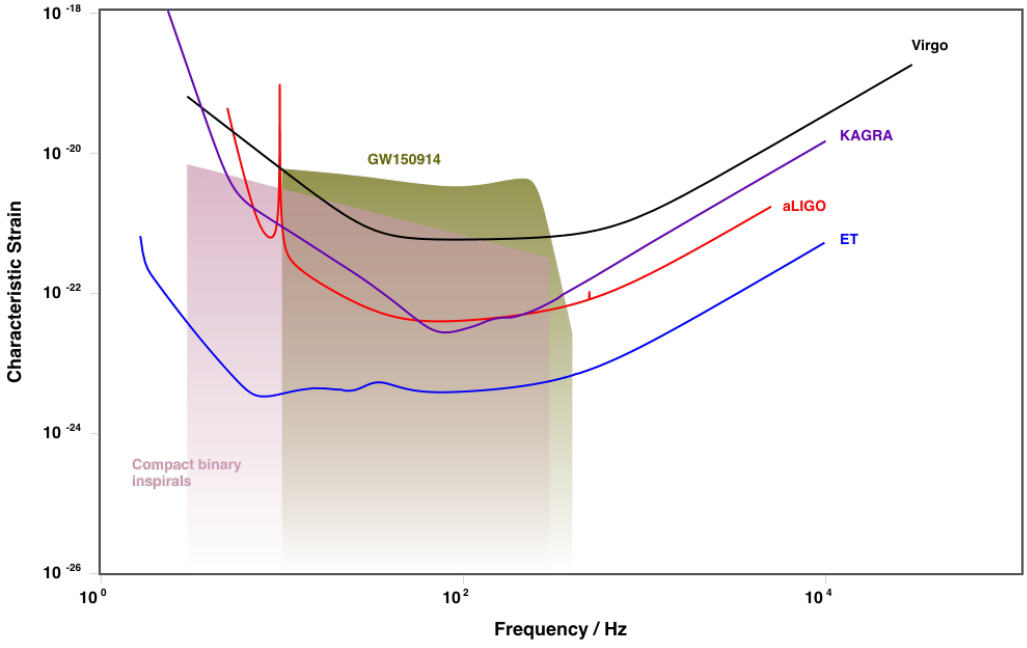

Fig. 22.: A plot of the characteristic strain sensitivities of all 4 discussed detectors so far: (1) aVIRGO (2) KAGRA (3) aLIGO (4) Einstein Telescope

The characteristic strain and root PSDs of KAGRA and the ET are shown in comparison with the current aLIGO and aVIRGO sensitivities.

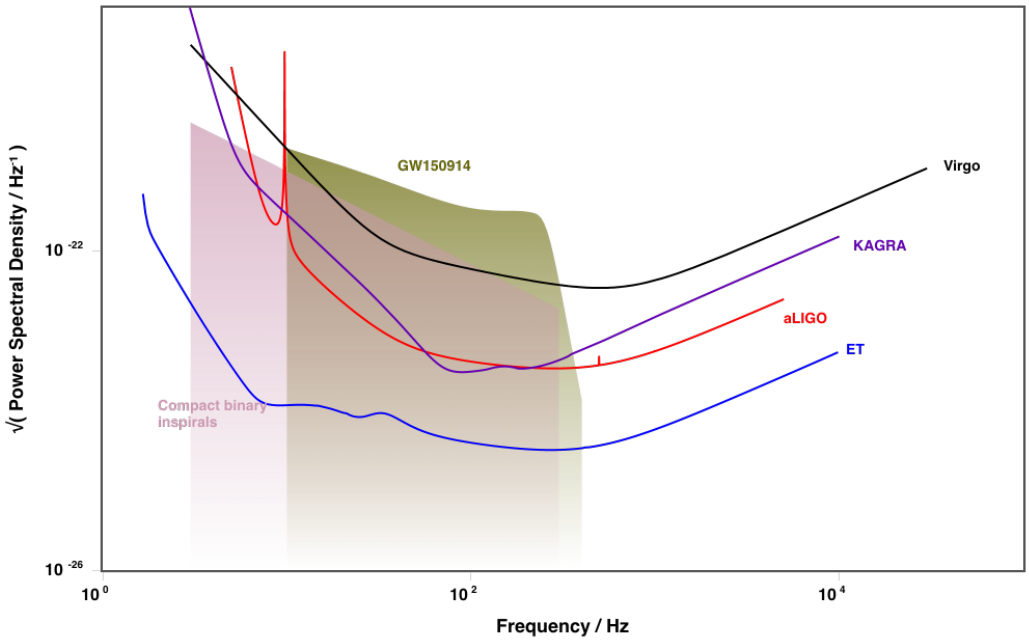

Fig. 23.: A plot of the root Power Spectral Density sensitivities of the discussed detectors: (1) aVIRGO (2) KAGRA (3) aLIGO (4) Einstein Telescope

In total, we have presented here a relatively brief development of a surface level interpretation of Einstein's field equations. The particularly important aspects of the current detector state and the ways in which GW signals are analyzed were considered. This was followed finally by the results obtained by the LVC in the detection of GW190814.

Though we have given a glance here into the future of two detectors, it should be noted this is nowhere near the full state of the developments in process within gravitational wave astronomy. We have not even begun to discuss the space interferometer LISA, which has already shown proof of concept and is expected to be up by 2030, or the other planned detectors aimed to reach into the ELF and VLF bands. We were unable to touch on numerous aspects of the LVC alone due to the number of collaborators involved in this process, and hope that nothing too crucial to the

subject has been omitted

Though the value of the gravitational wave astronomy field is at an all time high in terms of detections, the current methods of parameter estimation remain insufficient, namely the lack of fully explored numerical solutions to the complex combinations of parameter space that emit GWs in the first place. Not only in this corner, but also an expansion in the waveform modeling for both heavy NSs and light BHS in systems radiating GWs. Nonetheless, we expect in the coming years to see much growth in the parameter vector space used for comparison in the Bayesian analysis, particularly the components describing asymmetric mass ratios of compact binary systems.

Appendix A

ABBREVIATIONS

VCU	Virginia Commonwealth University
RVA	Richmond Virginia
EM	Electromagnetism
GR	General Relativity
SR	Special Relativity
GW	Gravitational Wave
LIGO	Laser Interferometer Gravitational-Wave Observatory
VIRGO	

REFERENCES

[1] Sean Carroll. *An Introduction To Spacetime and Geometry.* Addison-Wesley, 2003.

[2] J Aasi, B P Abbott, T Abbott, et al. Advanced ligo. *Classical and quantum gravity*, 32(7):074001, 2015.

[3] F Acernese, M Agathos, K Agatsuma, et al. Advanced virgo: a second-generation interferometric gravitational wave detector. *Classical and quantum gravity*, 32(2):024001–024001(52), 2015.

[4] Christopher Moore, Robert Cole, and Christopher Berry. Gravitational wave detectors and sources.

[5] C J Moore, R H Cole, and C P L Berry. Gravitational-wave sensitivity curves. *Classical and Quantum Gravity*, 32(1):015014, dec 2014.

[6] Elke Muller and Benjamin Knispel. Visualization of the binary black hole merger gw190814.

[7] Albert Einstein and John J et al. Stachel. *The collected papers of Albert Einstein.* Princeton Univ. Press, Princeton, NJ, 1987.

[8] G. M. Clemence. The relativity effect in planetary motions. *Rev. Mod. Phys.*, 19:361–364, Oct 1947.

[9] Clifford M Will. The 1919 measurement of the deflection of light. *Classical and Quantum Gravity*, 32(12):124001, jun 2015.

[10] Wikisource. Translation:on the dynamics of the electron (july) — wikisource,, 2019. [Online; accessed 4-December-2020].

[11] R. A. Hulse and J. H. Taylor. Discovery of a pulsar in a binary system. *Astrophysical journal. Letters*, 195:L51–L53, January 1975.

[12] B. P. Abbott, R. Abbott, T. D. Abbott, et al. Observation of gravitational waves from a binary black hole merger. *Phys. Rev. Lett.*, 116:061102, Feb 2016.

[13] Barry C Barish and Rainer Weiss. Ligo and the detection of gravitational waves. *Physics today*, 52(10):44–50, 1999.

[14] B. P. Abbott, R. Abbott, T. D. Abbott, et al. Gwtc-1: A gravitational-wave transient catalog of compact binary mergers observed by ligo and virgo during the first and second observing runs. *Phys. Rev. X*, 9:031040, Sep 2019.

[15] R. Abbott, T. D. Abbott, S. Abraham, et al. Gwtc-2: Compact binary coalescences observed by ligo and virgo during the first half of the third observing run, October 2020. arXiv:2010.14527.

[16] B. P. Abbott, R. Abbott, T. D. Abbott, et al. GW190425: Observation of a compact binary coalescence with total mass $\sim$ 3.4 m $\odot$. *The Astrophysical Journal*, 892(1):L3, mar 2020.

[17] R. Abbott, T. D. Abbott, S. Abraham, et al. GW190814: Gravitational waves from the coalescence of a 23 solar mass black hole with a 2.6 solar mass compact object. *The Astrophysical Journal*, 896(2):L44, jun 2020.

[18] Bernard F. Schutz. *A FIRST COURSE IN GENERAL RELATIVITY*. Cambridge Univ. Pr., Cambridge, UK, 1985.

[19] J.A. Wheeler C.W. Misner, K. Thorne. *Gravitation*. Princeton University Press, 2nd edition, 2017.

[20] Bernard F Schutz. *Geometrical methods of mathematical physics*. Cambridge University Press, Cambridge ; New York, 1980.

[21] R. Abbott, T. D. Abbott, S. Abraham, et al. Gw190412: Observation of a binary-black-hole coalescence with asymmetric masses. *Phys. Rev. D*, 102:043015, Aug 2020.

[22] C Cutler and K S Thorne. An Overview of Gravitational-Wave Sources. (gr-qc/0204090):40 p, Apr 2002.

[23] T Bulik, D Gondek-Rosinska, and K Belczynski. Expected masses of merging compact object binaries observed in gravitational waves. *Monthly notices of the Royal Astronomical Society*, 352(4):1372–1380, 2004.

[24] Colm Talbot and Eric Thrane. Measuring the binary black hole mass spectrum with an astrophysically motivated parameterization. *The Astrophysical Journal*, 856(2):173, apr 2018.

[25] M Punturo, M Abernathy, F Acernese, et al. The third generation of gravitational wave observatories and their science reach. *Classical and quantum gravity*, 27(8):084007, 2010.

[26] B P et al. Abbott. A guide to ligo–virgo detector noise and extraction of transient gravitational-wave signals. *Classical and quantum gravity*, 37(5):55002, 2020.

[27] C Buy, E Genin, M Barsuglia, et al. Design of a high-magnification and low-aberration compact catadioptric telescope for the advanced virgo gravitational-wave interferometric detector. *Classical and Quantum Gravity*, 34(9):095011, apr 2017.

[28] B. P. Abbott, R. Abbott, T. D. Abbott, et al. Gw170814: A three-detector observation of gravitational waves from a binary black hole coalescence. *Phys. Rev. Lett.*, 119:141101, Oct 2017.

[29] B. P. Abbott, R. Abbott, T. D. Abbott, et al. Gw170817: Observation of gravitational waves from a binary neutron star inspiral. *Phys. Rev. Lett.*, 119:161101, Oct 2017.

[30] Lee Samuel Finn and David F Chernoff. Observing binary inspiral in gravitational radiation: One interferometer. *Physical review. D, Particles and fields*, 47(6):2198–2219, 1993.

[31] John Veitch, Vivien Raymond, Benjamin Farr, et al. Parameter estimation for compact binaries with ground-based gravitational-wave observations using the lalinference software library. *Physical Review D*, 91(4):042003, 2015.

[32] R. Abbott, T. D. Abbott, S. Abraham, et al. Gw190521: A binary black hole merger with a total mass of 150 $M_{\odot}$. *Phys. Rev. Lett.*, 125:101102, Sep 2020.

[33] T. D Abbott, C Adams, V. B Adya, et al. Binary black hole population properties inferred from the first and second observing runs of advanced ligo and advanced virgo. *Astrophysical journal. Letters*, 882(2):L24, 2019.

[34] K Ackley. Observational constraints on the optical and near-infrared emission from the neutron star-black hole binary merger cadidate s190814bv. *Astronomy and astrophysics (Berlin)*, 2020.

[35] B. P. Abbott, R. Abbott, T. D. Abbott, et al. Properties of the binary neutron star merger gw170817. *Phys. Rev. X*, 9:011001, Jan 2019.

[36] B P Abbott, R Abbott, C Adams, et al. Effects of waveform model systematics on the interpretation of gw150914. *Classical and quantum gravity*, 34(10):104002, 2017.

[37] Prayush Kumar, Jonathan Blackman, Scott E. Field, et al. Constraining the parameters of GW150914 and GW170104 with numerical relativity surrogates. *APS*, 99(12):124005, June 2019.

[38] Laura Kreidberg, Charles D. Bailyn, Will M. Farr, and Vicky Kalogera. MASS MEASUREMENTS OF BLACK HOLES IN x-RAY TRANSIENTS: IS THERE a MASS GAP? *The Astrophysical Journal*, 757(1):36, sep 2012.

[39] Nai-Bo Zhang and Bao-An Li. GW190814s secondary component with mass 2.50–2.67 $m_{\odot}$ as a superfast pulsar. *The Astrophysical Journal*, 902(1):38, oct 2020.

[40] Vassiliki Kalogera and Gordon Baym. The maximum mass of a neutron star. *The Astrophysical Journal*, 470(1):L61–L64, oct 1996.

[41] Will M. Farr and Katerina Chatziioannou. A Population-Informed Mass Estimate for Pulsar J0740+6620. *Research Notes of the American Astronomical Society*, 4(5):65, May 2020.

[42] Masaru Shibata, Enping Zhou, Kenta Kiuchi, and Sho Fujibayashi. Constraint on the maximum mass of neutron stars using gw170817 event. *Phys. Rev. D*, 100:023015, Jul 2019.

[43] M. Linares, T. Shahbaz, and J. Casares. Peering into the dark side: Magnesium lines establish a massive neutron star in PSR j2215+5135. *The Astrophysical Journal*, 859(1):54, may 2018.

[44] Tyson B. Littenberg and Neil J. Cornish. Bayesian inference for spectral estimation of gravitational wave detector noise. *Phys. Rev. D*, 91:084034, Apr 2015.

[45] Jeroen Meidam, Ka Wa Tsang, Janna Goldstein, et al. Parametrized tests of the strong-field dynamics of general relativity using gravitational wave signals from coalescing binary black holes: Fast likelihood calculations and sensitivity of the method. *Phys. Rev. D*, 97:044033, Feb 2018.

[46] B. Sathyaprakash et al. Scientific Potential of Einstein Telescope. In *46th Rencontres de Moriond on Gravitational Waves and Experimental Gravity*, pages 127–136, 8 2011.

[47] T Akutsu, M Ando, K Arai, et al. Overview of KAGRA: KAGRA science. *Progress of Theoretical and Experimental Physics*, 08 2020. ptaa120.